Virtualisation of motorcycle customer usage profiles via multi-body simulation for durability

vorgelegt von
M.Sc.
Aptin Haerian

an der Fakultät V – Verkehrs- und Maschinensysteme
der Technischen Universität Berlin
zur Erlangung des akademischen Grades

Doktor der Ingenieurwissenschaften
– Dr.-Ing. –

genehmigte Dissertation

Promotionsausschuss:

Vorsitzender:	Prof. Dr.-Ing. Henning Meyer
Gutachter:	Prof. Dr.-Ing. Robert Liebich
Gutachter:	Prof. Dr.-Ing. Martin Meywerk

Tag der wissenschaftlichen Aussprache: 16. September 2022

Berlin 2022

Acknowledgements

First, I would like to thank Dr Öztürk, expert in durability, load and data analysis at BMW Motorrad, Germany, who supervised this thesis. Your contagious positive mindset resulted in a pleasant working atmosphere. Besides that, you also helped to improve the quality of the research with your expertise and our extensive professional discussions. The freedom and independency you granted me to try novel ideas were also pivotal for this thesis.

Another thank you belongs to Professor Liebich at the Chair of Engineering Design and Product Reliability at the Technische Universität Berlin, Germany. Your encouragement and feedback really drove me forward. Your overall knowledge in the relevant fields, but also scientific work in general, led to valuable discussions and helped to gain a different perspective on the work.

Furthermore, I would like to thank Professor Meywerk at the Chair of Vehicle Engineering at the Helmut-Schmidt-Universität / Universität der Bundeswehr Hamburg, Germany, for reviewing this thesis.

Additionally, I want to thank Professor Meyer at the Chair of Machine System Design at the Technische Universität Berlin, Germany, for chairing the exam.

Finally, I would like to thank my family and my friends for always supporting me and believing in me.

Munich, 2022
Aptin Haerian

Preface

This cumulative PhD thesis contains the manuscripts of the following publications:

[1] – A. Haerian, K. Öztürk and R. Liebich. 'Special and misuse events for motorcycles'. In: *International Journal of Vehicle Systems Modelling and Testing* (in press)

[2] – A. Haerian, K. Öztürk and R. Liebich. 'Damage equivalent virtual tracks for motorcycles'. In: *International Journal of Vehicle Design* (in press)

[3] – A. Haerian, K. Öztürk and R. Liebich. 'Influence of road and rider characteristics on durability of motorcycles'. In: *International Journal of Vehicle Systems Modelling and Testing* (in press)

Summary

This cumulative PhD thesis presents the development of methods for virtualising motorcycle customer usage profiles in terms of load analysis. As the amount of available usage data increases, the question arises how this source can be used in the vehicle development to make precise load assumptions. The transfer of the data into the virtual world is an essential component. The first publication within this cumulative PhD thesis deals with the load categories of special and misuse events. A new definition of these categories was introduced, converted into an equation, and confirmed by measurements. Furthermore, multi-body simulation models of full vehicle motorcycles were created and validated with measurements. In addition, a method has been developed to determine representative special events. The second publication includes a method for the identification of damage-equivalent virtual tracks, which allows a reduction of the simulation duration. Here, the tracks are segmented and evaluated for different use cases. For the simulation, test tracks measured with laser scanners were used. The third publication describes the transfer of classified data on road and rider characteristics into the simulation environment. First, a method was developed to determine the design-relevant customer with regard to service loads by means of synthetic riding manoeuvres. The roughness and the vehicle's velocity were taken into account. It was also shown how it is possible to transfer this data into an entire synthetic virtual track including data for curvature. The validation was carried out again with the measurement of a real motorcycle. In addition, a new method was developed to create speed profiles for simulations that considers the road characteristics and customer's riding skills. The presented methods enable a holistic virtual load data acquisition process. Possibilities to include the methods in the vehicle development process and further improvements are finally discussed.

Zusammenfassung

Die vorliegende kumulative Dissertation präsentiert die Entwicklung von Methoden zur Virtualisierung von Motorrad-Kundennutzungsprofilen in Bezug auf die Betriebsfestigkeit. Mit zunehmender Menge an verfügbaren Nutzungsdaten stellt sich die Frage wie diese nutzbringend in der Fahrzeugentwicklung verwendet werden können, um präzise Lastannahmen zu treffen. Dabei ist die Überführung der Daten in die virtuelle Welt ein essentieller Bestandteil. Die erste Veröffentlichung im Rahmen dieser kumulativen Promotionsschrift beschäftigt sich mit den Lastkategorien Sonder- und Missbrauchsereignisse. Eine neue Definition dieser Kategorien wurde eingeführt, in eine Gleichung überführt und anhand von Messungen validiert. Weiterhin wurden Mehrkörpersimulations-Modelle von Motorrad-Gesamtfahrzeugen erstellt und gleichermaßen validiert. Zusätzlich wurde eine Methode entwickelt, um repräsentative Sonderereignisse zu bestimmen. Die zweite Veröffentlichung umfasst eine Methode zur Identifikation von schädigungsäquivalenten virtuellen Strecken, welche eine Reduktion der Simulationsdauer ermöglicht. Hierbei werden Strecken segmentiert und für verschiedene Use Cases ausgewertet. Für die Simulation wurden laservermessene Teststrecken verwendet. Die dritte Veröffentlichung beschreibt die Überführung klassierter Daten von Straßen- und Fahrercharakteristiken in die Simulationsumgebung. Eine Methode wurde entwickelt, um mittels synthetischer Fahrmanöver auslegungsrelevante Kunden hinsichtlich Betriebslasten zu bestimmen. Dabei wurde die Rauigkeit und Fahrzeuggeschwindigkeit berücksichtigt. Weiterhin wurde gezeigt wie diese Daten in eine synthetische virtuelle Gesamtstrecke inklusive Kurven überführt werden können. Die Validierung erfolgte abermals mit der Messung eines realen Motorrads. Zusätzlich wurde eine neue Methode entwickelt, um Geschwindigkeitsprofile für Simulationen zu erstellen, welche die Straßeneigenschaften und das Fahrkönnen berücksichtigt. Die präsentierten Methoden ermöglichen eine ganzheitliche virtuelle Lastdatenerfassung. Abschließend werden Möglichkeiten die Methoden in den Fahrzeugentwicklungsprozess zu integrieren und weitere Verbesserungen diskutiert.

Contents

List of Figures

List of Tables

List of Abbreviations

Abbreviation	Description
ABS	Anti-lock Braking System
ASC	Automatic Stability Control
CAD	Computer-Aided Design
CAE	Computer-Aided Engineering
CAN	Controller Area Network
COG	Centre Of Gravity
CRG	Curved Regular Grid
DOE	Design Of Experiments
DOF	Degrees Of Freedom
DTC	Dynamic Traction Control
EIM	Effective Interface Mass
FE	Finite Elements
GPS	Global Positioning System
HCF	High Cycle Fatigue
IRI	International Roughness Index
ISO	International Organization for Standardization
LCF	Low Cycle Fatigue
LTF	Load Time Function
MBS	Multi-Body Simulation
OEM	Original Equipment Manufacturer
PSD	Power Spectral Density
SAS	Semi-Active Suspension
SUV	Sport Utility Vehicle

1 Introduction

1.1 Durability in vehicle engineering

Durability engineering assesses the design, dimensioning, and endurance of components and systems with regard to loads throughout the intended life cycle. Other common terms are: endurance strength, engineering strength, operating stability, operating strength, operational stability, structural durability. It is a discipline that inter alia has the goal to make valid load assumptions for components so they can later on be designed as precise as possible. To design full vehicles properly, the components have to be constructed with sufficient strength in order to endure the loads occurring during usage. Hence, load assumptions are part of the early phase in the vehicle development process where requirements are defined for the end product.

The pinpoint dimensioning and design of components and full vehicles has many advantages. In vehicle development, there is generally a need for weight and cost savings. The weight savings go hand in hand with lower fuel consumption. This is an important lever for the reduction of polluting exhaust gases. Increasing pressure from society, resulting customer demand, stricter regulations, and a look at the mobility of the future illustrate the need for action in this area. Durability engineering makes an important contribution in this regard. In contrast to fatigue strength, components are designed in such a way that they can endure the loads during operation over their intended life cycle. Fatigue strength as a requirement for the design of components would lead to oversized vehicles, which would be more expensive, consume more fuel, and might have worse driving characteristics due to the high mass. Furthermore, weight savings make it possible to use less raw materials, saving the manufacturers money and additionally making a contribution to sustainability.

However, these objectives should not upstage the main target of durability engineering, which is ensuring a functional product throughout the complete life cycle. This overarching goal is particularly relevant in the vehicle industry, as the safety

of customers is of great importance. If the loads occurring during usage would be higher than the assumed loads used for the design of the vehicle, component failure and warranty claims would result. Often, cases of damage can be traced to incorrect load assumptions [4]. To prevent this from happening, the detailed knowledge of customer behaviour and the integration into the vehicle development is important and has been a trend in the field of durability engineering in recent years. Customer behaviour has a significant impact on loads, for example, the riding style and the ridden roads. Acquiring relevant data can be achieved through different methods. One possibility is the use of questionnaires. They are, however, dependent on the kind of questions that are asked and the subjective assessment of the customer [5]. Using objective data is, thus, more valuable. A method to gain objective insight into customer behaviour is the collection of data through onboard signals that are logged and classified which was the focus in [6]. The classified data can, hereafter, be used for different use cases. As loads are currently derived from measurements of test riders on test tracks, the data can be used to find a combination of representative test tracks for specific customer usage profiles. However, test riders are often characterised by a supernormal riding style which cannot represent all customers. Therefore, the classified data can also be used as input for virtual models where a variety of use cases can be handled. This enables a virtual load data acquisition in contrast to the classical load data acquisition via measurement, see Figure 1.1. Two categories that are suited to characterise customer behaviour are road and rider characteristics. Exemplary parameters to describe the road are roughness, curviness, or also the occurrence of so-called special events. These events have to be considered for the dimensioning of components because they induce high loads that have to be endured without restrictions for the customer. The consideration of these events is of utmost importance with regard to product liability and warranty. Exemplary parameters to describe the rider are the velocity, longitudinal, or lateral acceleration.

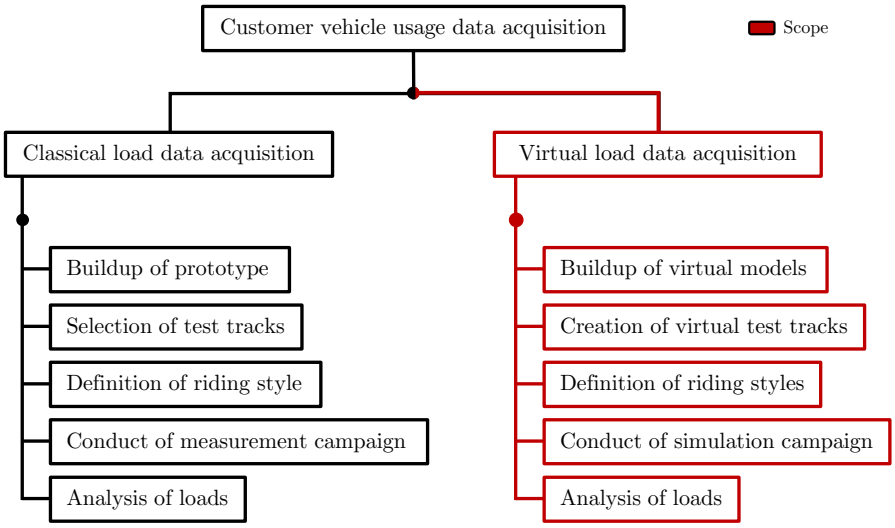

Figure 1.1 – Classical versus virtual load data acquisition.

According to Köhler et al. [4] the complete process of making load assumptions can be divided into the following steps:

- Definition of the total vehicle lifetime,
- differentiation between different operating states,
- weighting of the operating states,
- extrapolation of sub-spectrums,
- consideration of special events,
- creation of an overall spectrum.

The present work deals with the integration of operating states by utilising measured customer data to run simulations. For this work, the distinction and weighting of operating conditions could be combined into one step, the recording of operating conditions. The data used in this work allows a distinction to be made directly as the data is already classified with regard to relevant differentiators. At the same time, the weighting does not need to be performed separately as the collected data

indicates the frequency of occurrence for each specific operating state. Furthermore, special events were investigated in this work, as they can also be simulated with similar tools. This allows an overall assessment of the loads occurring throughout the product life cycle using one simulation environment. The resulting loads that are gained through the developed methods in this PhD thesis subsequently serve as inputs for the remaining steps of durability analyses which are not part of the scope.

1.2 Virtualisation

With increasing computer performance over the last decades, the vehicle development process has been provided with different methods to improve the aforementioned. Many of the methods belong to the topic of computer-aided engineering (CAE) that increase product quality or reduce costs and development time [7]. All three aspects are very appealing from a business point of view. A higher product quality, for example, can increase customer satisfaction and affect buying decisions. Reducing costs and development time also leads to lower costs for the end product. The fact that well executed durability engineering increases quality, company profitability, and customer satisfaction was also observed by Bergmann and Klefsjö [8].

CAE includes different types of simulations and data management tools. For simulations, all relevant aspects that exist in the real world have to be identified. Some simulations might require certain parameters or models where other simulations can neglect those due to the independency of the target quantity from these elements. Subsequently, these aspects need to be transferred into the virtual world.

In the present work, multi-body simulations (MBS) were used to derive loads which is also common practice in the four-wheeled vehicle industry. With these models, it is possible to calculate displacements, velocities, accelerations, and most importantly for this work, loads. As mentioned in [9, 10], a separation of the influencing factors on loads can be made. The three factors in the present work were titled Vehicle, Road, and Rider, see Figure 1.2. These factors interact with one another and influence the loads in the real world. Hence, they have to be represented in the virtual world as well.

The figure demonstrates that two factors interact in each case. These interactions, in turn, affect the loads which are the target quantity. The vehicle model influences the loads by its mechanical properties, such as mass and inertia distributions, or also

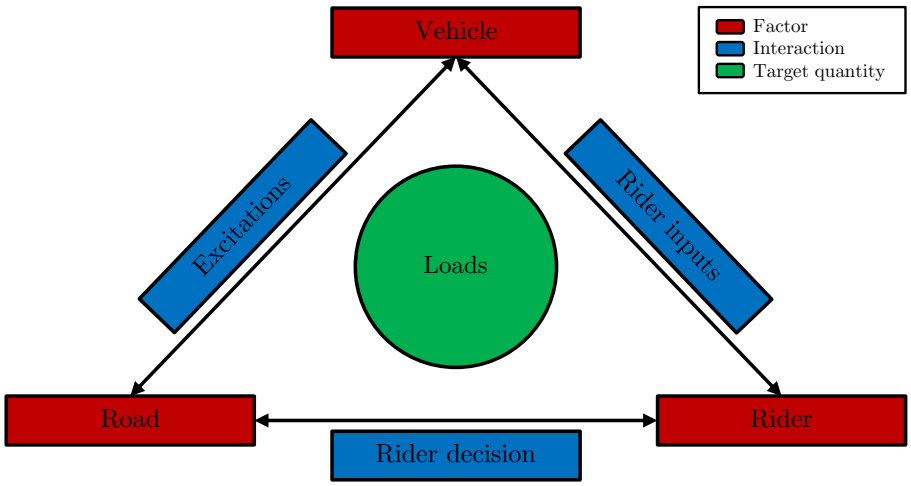

Figure 1.2 – Interaction of factors influencing loads.

the dynamic behaviour. Performing the same manoeuvre with two different vehicles will obviously cause different loads. However, a stationary vehicle does not lead to relevant loads as those are induced during riding, and therefore when the vehicle interacts with its environment. The road influences the loads in different ways. The most obvious one is the vertical excitation of the vehicle when it passes the respective road segment which causes vibrations. Furthermore, the trajectory, and hence lateral excitation is mainly given by the road that is ridden by the motorcyclist. The riding speed is also limited by road conditions. For example, tight curves cannot be ridden with excessive velocities. On the other hand, it is also unlikely that a motorcyclist will ride at a slow speed on a highway. As a result, the road characteristics influence the riding style when interacting with the rider. This interaction causes the rider to decide how a given road is ridden based on his or her preferences and riding skills. Additionally, the rider influences the loads by choosing the ridden roads. This decision can be influenced by different aspects. For instance, a rider might pick the shortest route to his destination to save time and fuel or an extra curvy road in order to perform dynamic riding manoeuvres and experience more lateral acceleration which can subjectively result in more riding pleasure. This influence is also indirectly included in the interaction between vehicle and road, as vehicles are used for different

routes on a segment-specific basis. For example, an enduro motorcycle will be used off-road more often than a superbike. The rider also interacts with the vehicle itself. Not only is the rider part of the system from a mechanical standpoint again with mass and inertia properties, but also with the inputs that are imposed on the vehicle. This aspect relates to the role of the rider as a controller. Parameters that need to be controlled by the rider are, for example, the steering angle, the velocity, the gear selection, the coupling position, or the brake pressures at the front and rear wheel. The reactions of the vehicle in turn influence this control task.

At present, load assumptions are generally derived from predecessor models in the motorcycle industry because appropriate methods that can be used in the early development stages are for the most part non-existent [11, 12]. According to Meywerk [7], CAE methods make it possible to detect errors at an early stage and make design changes. Using virtual models and simulations as in this work has further advantages. First, load assumptions can be made in the early development stages of the project. Therefore, it is not mandatory to have one or multiple prototypes to make predictions on the occurring loads. The independency of prototype measurement vehicles also enables a comparison of different concepts from a durability standpoint just using simulations. As a result, the accuracy of load assumptions increases while the number of revisions decrease resulting in a shorter development time. Furthermore, measurement campaigns are cost-intensive and time-consuming which is why only selected vehicles are tested with a limited time. The decision on which derivates or configuration variants should be measured can be supported by comparing all of them via simulation. In addition, tracks and manoeuvres can be prioritised based on simulation results if it is not possible to carry out all measurements in time. The reproducibility is also guaranteed through simulations and enables an objective comparison even for different vehicles. On the one hand, the virtual track is always the same. On real tracks and rides, vegetation, climate, and wear play a role which limits reproducibility [13]. On the other hand, the rider's behaviour is reproducible, as the virtual rider always rides the same way. A real rider can never exactly reproduce a manoeuvre, especially when considering form on the day. Another advantage of virtual load data acquisition is that even spots that are inaccessible on the real motorcycle can be evaluated. Moreover, costs are incurred for each measuring point on the real vehicle, on the one hand for the measuring technology per se, and on

the other hand for the application. Besides that, additional time is required. These difficulties do not exist with the virtual vehicle, as nearly any number of interfaces can be evaluated regardless of the location. Additionally, simulations ensure a secure database as results are always produced, whereas measurement data can only be examined after the rides. The drop out of sensors can only be noticed afterwards. In those cases, some measurements have to be repeated which again costs money and time. This is, however, not always possible due to time limitations, resulting in lack of data. A further advantage of determining loads by means of simulation instead of measurement is the independency of wheel load transducers. It is state of the art in the motorcycle industry to determine the loads at the wheel hubs with these measuring tools [14]. The loads at the wheels are particularly important as they represent the loads that are induced into the motorcycle due to the interaction between environment and vehicle. However, this technology is very expensive and in the motorcycle industry there are only a few suppliers that have the know-how. Virtual load data acquisition allows slimmer measurement setups without wheel load transducers that can be used to validate virtual models. Subsequently, the loads can be obtained from the simulation instead of measurements. For Original Equipment Manufacturers (OEMs), this would lead to a wider choice of suppliers and could reduce strong dependency relationships. Additionally, the wheel load transducers are very sensitive, which is why critical manoeuvres, such as special events, often have to be performed at reduced speed in order to avoid damage. As a result, it is not possible to accurately represent customer behaviour. Moreover, the wheel load transducers influence the loads and vehicle dynamics, as the vehicle empty weight and the unsprung masses increase compared to the series vehicle. The aforesaid influence is even higher for motorcycles than for four-wheeled vehicles. In the present work, for example, the wheel load transducers increased the unsprung masses at the front and rear wheel by 12% to 15%. Finally, simulations do not cause damage to vehicles or persons. In measurement campaigns, components can be damaged, and thereby need to be replaced. Apart from that, there is always a risk of accidents during measurements which can result in personal damage. This could also potentially be prevented by looking at simulations to see which manoeuvres are particularly critical and exceed vehicle limits in terms of durability or riding dynamics.

1.3 Multi-body simulation model

Multi-body models are commonly used in science, research, and the vehicle industry [15]. In the simplest form, they consist of rigid bodies that are connected via joints [7]. They have associated masses and are exposed to forces and torques at discrete points. These loads are transferred to springs, dampers, joints, and other types of bearings. Besides that, impressed volume loads can act on the respective body [16]. As non-deformable rigid bodies have no strains, and hence no stresses can be calculated, these types of models are used to calculate inner loads. Afterwards, the detailed fatigue analysis can be performed with finite element (FE) models of the components. Here, detailed component geometry and material properties can be included. The calculated inner loads from the MBS are hence used as inputs for FE calculations and in-depth load analysis [17].

For the present work, full vehicle MBS models of motorcycles were created in ADAMS®. The models include all relevant mechanical subsystems and a rider. Additionally, the FTire by Gipser [18] was incorporated through a co-simulation as it has been used and analysed in many publications for four-wheeled vehicles [19–28]. This physical model is the most suited for simulations that include vertical excitations and durability related manoeuvres because it is the best compromise between computing time, accuracy, and parametrisability [26]. Additionally, the tyre model can easily be implemented in a commercial software like ADAMS®. A further co-simulation was integrated by considering the control systems anti-lock braking system (ABS), semi-active suspension (SAS), and wheelie control. The control systems were modelled in Simulink® and included due to the presence in the real motorcycle that was used for validation. Different types of road models were created. For the simulation of special events, the geometry of multiple obstacles was measured on a test track and replicated in the virtual environment. For the simulation of service loads, test tracks that were measured in the past with laser scanners were transferred into the virtual environment via the CRG data format. With this data, the trajectory and vertical profile of a measured track can be mapped. For more information on CRG data, the reader is referred to [29, 30]. Furthermore, synthetic virtual tracks were created based on road characteristics. The rider was modelled in two different ways. For validation purposes, measured velocities and manoeuvres were recreated in the virtual environment. For the simulation of typical customer behaviour, rider characteristics

were used to create speed profiles. The remaining quantities were determined by the controller models provided by ADAMS®.

An enhancement of a multi-body model can be achieved by substituting rigid bodies with flexible bodies. As the dynamic behaviour of technical systems, in general, is influenced by the elastic properties and deformations of the individual bodies, the implementation is reasonable [31]. The detailed procedure for the inclusion of flexible bodies is described in Appendix A. In general, the implementation of flexible bodies instead of rigid bodies leads to a higher modelling effort as more know-how is required. In addition to that, the generation of necessary models and preparation for the MBS is very time-consuming. The computing time increases significantly when using flexible bodies as well. For this reason, it is beneficial to understand which components can be modelled as rigid instead of flexible bodies. Another advantage of rigid bodies is that during an early stage of the vehicle development process, concepts can be compared quicker. The possibility of substituting flexible with rigid bodies was investigated by means of a study in this work.

Apart from the mechanical components, the rider mass and positioning were also considered for the full vehicle MBS models in ADAMS®. The mass of the rider was determined by using an axle load scale. These scales are used to determine the load distribution on the two wheels of a motorcycle and also for passenger cars to measure the loads on the two axles. The axle load scale outputs one value for the front wheel (m_{ft}) and one for the rear wheel (m_{rr}). The sum of the two measured values equals the total mass of the vehicle m_{tot}, see Equation 1.1. The mass of the rider m_{rid} can be determined by positioning the vehicle on the scale once with the rider and once without. The difference between the two measured values for the total mass of the vehicle with the rider $m_{\mathrm{tot,veh,rid}}$ and without the rider $m_{\mathrm{tot,veh,emp}}$ equals the rider mass, see Equation 1.2.

$$m_{\mathrm{tot}} = m_{\mathrm{ft}} + m_{\mathrm{rr}}, \tag{1.1}$$

$$m_{\mathrm{rid}} = m_{\mathrm{tot,veh,rid}} - m_{\mathrm{tot,veh,emp}}. \tag{1.2}$$

The position of the rider was adjusted iteratively in the virtual model by running static simulations. Before each simulation, the position of the rider was shifted forward or backward along the riding direction in relation to the centre of grav-

ity (COG) of the motorcycle. The target quantities, that were compared with the measurements of the axle load scale, were the loads at the front and rear wheel.

Further parameters that were measured on the real vehicle and adjusted for the virtual model were the tyre pressure for the front and rear wheel, the spring preload, and the riding mode. The tyre pressure was set in the FTire model. The spring preloads were applied to the front and rear suspension systems. The riding mode was considered in the Simulink® model of the SAS. The SAS control system adjusts the damping characteristics, and hence has a major influence on the vehicle dynamics. The characteristics can be adjusted by the rider before and during the ride by selecting a certain mode and loading. Exemplary modes of the motorcycle used for the present work (BMW R1200GS) are Road, Dynamic, or Enduro. The loading can be configured in three stages: solo operation, solo operation with luggage, and pillion operation with luggage.

1.4 Experimental set-up

For the validation of the MBS model and the developed methods, measurement campaigns were carried out with a real motorcycle on test tracks. The motorcycle was equipped with wheel load transducers from AIM Arnold Intelligente Messysteme GmbH & Co. KG at the front and rear wheel as well as data-logging devices. Using the wheel load transducers, the loads at the two wheel hubs were measured. Figure 1.3 shows the motorcycle with the wheel load transducers.

Wheel loads are of particular interest in the vehicle development because they provide information on which loads are induced by the external influences in the vehicle. Wheel loads are also typical inputs for other simulations, for instance, FE calculations of components. Besides the transducers, data-logging devices recorded signals that can be accessed via the vehicle's Controller Area Network (CAN) bus. The source of the signals are onboard sensors. In addition to the CAN logging device, a global positioning system (GPS) module was used. The GPS data provides the position of the vehicle and was used to validate virtual tracks. Both devices are from 2D, Debus & Diebold Meßsysteme GmbH and depicted in Figure 1.4. The devices have negligible weights and dimensions, and hence do not affect the vehicle dynamics and enable offline applications after the measurements, for example, comparisons with simulation results.

Figure 1.3 – Exemplary measurement motorcycle with wheel load transducers ©BMW AG.

(a) Data-logging device (b) GPS module

Figure 1.4 – Logging devices.

Table 1.1 – Overview logged signals.

Component	Measurand
Vehicle	Velocity GPS longitudinal GPS lateral Banking angle
Front suspension	Displacement Compression speed (indirect)
Rear suspension	Displacement Compression speed (indirect)
Front wheel hub	X force Z force
Rear wheel hub	X force Z force

All logged signals are listed in Table 1.1. The compression speeds of the front and rear suspensions were not measured directly, but calculated from the suspension displacements.

1.5 Brief literature survey

The present work combines two aspects in the context of durability engineering. The first one is the simulation of full vehicles riding over rough roads and obstacles. The second one is the implementation of customer usage profiles for load assumptions.

Many publications in the field of four-wheeled vehicles have already shown that simulation of durability-relevant manoeuvres by means of MBS models is possible. The manoeuvres include driving over obstacles or rough roads. Riepl et al. [23] used an MBS model of a passenger car coupled with FTire to run simulations on digitalised road surfaces. Bäcker et al. [32] ran full vehicle simulations for passenger cars on synthetic vertical profiles to recreate measurement results. Waser et al. [26] compared different tyre models for simulations with the MBS model of a truck driving on rough roads. Benz [16] created rigid and flexible full vehicle models for passenger cars and ran simulations for deterministic road excitations like sleeper events and

stochastic road excitations like rough roads. Lepold and Kroschwald [22] simulated a passenger car riding over a kerb with an MBS model including the FTire. Kang et al. [33, 34] created random road profiles to excite MBS models of passenger cars and determine transfer functions. Kollmer et al. [21] simulated special events and service loads for passenger cars. The influence of the geometry for potholes and bumps on the loads was examined. Additionally, different waviness and unevenness parameters were used to calculate vertical wheel forces. They employed the FTire model as well. Engelmann [20] examined misuse events like potholes and kerb impacts for passenger cars with FE models. Additionally, he simulated a pothole event with a rigid full vehicle MBS model including FTire. Londhe and Kangde [35] proved that kerbs and uneven roads can be simulated with MBS models for a sport utility vehicle (SUV). Roy and Villaire [25] also created virtual roads and validated the MBS model of a passenger car with an FTire. Weber [28] digitalised a handling circuit and analysed the induced loads for a passenger car via MBS and FTire. Morr et al. [36] combined the simulation of passenger cars via MBS with methods from testing on real tracks and test beds. Rönicke et al. [24] improved test track design using simulations of passenger cars, including FTire, on previously digitalised tracks. Blanchette et al. [37] simulated different manoeuvres including a speed bumper crossing with the MBS model of a tricycle.

The consideration of different customer usage has been a topic of multiple publications as well. The 3D method presented in [9, 38] divides the influencing factors on loads for powertrain and chassis components into driver, driving environs, and driven vehicle. Based on this method, the operating states can be examined more precisely by subdiving the three factors into further categories and subcategories. Measured load spectrums, as well as simulations, are employed to generate a database for dimensioning components. Wagner et al. [39] included Monte Carlo simulations for the 3D method to randomly select the share of operating states and also to determine load values from measurements. This enables the derivation of a more customer-correlated load spectrum. Dreßler et al. [40] presented a method to determine representative load spectrums by differentiating between vehicle, specific operating and load states, as well as usage behaviour for trucks. The identified operating states are mapped on the basis of representative load measurements during customer usage. Furthermore, Monte Carlo simulations are applied to create differ-

ent synthetic customer profiles. Based on the distribution of the individual operating states, synthetic customers are assigned a pseudo-damage. The damage is afterwards used to determine which combination represents the design-relevant load spectrum. Additionally, a schedule for test tracks can be derived. In contrast to [9, 38], the parameter space is not prescribed. This allows more flexibility but also requires the elaboration of the said parameter space. Streit et al. [41] enhanced the approach by including correlation and variance analysis to identify important quantities and operating states which reduces data amount. They also analysed excavators that have different operating states compared to other vehicles. Speckert et al. [10] adapted the existing approaches from [40, 41] in the context of virtualisation by presenting the idea of a virtual measurement campaign. In their concept, they differentiate between vehicle model, environment model, and usage model which coincides with the assumption in [9]. They state that a complete environment model should contain data on the road network, legislation, topography, road quality, traffic, socioeconomic data, and climate. They use data from different online sources and condense them into operating states. Variability of different factors is accounted for by statistical models. The authors also describe how the planning of real measurement campaigns can be improved with their concept. Eckstein's works [42, 43] are closely related to [40, 41] as he derived representative load spectrums for tractors. He distinguishes between the operating states and utilises variance analyses. The operating states are again portrayed using load measurements that are closely related to customer usage. He also uses Monte Carlo simulations to identify a combination of states that is design-relevant. Müller et al. [44] collected data from measurement campaigns of trucks and classified the data. The data was used to define operating states and run Monte Carlo simulations to pick segments from load measurements in order to create synthetic customer load profiles. These, again, form a customer population from which a reference customer can be determined for the design via quantile formation. Biedinger [45] applied the virtual measurement campaign idea from [10], analysed operation conditions, and found representative routes for different user types. Her presented algorithms consider geographical and statistical data. Furthermore, she compared the loads for two different driving styles that result in different speed profiles.

To sum up, MBS of special events and service loads are state of the art for passenger

cars and commercial vehicles like trucks. The inclusion of customer usage is often performed by means of load measurements or representative simulations that are combined through different models for operating states. The present work aims to simulate realistic customer load profiles while implementing classified data that can be derived from the customer field in the future. The necessary representation in the virtual world is given by an MBS model of a motorcycle, virtual roads, and a virtual rider. The direct transfer of classified customer data, as well as the simulation of relevant manoeuvres, is a novelty, especially for the motorcycle industry. With the developed methods, road and rider characteristics can be considered more detailed in comparison with existing approaches of general operating states. This is expected to enable more precise load assumptions for the design of vehicle components. Misuse and crash events are touched upon in the present work, but not simulated as standard MBS models are not suited for manoeuvres that result in plastic deformation of components.

1.6 Overview of published papers

Special and misuse events for motorcycles

The first publication [1] deals with the load categories special and misuse events. These types of loads have to be analysed separately from service loads due to their high load amplitudes. As there is no uniform definition of these events, a novel definition was developed. This definition includes the damage as an important durability quantity. Another goal was to keep the definition general and as short as possible so that it can be applied cross-industrial. The definition for special events was verified by means of measurements of a real motorcycle riding over obstacles. Furthermore, the measurements were recreated in the virtual world with an MBS model. The vehicle's dynamic behaviour and the wheel loads were compared between simulation and measurement where sufficient agreement could be achieved. Additionally, a novel method is presented to choose the most decisive special events. In the future, MBS simulations can be used to obtain special event loads or prioritise measurements if not all manoeuvres can be measured due to time restrictions. The novel definitions can be used to identify special and misuse events and extract them from service loads measurements.

Research questions:

- What are special events and how can they be characterised?
- Is it possible to simulate special events for motorcycles with MBS models?
- How can relevant special events be identified to reduce development time?

Damage equivalent virtual tracks for motorcycles

The second publication [2] presents a novel method to create damage equivalent virtual tracks. For the simulation of service loads, laser-scanned tracks were recreated in the virtual world. A synthetic customer usage profile was analysed by considering all relevant roughness classes and curved tracks. As the simulation of all tracks has a high expenditure of time, the aim was to reduce the simulation duration by creating a virtual track that causes similar damage. The presented method distinguishes between different loads and tracks and identifies the most damaging track segments. The remaining sections are neglected through an omission approach.

Research questions:

- Is it possible to simulate service loads for motorcycles with MBS models on virtual roads?
- How can simulation duration be reduced for service loads while retaining a majority of the information on loads?

Influence of road and rider characteristics on motorcycle durability

The third publication [3] shows how customer behaviour influences service loads. It also demonstrates how classified data from onboard sensors can be used to create virtual tracks and specify speed profiles. As not all customers can be recreated in the virtual world, a method to identify design-relevant customers is presented. In the course of the investigations, the influence of roughness and velocity on the load category was analysed in order to assess which combinations belong to service loads and need to be considered. The method takes the velocity and the roughness of the

road into account. After the design-relevant customer is identified, a virtual track can be created with the same database. The addition of curvature is also presented. The roughness was recreated with a sine curve superposition, while the trajectory was recreated with a symmetric trapezoid approach. Furthermore, an algorithm that determines the speed profile for simulations was developed which considers rider skills and road characteristics. The rider skills include maximum velocities and accelerations. The models and assumptions were validated by measurements on a real test track. With the novel methods, it is also possible to consider scatter in the simulation. Overall, the simulation of realistic load profiles for different customer usage profiles was analysed.

Research questions:

- How can design-relevant customers be identified with synthetic riding manoeuvres?
- How can tracks ridden by customers be recreated with a minimum dataset?
- Which road and rider characteristics can be used and scattered to simulate customer behaviour?

2 Special and misuse events for motorcycles

Special and misuse events for motorcycles

Aptin Haerian[a], Kemal Öztürk[b], Robert Liebich[a]

[a]*Chair of Engineering Design and Product Reliability, Technische Universität Berlin, Berlin, Germany;*[b]*BMW AG, Munich, Germany*

(This is an Accepted Manuscript of an article in International Journal of Vehicle Systems Modelling and Testing, available online: https://www.inderscience.com/jhome.php?jcode=ijvsmt .©Inderscience.)

The present work deals with the topic of special and misuse events for motorcycles. First, a novel approach was found to define these events based on signal characteristics related to durability engineering. Furthermore, a multi-body simulation (MBS) model of a motorcycle was created to determine loads for special events. A suitable tyre model and relevant control systems were integrated for co-simulations. To validate the virtual model, wheel forces and selected onboard signals were compared with measurements of a real motorcycle ridden on a proving ground. The model showed sufficient agreement as the maximum wheel forces could be predicted with accuracies between 80% and over 99%. Afterwards, the loads were used to define representative special events. The kerb, sleeper, and bumper impacts were the most important events as they led to the highest forces. The gained perceptions enable a faster and more target-oriented definition of design loads while additionally saving costs.

Keywords: Special events, multi-body simulation, motorcycle, durability, misuse events, impact

2.1 Introduction

The precise knowledge of occurring operating loads and their magnitude is essential for the vehicle development process to design components and complete vehicles correctly so that they can withstand the loads without being oversized. In that regard, it is important to distinguish between loads that a vehicle has to sustain and

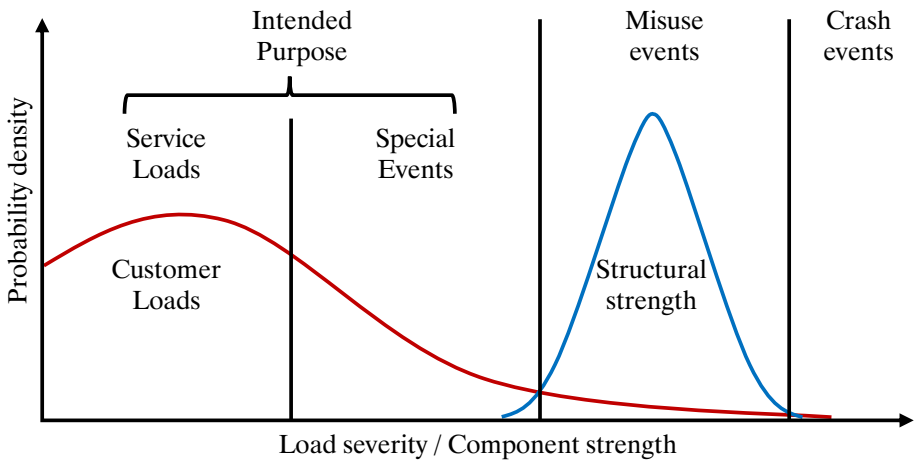

Figure 2.1 – Distribution of customer loads and structural strength.

loads that it does not need to sustain. A general distinction is made by defining four categories of loads:

- Crash event loads,
- misuse event loads,
- special event loads,
- service loads.

Figure 2.1 shows a fictional customer load distribution as well as a distribution of the structural strength. The figure highlights the fact that the four named categories of loads differ in severity and also probability of occurrence.

Crash events have the highest load severity and exceed the structural strength [1]. Crash events are, however, no specific manoeuvres and are mostly a consequence of accidents with other vehicles or objects. Misuse events also have high load severities that often exceed the structural strength. They are characterised by exceeding a threshold and often appear during impact situations [2, 3]. That is the reason for the fail-safe principle which ensures that components affected by overloading deform

plastically along the load path. This principle is indispensable for safety-related issues and allows the customer to bring the vehicle to a standstill, and therefore prevents customer and vehicle from hazard. In addition to that, the fail-safe principle is designed in a way that the customer can notice the damage, for example visually, and realise that the carried out manoeuvre was a misuse. Misuse events are not part of the so-called intended purpose. A definition of misuse events is difficult because they can only be identified as such through their effect on components and their damage [1]. Hence, the consideration of such events in the vehicle industry is dependent on the design philosophy of each manufacturer. Outside of the vehicle industry, often a distinction between service loads and overloads is made only [4]. Therefore, it is useful to find a concise definition of these events that can be used cross-industrial.

On the other hand, special events must be sustained without plastic deformation and should not restrict customer usage in the long term [3]. They are part of the intended purpose which can differ for specific motorcycles. For example, an off-road motorcycle has to meet different requirements than a superbike. They also occur less often while having a higher load severity. Some examples of special events are: riding up a kerb, over bumpers, or through a pothole [2]. Special events can also be component-specific [5]. In this context, component-specific events are those that lead to loads that are relevant for the dimensioning of one component but might not be relevant for others. The damage mechanism for special events is a mixture of component fatigue in the low cycle fatigue (LCF) and the accumulation of single deformations to a total deformation causing functional damage [1]. Special events are becoming increasingly relevant for the vehicle development process of passenger cars as more and more regions with poor road conditions are being developed as relevant markets. At the same time, requirements for vehicle dynamics are increasing, low profile tyres are used for cars, the engine power is increasing, as well as the vehicle weight [6]. All of these factors influence the loads, especially for borderline cases like special events. The same statements can be made for motorcycles. The changing vehicle dynamics play a major role, especially in regards to control systems that are used, for example, anti-lock braking system (ABS), automatic stability control (ASC), and dynamic traction control (DTC). Another aspect that should not be ignored is the upcoming customising trend. Motorcycle customers have the desire to

individually configure their vehicles with parts that lead to a unique appearance of the motorcycle. This customer demand is nowadays supported by the main motorcycle manufacturers and leads to a variety of possible combinations that have to be considered in the durability assessment. One decisive example is the possibility to order a motorcycle with different available wheel diameters directly from the factory. This is in particular decisive because the wheel is an important component when load assumptions are made as the loads induced by the road are transmitted through the road-tyre contact. Finally, special events can make up to 20% of the road-induced damage, and therefore should not be neglected [7].

The remaining share of damage belongs to the category of service loads. These loads are also part of the intended purpose and occur during normal usage of the vehicle including accelerating, braking, cornering, and vibrations induced by the roughness of the road [2]. Bracing of the vehicle, as well as pitching and rolling momentum also belong to service loads. Driving on an even road with constant friction coefficient is also considered as standard vehicle operation. Further on, the service loads have to be sustained throughout the entire intended vehicle lifetime [3]. The damage mechanism for service loads is the occurrence of micro-cracks that generate macro-cracks and eventually lead to fatigue failure, and hence structural failure [1].

In order to make valid load assumptions for vehicles, it is of the utmost importance to define special and misuse event loads clearly and examine them separately from service loads and crash events. This distinction is also important with regard to warranty issues. Therefore, the present work aims to provide a concise defintion of these two load categories. Furthermore, a feasibility study is conducted to find out whether virtual models for motorcycles can be used to simulate events of this severity and obtain precise loads. Additionally, a method is presented to identify relevant component-specific special events. Focusing only on important events can reduce the number of measurements and simulations, and thus saves resources.

Determining loads of this severity through simulation, as in this work, has various advantages. First and foremost, test vehicles and components are not damaged or even destroyed. Currently, wheel forces are measured with wheel load transducers [8]. These transducers are, however, expensive, fragile, and require a lot of expertise that only a few suppliers have. Establishing a virtual load data acquisition would,

therefore, lead to a wider pool of suppliers that can be used for measuring technology as less complex devices can be utilised for the validation of virtual models. Another disadvantage of wheel load transducers is the weight that is not negligible as it increases the weight of the motorcycle [9]. This influences the vehicle dynamics, and hence the measured loads cannot exactly represent the ones occurring during customer usage. For motorcycles, the weight of the transducers is even more critical than for passenger cars as the relative weight increase for the measurement vehicle is greater. The wheel load transducers used for the present work increased the empty weight of the vehicle by more than 3%, for example. A further advantage of the virtual determination of loads is that they can also be ascertained for components that cannot be measured in real tests or only with great effort. The reason being that some areas are not accessible for measurement devices or that the measurement devices and methods do not provide meaningful results. One example that was examined in the present work are the forces acting on bolt joints of the frame. With virtual models for load data acquisition, it is also possible to evaluate different vehicle concepts or designs better during the early stages of the development process where the real or physical vehicle does not exist yet. At present, the definition of special and misuse events for motorcycles is mainly based on field experience from predecessor models [9]. This can result in imprecise load assumptions.

The present work is organised as follows. Section 2.2.1 presents a novel definition of special and misuse events for durability engineering. Section 2.2.2 portrays the used multi-body simulation (MBS) model. Section 2.2.3 demonstrates a novel method to identify the most decisive special events. Section 2.3 describes the measurements of special events with a real motorcycle on a proving ground. Section 2.4.1 shows the validation of the MBS model based on these measurements. In Section 2.4.2 representative special events are identified. Section 2.4.3 shows the validation of the novel definition for special events. Finally, Section 2.5 summarises the findings of the present work and explains which aspects need to be considered for future research.

2.2 Methods

2.2.1 Definition of special and misuse events

In vehicle development, two concepts are employed for the dimensioning and design of components. For the dimensioning, maximum loads serve as specifications. According to the current state of the art, maximum loads are examined for crashes, misuse, and special events separately. Apart from that, service loads are relevant for the detailed design of components. Service loads are handled as a load time function (LTF) and used as inputs for algorithms to calculate durability related indicators. As previously shown, many publications describe the different load categories. Nevertheless, a clear distinction including durability related parameters is nonexistent. Especially the threshold between service loads and special events is crucial because special events are only considered with the maximum load.

The decision on whether a component has to be designed based on service loads or special event loads can be enhanced by an approach from K. Pötter (personal communication). Hereafter, the approach will be portrayed in a generalised variant. First, the load ratio l_r and strength ratio s_r according to Equations 2.1 and 2.2 have to be obtained.

$$l_\mathrm{r} = \frac{l_\mathrm{se}}{l_\mathrm{sl}}, \tag{2.1}$$

$$s_\mathrm{r} = \frac{s_\mathrm{se}}{s_\mathrm{sl}}. \tag{2.2}$$

The values needed for the ratio l_r are the maximum load occurring during the special events l_se and the maximum service load l_sl. The associated strengths can be derived from the S-N curve and the stress-strain chart respectively and represent the permissible stress for the component. For special events, the permissible plastic strain ε_per is used as a starting point and extended parallel to the line described by Hooke's law in order to receive the deformation resistance s_se, see Figure 2.2a. The vibration resistance s_sl is derived from the S-N curve with a pre-defined number of cycles N_sl, see Figure 2.2b.
Both N_sl and ε_per are parameters that can vary for different components, vehicles, and also manufacturers. Therefore, no exact value will be proposed at this point.

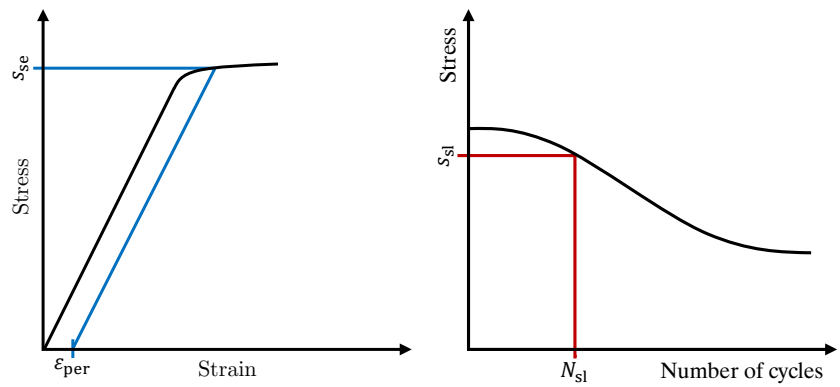

(a) Stress-strain chart (b) S-N curve

Figure 2.2 – Material characteristic curves.

However, the decision should be plausible from an engineering point of view. It is recommended to choose N_{sl} in the area of high cycle fatigue (HCF), e.g. between 10^4 and 10^6 cycles. $\varepsilon_{\mathrm{per}}$ should also have a plausible order of magnitude, and therefore should not exceed 1%.

For the design factor f_{d} in Equation 2.3, only two scenarios exist. The factor can either exceed the value of one or not. For values greater than one, the special events lead to the decisive load for the design of the component. For values below one, the service loads are decisive for the design process.

$$f_{\mathrm{d}} = \frac{l_{\mathrm{r}}}{s_{\mathrm{r}}}. \tag{2.3}$$

The existing definitions and classifications of special events lack the inclusion of damage or pseudo-damage. This is, however, important, as special events are part of the intended purpose and need to be sustained multiple times. Furthermore, the state of the art provides methods to identify special events that are related to impact situations of vehicles. However, considering the damage as a durability related indicator enables an identification of special events that are not exclusively results of impact situations. Therefore, these aspects were included together with the existing descriptions for the following novel definition.

First, the event character will be described. In this case that relates to the fact

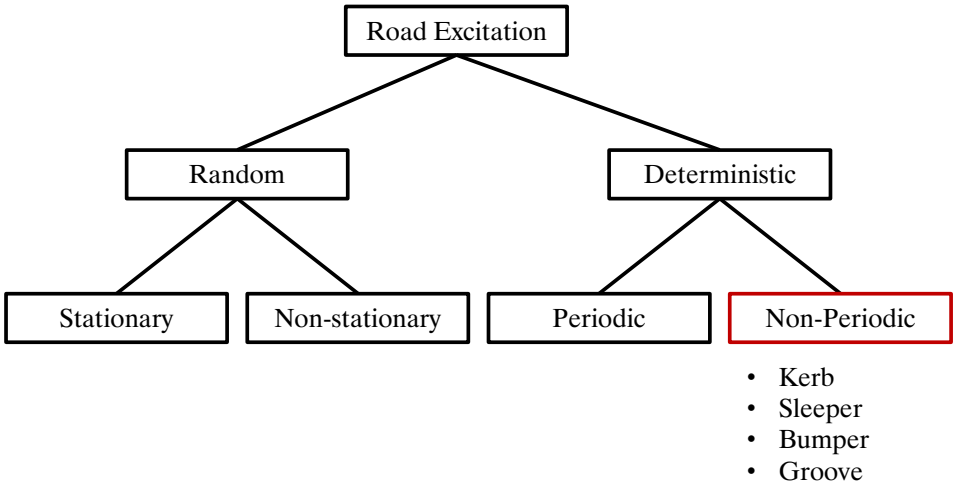

Figure 2.3 – Signal types for road inputs.

that a special or misuse event only accounts for a specific track segment which is short compared to the travelled distance during the designated operating life. A bumper, for example, is only a few metres long while a motorcycle has a product life cycle of many kilometres. This aspect is, therefore, essential for a fundamental definition.

If the signal characteristics of the road input are considered, it can be observed that there are two categories of signals that are used to describe the road, see Figure 2.3. The first category comprises random signals which can be divided into stationary and non-stationary ones. The second category covers deterministic signals which can be either periodic or non-periodic. The present work deals with special events such as kerb strikes or riding over bumpers. The mentioned road inputs belong to the non-periodic deterministic signals as they can be described with simple geometrical shapes and are not repetitive. The deterministic character of these road inputs goes hand in hand with the earlier mentioned assumption that special and misuse events take place during a specific track segment.

The fact that deterministic road obstacles have a significant impact on the damage of vehicles was observed by Oijer and Edlund [10]. The authors calculated the forces, and subsequently damage for a tractor-trailer combination driving over a road profile

before and after it was resurfaced. The measurements showed that the number of road obstacles changed over the years and along with it the induced damage. A higher number of road obstacles led to significantly higher damage which indicates that consideration of damage for those events could be of relevance.

Based on that finding, the definition of special and misuse events presented in this work additionally involves the concept of damage accumulation resulting from load signals. Here, the damage term is used from a fatigue standpoint and displays the degree of utilization for a component. There are several methods to determine the damage in durability engineering. Usually, an LTF serves as a database. A classification is then applied to reduce the amount of data and computational effort. In the present work, the rainflow counting method was used because it has a background that is physically justifiable. It is based on the Masing memory rule, and therefore has a direct physical connection to the material's properties. At the same time, it is well established as a standard method. Another benefit of the rainflow counting method is the option to transfer the derived results (e.g. rainflow matrix) into outcomes of other counting methods [11]. For the rainflow counting method, different possible algorithms exist. In the present work, the four-point algorithm according to Clormann and Seeger [12] was implemented. The resulting rainflow matrix can subsequently be used to retrieve the amplitudes L_i of the signal and also to calculate a pseudo-damage. The pseudo-damage makes a comparison between different LTFs possible with only one characteristic value and at the same time reduces the amount of data immensely. The stress cycle curve (S-N curve) and the Palmgren-Miner rule are further technical background information needed for the calculation of the pseudo-damage. The Palmgren-Miner rule postulates that the damage contributions of all considered cycles can be added up. The S-N curve provides the damage exponent β. According to Johannesson and Speckert [13], the pseudo-damage d can be calculated with Equation 2.4.

$$d = \sum_i L_i^\beta. \tag{2.4}$$

This equation only allows a comparison between two different LTFs as the proportionality constant is left out of the equation. The reason for this is the desired capability of the calculations to be independent of the specific material or component properties. The damage exponent in the present work was set to $\beta = 5$ as it is a

typical value for automotive components [13].

Lastly, it is important to exclude crash scenarios from misuse events. On the one hand, crashes occur during accidents and are not part of the normal operation. Misuse events, on the other hand, are manoeuvres that are comparable to special event manoeuvres and might only differ in velocity or shape of the obstacle ridden over, for example. This means that misuse events are limited by two thresholds. One separates the special events from the misuse events and the other separates misuse events from crash events. Special events also have two thresholds. The upper one is the same threshold that applies for the misuse events while the lower threshold separates special events from service events.

With the mentioned concept of damage as well as the road characteristics of special and misuse events, it is possible to combine them in a definition for those events:

A special event is characterised by over-proportional damage during a short track segment compared to the whole product lifecycle and is part of the intended purpose.

A misuse event is characterised by the exceedance of a permissible load during a short track segment compared to the whole product lifecycle and is neither part of the intended purpose nor part of crash scenarios.

These definitions can be used to look at specific events or track segments and classify the loads as either service, special event, or misuse loads. In order to classify an event, the maximum load has to be considered as well as the occurring damage during the event. The maximum load can be compared to the threshold separating special and misuse events. If the maximum load of the event exceeds the threshold, it is classified as a misuse event. The maximum load is decisive for this threshold as misuse events can only take place once because the plastic deformation is too high to use the vehicle subsequently. On the other hand, special events occur frequently and need to be endured as part of the intended purpose. Therefore, the occurring damage needs to be compared to the threshold separating service from special events. If the damage exceeds the threshold, it is classified as a special event.

In order to ascertain if an event needs to be regarded as a special event in the durability assessment, a novel factor was defined and called damage ratio r_{e}. This

factor is based on the previous definition for special events which involves the over-proportional damage during a short track segment compared to the vehicle life cycle. The factor can be calculated by dividing the occurring or additional damage during an event d_e by the ridden distance l_e, see Equation 2.5. The factor represents the damage per distance, and therefore can also be seen as the first derivative of the damage.

$$r_\mathrm{e} = \frac{d_\mathrm{e}}{l_\mathrm{e}}. \tag{2.5}$$

2.2.2 MBS model

The simulation models used for the present work were created using ADAMS® and are composed of the flexible MBS model of a motorcycle including the rider. The usage of MBS models for analysing vehicles driving over obstacles is common practice. Models for other vehicles like passenger cars have been utilised by other authors like [1, 7, 14, 15]. The flexible bodies were imported from FE models using the Craig-Bampton method [16]. Figure 2.4 displays the flexible components. According to [13], including between 10 and 100 modes for flexible bodies in multi-body simulations is accepted. For the simulation model in the present publication, therefore, 10 normal modes were computed for each flexible body in addition to the constraint and rigid body modes. This value was chosen in order to ensure consistency of the flexible body modelling and also to reduce computational time while obtaining meaningful results. The number of total modes are listed in Table 2.1. The damping characteristics of the front and rear suspension were measured on test stands for compression speeds up to up to $1\,\mathrm{m\,s^{-1}}$ and linearised outside of this range. Figure 2.5 shows the MBS model of a motorcycle including the rider and the different elements of the co-simulation. The rider had a height of 182 centimetres and weighed 80.5 kilogram. The inertia properties of the virtual rider were automatically calculated by ADAMS®using an internal dataset. In the MBS model, the rider was rigidly connected to the frame. For the simulations, a standard closed-loop rider model provided by ADAMS® was used.

For the present work, two models were created with different wheels. One model was created with the wheel load transducers for validation purposes and the other one with serial wheels to specify loads for customer usage. In addition to the mechanical

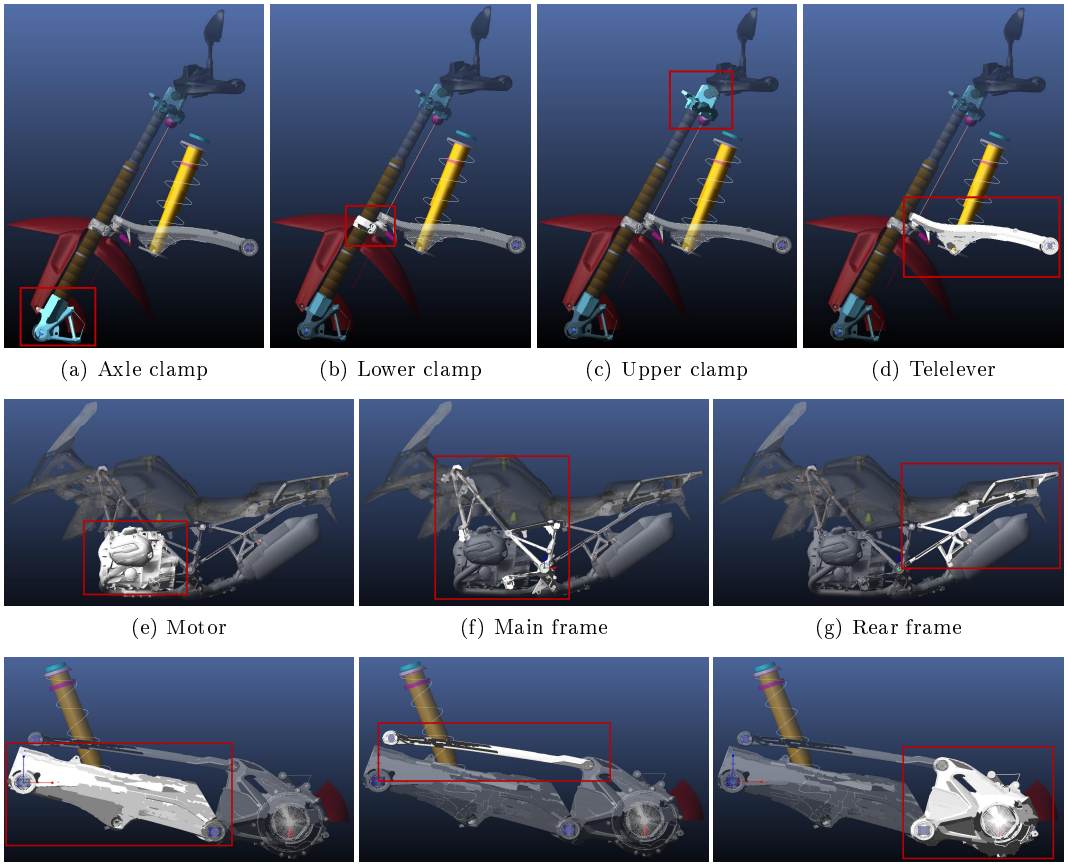

(a) Axle clamp (b) Lower clamp (c) Upper clamp (d) Telelever

(e) Motor (f) Main frame (g) Rear frame

(h) Swingarm (i) Paralever (j) Rear axle drive

Figure 2.4 – Flexible components.

Table 2.1 – Flexible components and total number of modes.

Component	Total number of modes
Axle clamp	46
Lower clamp	40
Upper clamp	46
Telelever	46
Motor	88
Main frame	136
Rear frame	136
Swingarm	46
Paralever	28
Rear axle drive	46

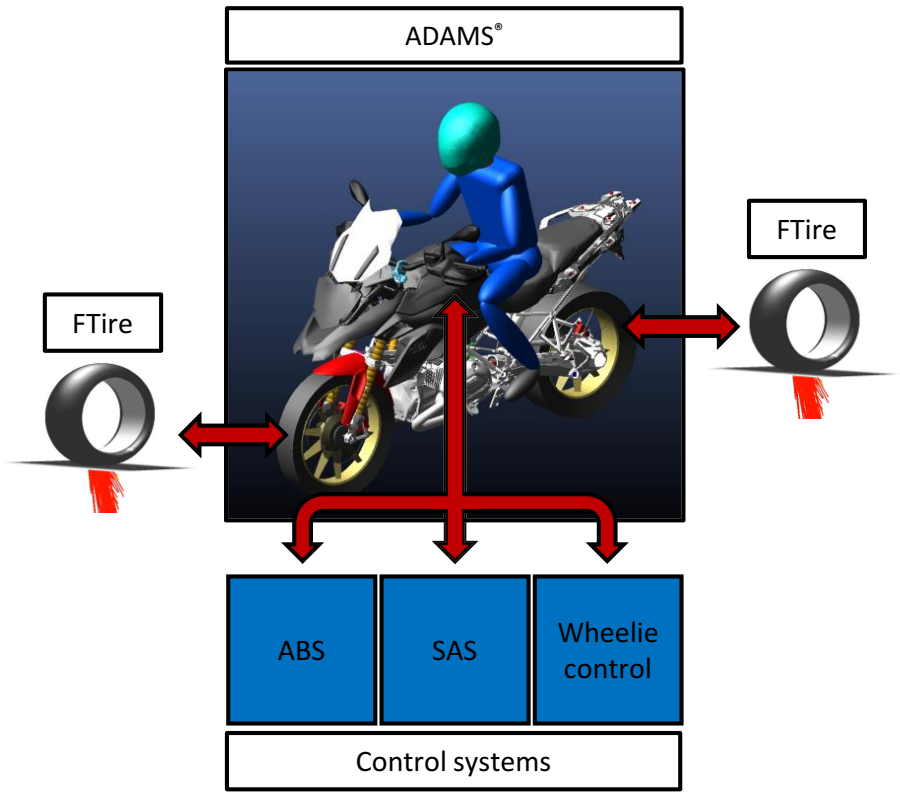

Figure 2.5 – ADAMS® model of motorcycle and co-simulation elements.

components, the real motorcycle used for the measurements was also equipped with control systems like ABS, semi-active suspension (SAS), and wheelie control. Hence, a Simulink® model was implemented in the simulation process. The ABS regulates the brake pressure so that the steerability and directional stability of the vehicle are still guaranteed during braking manoeuvres. The wheelie control serves the purpose of preventing the front wheel to lift off from the ground and as a result enabling better acceleration of the motorcycle. In order to achieve that, the engine torque is regulated by the control system. The SAS regulates the suspension behaviour, and therefore the vertical movement between wheel and chassis. Ultimately, it improves riding stability and comfort. During measurements of several events, the wheels temporarily lost contact with the ground. In addition to that, events like kerb strikes lead to a large suspension displacement. Therefore, the implementation of the control systems was necessary. Data exchange between the ADAMS® and Simulink® subsystems takes place at each time step. Between two steps, each software independently uses the calculated inputs from the last time step to calculate the corresponding outputs. In the following time step, the two environments communicate again and the respective outputs are defined as inputs for the other environment. The Simulink® model consists of four main parts which are the ADAMS®, ABS, SAS, and wheelie control block. The outputs of the ADAMS® block are handed over to the control system blocks as inputs. The outputs of the control system blocks are, on the other hand, returned as inputs to the ADAMS® block. The discrete-time step size was set to 0.0025 seconds. The inputs and outputs of the different blocks are listed in Table 2.2. For the connection between the ADAMS® and SAS block, a schematic representation is given in Figure 2.6.

The interaction between the vehicle and environment is another factor that plays a major role in multi-body simulations. Particularly the contact between the tyre and the road or obstacles should be paid attention to. The first task is to specify the road profile that the motorcycle travels on. The road excitation, or also the road profile in this case, for the simulated events was defined as a deterministic signal, as described previously. In doing so, the measured obstacles were modelled as two-dimensional curves and extruded in the third direction in space.

For events in which the tyre can penetrate into the carcass due to high loads, it is essential to use a correct tyre model and associated parameters. Finding and studying

Table 2.2 – Inputs and Outputs of Simulink® model.

Block	Inputs	Outputs
ADAMS®	Damping force front Damping force rear Damping coefficient front Damping coefficient rear Adjusted engine torque Adjusted brake pressure front Adjusted brake pressure rear	Suspension displacement front Suspension displacement rear Throttle position Vehicle speed Engine Torque Normal force front wheel Angular speed front wheel Angular speed rear wheel Radius front wheel Radius rear wheel
ABS	Angular speed front wheel Angular speed rear wheel Radius front wheel Radius rear wheel Vehicle speed	Adjusted brake pressure front Adjusted brake pressure rear
SAS	Suspension displacement front Suspension displacement rear Throttle position Vehicle speed	Damping force front Damping force rear Damping coefficient front Damping coefficient rear
Wheelie control	Engine Torque Normal force front wheel	Adjusted Engine Torque

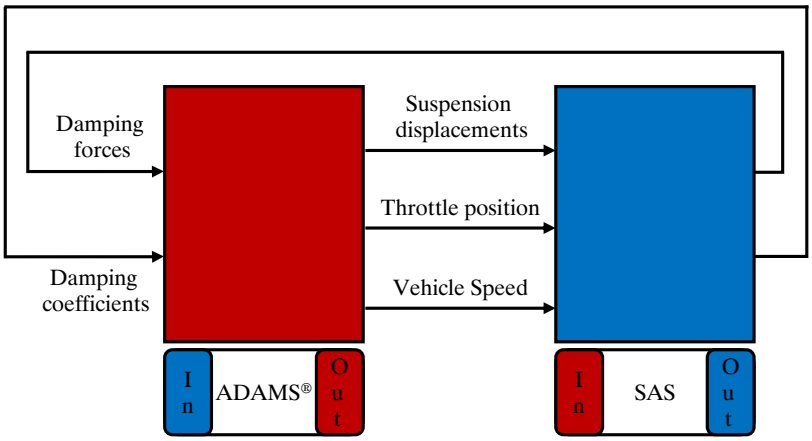

Figure 2.6 – Connection between ADAMS® and SAS block.

tyre models for vehicle dynamics, but also simulation models of vehicles driving over obstacles, was the topic of many publications like [17–23]. According to Adamski [24], three tyre models are well suited for driving comfort and load spectrum simulations. These three tyre models are the FTire by Gipser [25], RMOD-K by Oertel [26], and the CDTire by Gallrein and Bäcker [27].

The usage of FTire for other vehicles (e.g. passenger cars) in other publications led to accurate results, and hence was also employed in the present work as another element in the co-simulation. Engelmann [14] implemented FTire models for the simulation of misuse events like potholes with a rigid full vehicle MBS model of a passenger car. Kollmer et al. [7] investigated the influence of bump and pothole geometry on loads and damages with an MBS model of a passenger car including the FTire model. Lepold and Kroschwald[28] displayed how loads acting on components can be determined through MBS and finite element analysis. The identification of critical components was accomplished through a parameter study as well. The tyre model used was also FTire. Riepl et al. [29] described the application of multi-body systems in the context of minimising development risks and likewise integrated the FTire model for a complete vehicle model of a passenger car.

The FTire presents a fully non-linear three-dimensional tyre model for in-plane and out-of-plane simulations and is applicable for frequencies up to 200 Hz. It is also possible to conduct simulations that include obstacles with wavelengths less than half of the contact patch. Unlike other tyre models, FTire additionally has the advantage that the data representing the road surface does not need to be preprocessed. Additionally, the tyre model can also deal with sharp obstacles. As mentioned before, during some events the tyres lose contact with the road surface for a short period of time. Due to the FTire's internal structural stiffness, however, forces are still calculated even for such scenarios which is also an advantage of this model. In conclusion, the FTire is well suited for misuse events, see [24], and therefore valid for the studies that were carried out in the present work.

2.2.3 Design of simulation study

For the study of representative special events, a set of obstacles and associated velocities was defined. The maximum velocities for the comparison of the events were chosen based on realistic riding scenarios. Events with lower velocities were

Table 2.3 – Simulated velocities and events.

Event	Velocities ($\mathrm{m\,s^{-1}}$)
Kerb	5, 5.3, 5.6
Sleeper	12.5, 13.2, 13.9
Bumper	15, 15.8, 16.6
Groove	12.5, 13.2, 13.9

also simulated so that not only worst case scenarios were compared and velocity-specific influences could be neglected. Therefore, for each event, 95% and 90% of the maximum velocity were simulated additionally. The events and their respective velocities for the study are listed in Table 2.3.

The simulation model was used to calculate forces not only acting at the wheel hub but also on specific components that cannot be measured during real testing or are hard to access with measurement devices. Therefore, decisive spots and loads had to be determined for the evaluation. Besides the loads at the wheel hubs of the front and rear wheel, spots were chosen for the front suspension, the frame, and the rear suspension. The loads at the wheel hubs are important as they are often used as input for further simulations. These loads are also of high interest as they indicate which forces are induced by the road or obstacle. The other decisive spots were chosen based on experiences from predecessor models and other motorcycles which means that these spots were critical in terms of high stresses. For the front suspension, the forces in the longitudinal and normal direction of two ball joints were chosen. For the rear suspension, the swingarm bearing as well as the connection of the spring strut to the frame were selected, again with the longitudinal and normal forces. For the frame, four bolt joints that connect the engine and gearbox with the frame were chosen. Because bolt joints are designed against transverse shear, the resulting force of longitudinal and normal direction was used as an indicator, see Equation 2.6. Lateral forces were not considered for all components as the manoeuvres that were executed did not contain significant lateral components. The mentioned spots and the respective loads are listed in Table 2.4 and highlighted in Figure 2.7.

$$F_T = \sqrt{F_X^2 + F_Z^2}. \tag{2.6}$$

Table 2.4 – Decisive spots and loads.

Motorcycle part	Spot	Loads
Front wheel	Wheel hub	F_X, F_Z
Front suspension	Ball joints	F_X, F_Z
Frame	Bolt joints	F_T
Rear suspension	Swingarm bearing, Spring strut	F_X, F_Z
Rear wheel	Wheel hub	F_X, F_Z

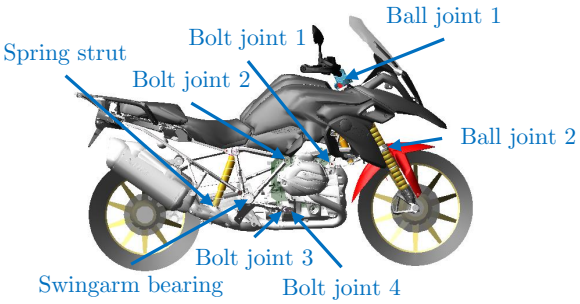

Figure 2.7 – Decisive spots.

Figure 2.8 – Test motorcycle with the global reference coordinate system ©BMW AG.

For each simulation, the maximum value of the mentioned loads was extracted and compared. The maximum loads were chosen as an indicator as they are used to define the maximum loads that the components need to endure. Therefore, these loads also represent the threshold between special and misuse events.

2.3 Measurement campaign

The purpose of the carried out measurements was to create a database to validate the simulation model described previously. For the measurements, a motorcycle of the type BMW R1200GS was equipped with sensors and data-logging devices. Figure 2.8 shows the standard motorcycle model along with the global reference coordinate system.

The wheel loads were measured with wheel load transducers from AIM Arnold Intelligente Messysteme GmbH & Co. KG. Using wheel load transducers is valuable because the loads at the wheel hubs are essential when it comes to load assumptions as they represent the outer forces acting on the full vehicle. Furthermore, it is important to ensure that, particularly, calculated loads of the virtual model are comparable to measurements since loads are the most important target quantity for durability assessments.

In order to validate the dynamic behaviour of the simulation model, the suspension displacement was logged for the front and rear suspension. The compression speeds were calculated based on the displacement signals. Additionally, the velocity of the vehicle was logged in order to specify the velocities for the simulations. The logged

Table 2.5 – Logged signals for simulation validation.

Component	Measurand	Symbol
Vehicle	Velocity	v
Front suspension	Displacement Compression speed (indirect)	s_{ft} $\dot{s}_{\mathrm{ft}}$
Rear suspension	Displacement Compression speed (indirect)	s_{rr} $\dot{s}_{\mathrm{rr}}$
Front wheel hub	X force Z force	$F_{X,\mathrm{ft}}$ $F_{Z,\mathrm{ft}}$
Rear wheel hub	X force Z force	$F_{X,\mathrm{rr}}$ $F_{Z,\mathrm{rr}}$

signals are listed in Table 2.5.

The obstacles that were ridden over are depicted in Figure 2.9. The kerb ridden upwards had a height of 14 centimetres. The sleepers had a height of seven centimetres, a length of 15 centimetres, and were placed at a distance of 10 metres. The bumper had a slope on both sides and a height of 13 centimetres while being five metres long. The bumper was followed by another bumper with the same geometry at a distance of 3.2 metres. Lastly, the groove had a depth of six centimetres and a length of 74 centimetres.

The ridden velocities were chosen based on real riding scenarios from predecessor measurement campaigns without wheel load transducers. However, in order to prevent the transducers from being damaged during this measurement campaign, the events had to be ridden with lower velocities than for the vehicle with serial wheels due to the additional weight of the transducers. This again highlights why it is important to use virtual models to obtain realistic customer loads when manoeuvres would lead to damaged components during measurement. The range of measured velocities is listed in Table 2.6. Compared to Table 2.3 where realistic maximum velocities were simulated, the values are lower except for the groove events.

(a) Kerb

(b) Sleeper

(c) Bumper

(d) Groove

Figure 2.9 – Road obstacles ©BMW AG.

Table 2.6 – Velocity ranges for events.

Event	Measured velocities ($\mathrm{m\,s^{-1}}$)
Kerb	3.6–4.1
Sleeper	9.5–10.1
Bumper	12.9–15.4
Groove	13.6–14.1

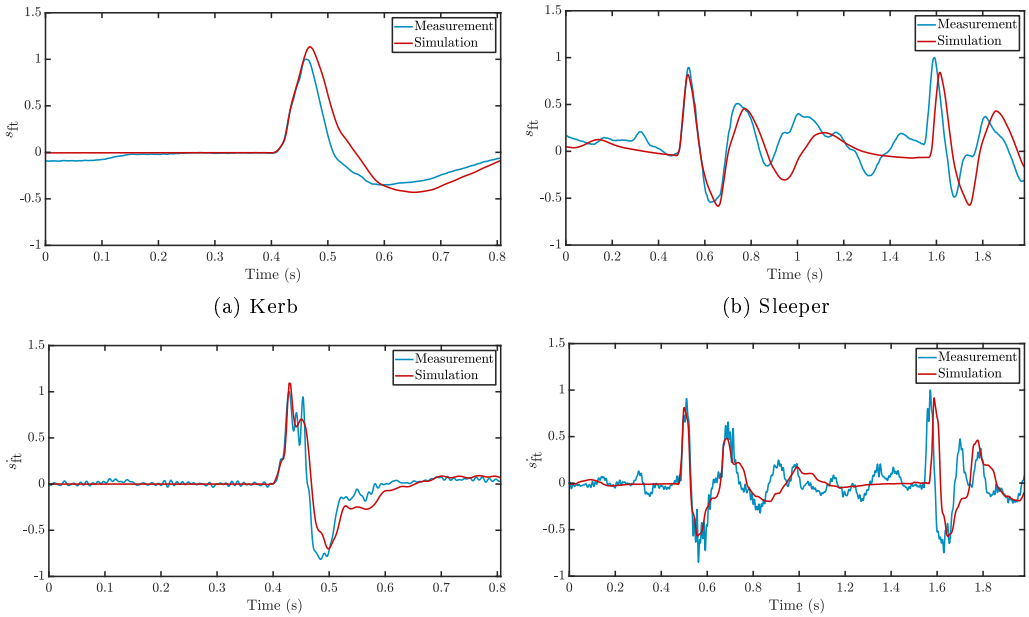

(a) Kerb (b) Sleeper

(c) Kerb (d) Sleeper

Figure 2.10 – Validation front suspension.

2.4 Results

2.4.1 Comparison with measurements

As described previously, the velocities were logged during the measurements on the proving ground and used as inputs for the simulation. The kerb and sleeper events did not show relevant accelerations, and therefore the simulations were run with constant velocity. The bumper and groove events showed relevant accelerations during the measurements which were replicated virtually.

In order to validate the dynamic behaviour of the vehicle, the suspension displacements and compression speeds from simulation and measurement were compared. Figure 2.10 shows comparisons of the front suspension behaviour for exemplary events, while Figure 2.11 displays the same for the rear suspension. All variables were normalised in relation to the maximum value from the respective measurement. The figures show that the characteristic dynamic behaviour of the real vehicle can be represented by the virtual model.

As this research aims to present a method on how decisive special events can be

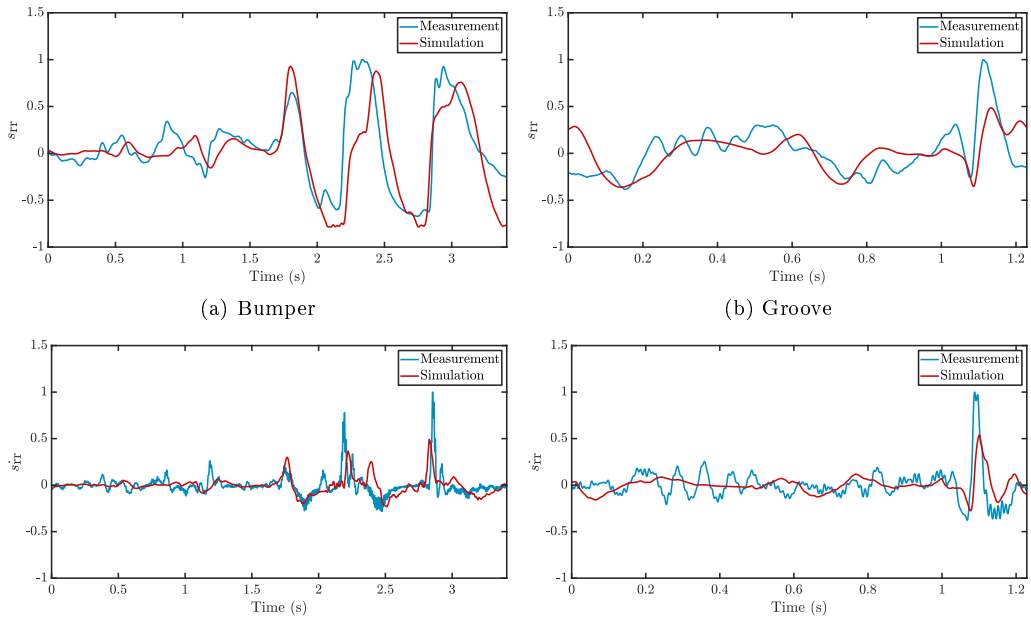

(a) Bumper (b) Groove

(c) Bumper (d) Groove

Figure 2.11 – Validation rear suspension.

identified in terms of durability engineering, it is necessary to have a virtual model that can precisely predict loads. The comparison was made for the longitudinal and vertical forces of the front and rear wheel hub. The kerb and sleeper events were especially critical for the front wheel, while the bumper and groove events led to high forces at the rear wheel. Figure 2.12 shows comparisons for the front wheel hub of exemplary events, whereas Figure 2.13 illustrates the forces at the rear wheel hub.

The figures demonstrate that the virtual model can predict the considered maximum forces at the wheel hubs with adequate accuracy. Since peak loads are the most important outputs for special event load assumptions, the comparison and consideration of these values is sufficient. For the sleeper event, a phase shift can be observed which results from the slight deviation between the speed profiles of the virtual and real rider. Furthermore, overdamping is an issue for the kerb and sleeper event in the longitudinal direction. This could result from imprecise parametrisation of damping characteristics for the front suspension. The longitudinal forces at the rear wheel also show noticeable deviations. These events were simulated with speed profiles. Jumps in the throttle and brake demand by the virtual rider could also be

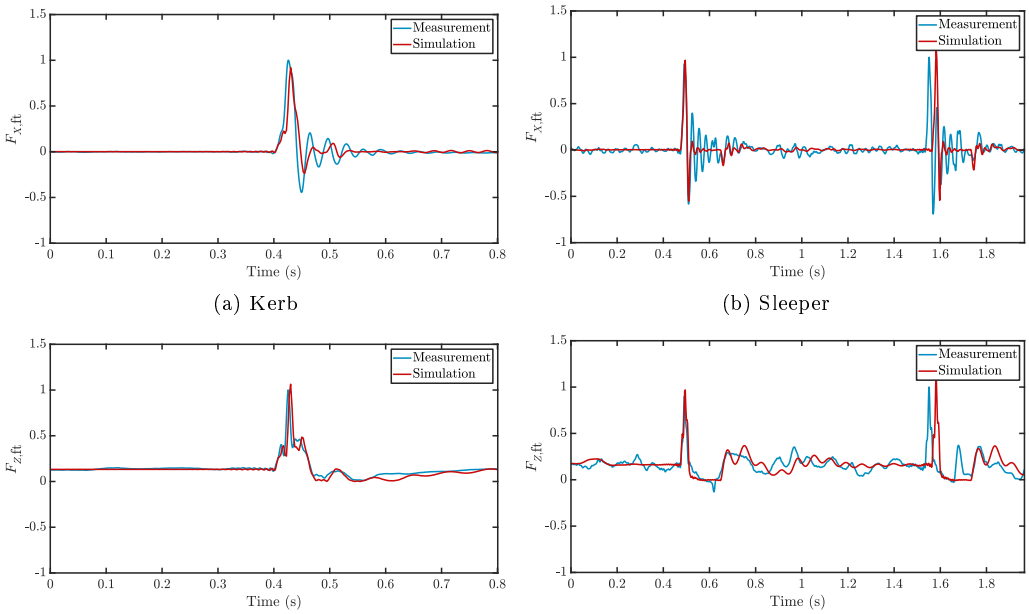

(a) Kerb (b) Sleeper

(c) Kerb (d) Sleeper

Figure 2.12 – Validation front wheel.

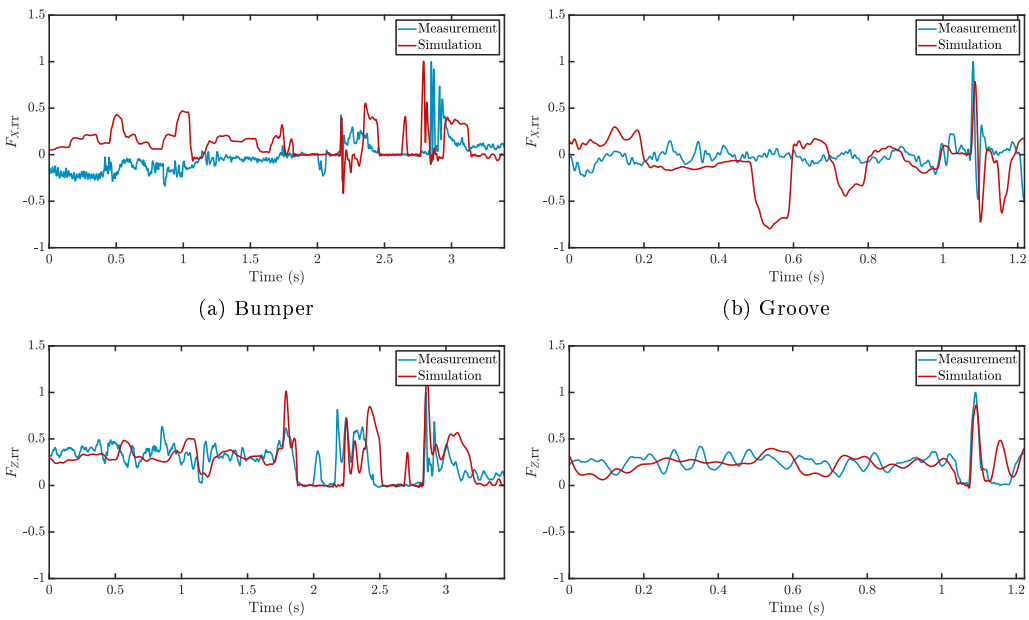

(a) Bumper (b) Groove

(c) Bumper (d) Groove

Figure 2.13 – Validation rear wheel.

Table 2.7 – Accuracy ranges for analysed loads.

Load	Range a_{sim} (%)
$F_{X,\text{ft}}$	85.7–99.9
$F_{Z,\text{ft}}$	96.3–99.6
$F_{X,\text{rr}}$	82.1–99.6
$F_{Z,\text{rr}}$	80.5–96.4

observed. Hence, the source of inaccuracy is assumed to be the virtual rider model that tries to replicate the speed profile. The maximum loads at the rear wheel are also subjected to more deviations as the vehicle dynamics and rider behaviour affect the loads after the initial impact of the front wheel and before the rear wheel hits the obstacle more than before the initial impact. Table 2.7 summarises the comparison of the maximum loads for all measured and simulated events separately for each load. The accuracy a_{sim} for each load and event was calculated with Equation 2.7 where F_{sim} and F_{meas} are the maximum loads from the simulation and measurement respectively.

$$a_{\text{sim}} = 1 - \left| \left(\frac{F_{\text{sim}}}{F_{\text{meas}}} - 1 \right) \right|. \tag{2.7}$$

2.4.2 Representative special events

Figure 2.14 shows exemplary bar charts for two loads from Table 2.4, one being a wheel load and one an inner load. For each decisive load, the event with the highest resulting load was defined as the representative one. As an abbreviation, the events were numbered from one to three for each obstacle with one being the event with the lowest velocity and three the one with the highest. Table 2.8 gives an overview of the findings resulting from the analysis.

To sum up, the kerb, sleeper, and bumper event led to the highest loads while the groove event can be neglected. The kerb and sleeper events were critical for the front part of the motorcycle and the frame, whereas the bumper event was mainly decisive for the rear part of the motorcycle. While the kerb impact led to the highest loads in the longitudinal direction of the front wheel and the lower ball joint, the sleeper impact led to higher loads in the vertical direction for these spots. The effect

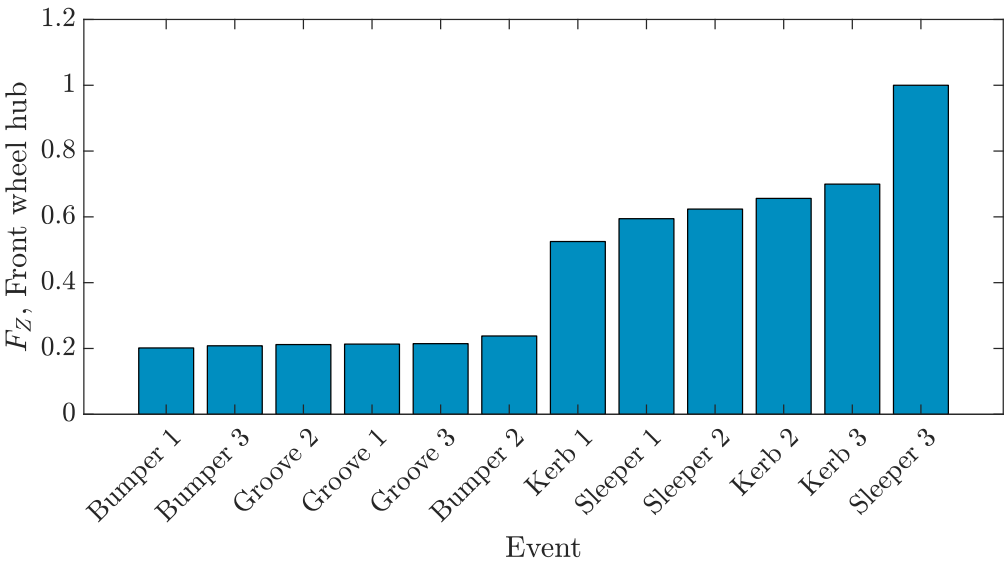

(a) Exemplary wheel load

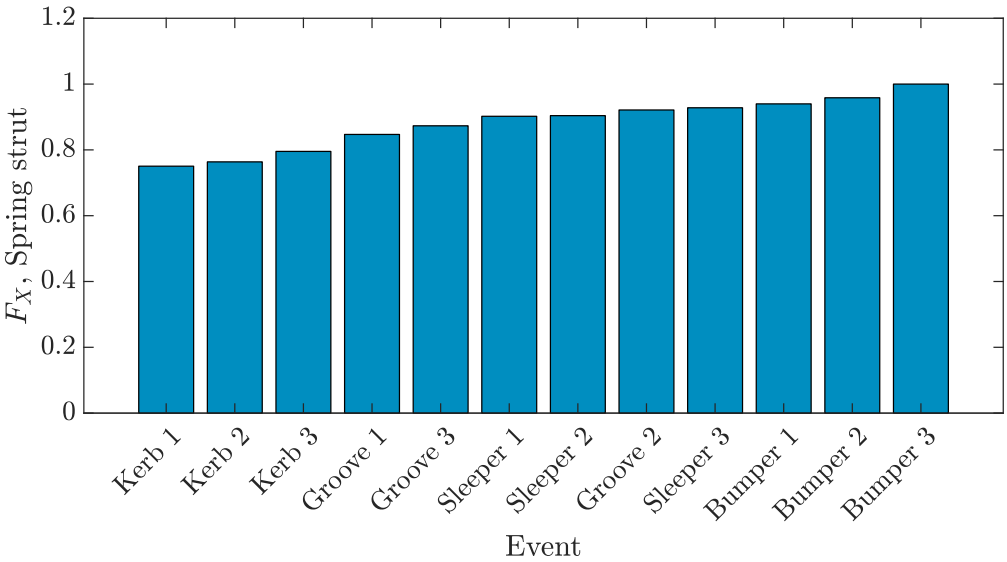

(b) Exemplary inner load

Figure 2.14 – Loads for events.

Table 2.8 – Resulting representative special events.

Motorcycle part	Spot	Load	Representative event
Front wheel	Wheel hub	F_X F_Z	Kerb Sleeper
Front suspension	Ball joint 1	F_X F_Z	Kerb Kerb
Front suspension	Ball joint 2	F_X F_Z	Kerb Sleeper
Frame	Bolt joint 1	F_T	Kerb
Frame	Bolt joint 2	F_T	Kerb
Frame	Bolt joint 3	F_T	Kerb
Frame	Bolt joint 4	F_T	Sleeper
Rear suspension	Swingarm bearing	F_X F_Z	Sleeper Sleeper
Rear suspension	Spring strut	F_X F_Z	Bumper Bumper
Rear wheel	Wheel hub	F_X F_Z	Bumper Bumper

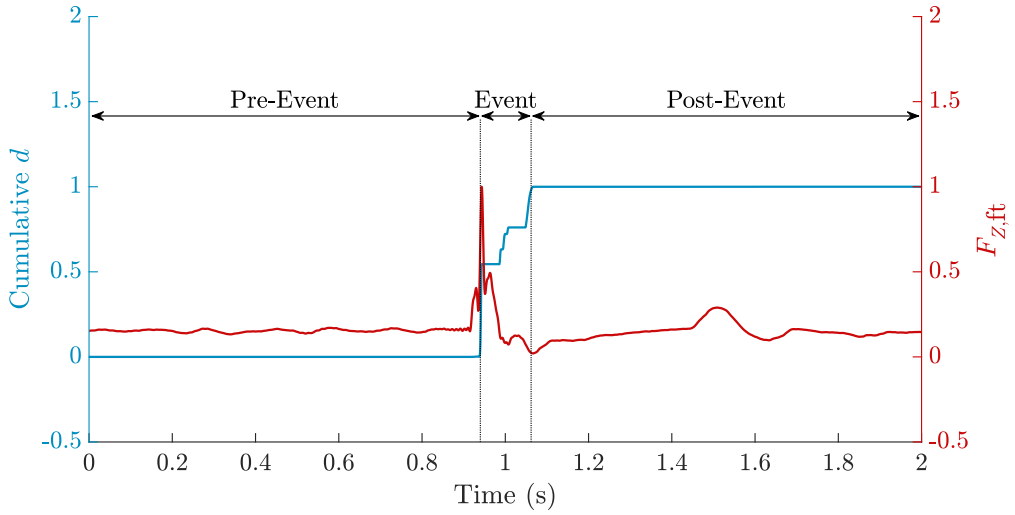

Figure 2.15 – Determination of damaging time window.

of differing representative special events for different directions in space highlights the importance of such a divided analysis.

2.4.3 Validation of damage ratio

With the measured events from Table 2.6, the approach described in Section 2.2.1 was examined. The service loads were obtained by measurements of the forces at the wheel hub on test tracks with wheel load transducers. For the service loads, the damage ratio r_e was calculated every second, according to Equation 2.5. The ridden distance per second was calculated by multiplying the time window with the mean vehicle velocity during the respective window. For the special events, it is important to isolate the obstacle from the track before and after the impact. Therefore, the cumulative pseudo-damage was calculated and analysed for every new data point which corresponds to a continuous rainflow counting. Figure 2.15 shows the normal force of the front wheel during the event riding up a kerb as well as the cumulative pseudo-damage.

The figure highlights that before the event the increase in pseudo-damage is negligible. During the event, the damage rises significantly and reaches a saturation point. This noteworthy observation underlines the assumption that a major part of

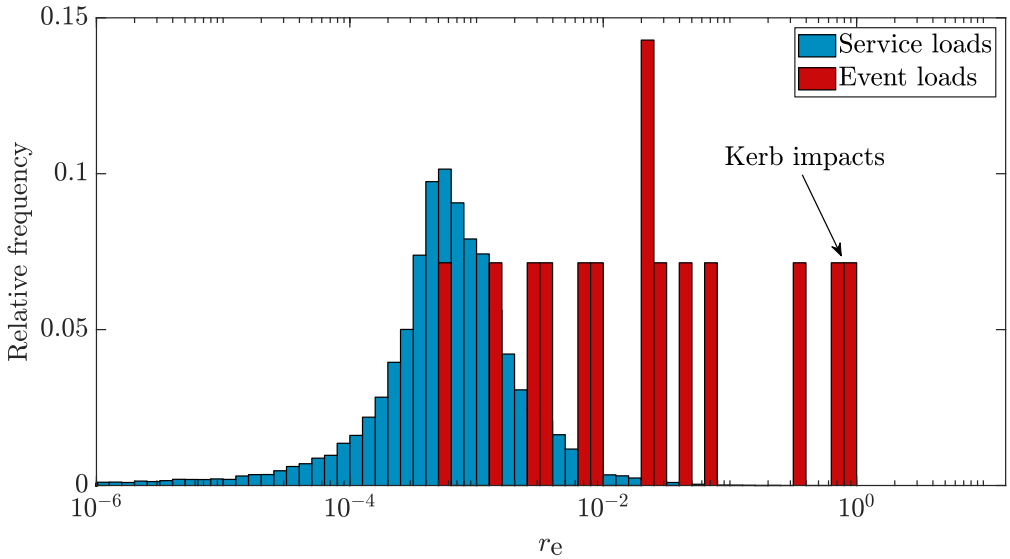

Figure 2.16 – Distribution of r_e for F_Z at the front wheel hub.

the damage occurs during a short track segment. The boundaries for the window were chosen to be 2.5% and 97.5% of the cumulative pseudo-damage so that the window covers 95% of the total damage during the event. The resulting window was considered for the calculation of the damage ratio for each special event. Figure 2.16 shows the comparison between service loads and special events for the damage ratio of the normal force at the front wheel hub as a distribution chart.

It can be observed how big the difference between the worst special events (kerb impacts) and the service loads is. Even though some events are in the medium range of service loads, most events are in the higher ranges. It should also be noted that the scale is logarithmic and that the damages from the event measurements are not even worst case scenarios as lower velocities were ridden due to the wheel load transducers. This means that during customer usage the damage ratios are significantly higher. However, the figure also demonstrates that events can be similar to service loads in terms of caused damage.

2.5 Discussion

The present work showed how special and misuse events can be defined from a load analysis standpoint, which events are relevant for motorcycles, and how the loads can be virtually acquired and validated.

First, a novel definition for special and misuse events was presented including damage, and hence an important value for durability assessments. The objective was the characterisation of these events with elementary signals. The definition was, furthermore, used to calculate the novel damage ratio which displays the average damage during a small track segment. The hypothesis that the major part of damage occurs during a short segment was observed by using a continuous rainflow counting. The damage ratio was significantly higher for certain special events compared to measurements from service loads. The definition is also applicable to different products or components and is not limited to motorcycles only. Many publications show how it is possible to identify road obstacles, but with the presented parameter it is now also possible to identify special events that are not related to impact situations with obstacles. Additionally, special events can be extracted from LTFs of service loads, even without prior knowledge of the track condition. An event that appears during the testing procedure of service loads and causes damage that exceeds the average damage significantly can be fused separately and does not influence the assumptions for the service loads. Due to time limitations, service load measurement campaigns are performed with selected acceleration factors. Thus, the calculated damage from the measured load profile is extrapolated based on these factors. If an unexpected special event occurs during a measurement campaign, for example, due to unnoticed defects on the test track, the resulting loads would also be multiplied by the factor. This would lead to unrealistic requirements and ultimately over-dimensioned vehicles. Identifying those segments is, thus, very useful. Therefore, a reasonable threshold must be defined. As this threshold is component, vehicle, and manufacturer dependent, the present work will not propose an exact value. Another aspect that could be implemented into the definition of special events is the frequency of occurrence. If an event or manoeuvre is performed by a large number of customers frequently, it can also be included in the service loads. As mentioned by Berger et al. [30], however, considering special events for load determination requires years of studying customer behaviour in terms of frequency of occurrence. Further research should, therefore,

focus on algorithms to identify special events from LTFs including realistic customer usage behaviour. Data science methods, for example, machine learning, are assumed to be promising and could calculate thresholds based on corrected service and special event load profiles.

After clarifying the properties of special events, a measurement campaign was carried out with a real motorcycle equipped with data-logging devices, sensors, and most importantly wheel load transducers. The measurement campaign included riding over different obstacles. Additionally, multi-body co-simulation models with control systems and FTire models were created. The implementation of control systems was necessary due to the presence in the real motorcycle and higher accuracy. However, the findings of the present work can also be applied for motorcycles without such control systems, and hence simpler models. The simulation models were successfully validated based on the measurements. The vehicle's dynamic behaviour was validated with the comparison of suspension behaviour, while the loads were validated by means of the forces at the wheel hub. The maximum loads could be computed with an accuracy of more than 80% and up to over 99% for each load which is a big leap compared to the current approach in the motorcycle industry where load assumptions in the early development stage are afflicted with more inaccuracy. The deviations between simulation and measurements have multiple reasons. First of all, the roughness of the tracks was not modelled for the obstacles. However, the roughness is not expected to have a big influence on the maximum loads. Additionally, the modelling would become more complex as the roughness of every surface needs to be determined, also, for example, the front surface of kerbs and the surface on the bumpers. Another reason for the deviations is the damping characteristic of the real vehicle compared to the virtual vehicle. The damping properties for the suspensions were only measured for compression speeds up to $1\,\mathrm{m\,s^{-1}}$ on test stands. Therefore, the virtual model could only provide correct results for values under this threshold. Outside of this range, the damping characteristics had to be linearised. However, real damping characteristics are highly non-linear. During the measurements of all events, compression speeds higher than $1\,\mathrm{m\,s^{-1}}$ and up to $2\,\mathrm{m\,s^{-1}}$ occurred. To reach more accordance between measurement and simulation, the measurement range for the damping characteristics needs to be extended. Lastly, the movement of the rider influences the dynamic behaviour of the motorcycle. The movement shifts the centre

of gravity of the rider in relation to the motorcycle and can also lead to low-frequent excitations, and hence also influence the loads. The virtual rider does not perform these movements and is connected rigidly to the frame which leads to deviations, especially in extreme situations like special events. In order to eliminate these deviations, the movement of the rider needs to be replicated in the virtual environment. Therefore, the movement and influence on the loads need to be examined in future research. Additionally, suitable virtual rider models should be developed that ensure stable simulation of special events.

With the validated simulation model, events were simulated to obtain representative special events. The results show that, when it comes to structural components of motorcycles, the most important special events are the events of riding up a kerb, over sleepers, and bumpers with high velocities. Time and cost savings are possible as measurements and simulations can be prioritised or reduced in their amount. In contrast to simulations and measurements, the real customer will rarely ride a specified velocity exactly. Hence, it is necessary to consider a range of velocities and investigate the influence more closely in order to fully cover customer usage.

Future research should focus on analysing other obstacles and their geometries as well as different motorcycle concepts. With the methods presented in this work, it is possible to objectively assess new studies and identify relevant special events via measurement or simulation.

References

[1] M. Hauke. 'Simulation des Missbrauchverhaltens von Gesamtfahrzeugen'. PhD thesis. Technische Universität München, 2004.

[2] C. Gorges, K. Öztürk and R. Liebich. 'Impact detection using a machine learning approach and experimental road roughness classification'. In: *Mechanical Systems and Signal Processing* 117 (2019), pp. 738–756.

[3] C. Matz. 'Online Berechnung von Fahrwerkskräften auf Basis von Onboard-Sensorik'. PhD thesis. Technische Universität Clausthal, 2016.

[4] H. Jung. 'Einfluss von Überlasten auf die Betriebsfestigkeit von Walzwerksantrieben'. PhD thesis. Technische Universität Clausthal, 1993.

[5] M. Köhler, S. Jenne, K. Pötter and H. Zenner. *Zählverfahren und Lastannahme in der Betriebsfestigkeit.* Berlin, Heidelberg: Springer Berlin Heidelberg, 2012.

[6] B. Zeichfüßl, M. Grabenstein, S. Kirschner and R. Witt. 'Ableitung von Sonderereignis-Lastannahmen für die Fahrzeugauslegung'. In: *Materials Testing* 50 (2008), pp. 665–670.

[7] H. Kollmer, F. Küçükay and K. Pötter. 'Measurement and fatigue damage evaluation of road profiles in customer operation'. In: *International Journal of Vehicle Design* 56 (2011), pp. 106–124.

[8] M. Kuchler and R. Schrupp. 'Multiaxial motorcycle wheel load transducer'. In: *VDI* 1616 (2001), pp. 249–278.

[9] M. Sautter and G. Greim. 'Betriebsfester Leichtbau von Motorrädern'. In: *Materials Testing* 47 (2005), pp. 396–403.

[10] F. Oijer and S. Edlund. 'Identification of transient road obstacle distributions and their impact on vehicle durability and driver comfort'. In: *Proceedings of the 18th IAVSD symposium; 2003 Aug 24-30; Kanagawa.* Abingdon: Routledge, 2004, pp. 744–753.

[11] E. Haibach. *Betriebsfestigkeit.* Berlin, Heidelberg: Springer Berlin Heidelberg, 2006.

[12] U. H. Clormann and T. Seeger. 'Rainflow-HCM. Ein Zählverfahren für Betriebsfestigkeitsnachweise auf werkstoffmechanischer Grundlage'. In: *Stahlbau* 55.3 (1986), pp. 65–71.

[13] P. Johannesson and M. Speckert. *Guide to load analysis for durability in vehicle engineering.* Chichester: Wiley, 2014.

[14] S. Engelmann. 'Simulation von fahrwerkdominierten Misuse–Lastfällen zur Unterstützung der virtuellen Crashsensorik'. PhD thesis. Helmut-Schmidt-Universität / Universität der Bundeswehr Hamburg, 2013.

[15] H.-J. Hong, J. Kline, R. Geisler and P. Kodali. 'Dynamic front wheel curb impact study'. In: *SAE transactions* 114 (2005), pp. 1676–1680.

[16] R. Craig and M. Bampton. 'Coupling of substructures for dynamic analyses'. In: *AIAA journal* 6 (1968), pp. 1313–1319.

[17] M. Bäcker, A. Gallrein and H. Haga. 'Simulating very large tire deformations with CDTire'. In: *SAE International Journal of Passenger Cars-Mechanical Systems* 2 (2009), pp. 765–771.

[18] J. R. Cho, K. W. Kim, D. H. Jeon and W. S. Yoo. 'Transient dynamic response analysis of 3-D patterned tire rolling over cleat'. In: *European Journal of Mechanics-A/Solids* 24 (2005), pp. 519–531.

[19] D. Guan, C. Fan and X. Xie. 'A dynamic tyre model of vertical performance rolling over cleats'. In: *Vehicle System Dynamics* 43 (2005), pp. 209–222.

[20] H. Haga. 'Evaluation of tyre models for durability loads prediction using a suspension-on-a-drum environment'. In: *Vehicle System Dynamics* 43 (2005), pp. 281–296.

[21] A. J. C. Schmeitz. 'A semi-empirical three-dimensional model of the pneumatic tyre rolling over arbitrarily uneven road surfaces'. PhD thesis. Delft University of Technology, 2004.

[22] H. von Chappuis, G. Mavros, P. D. King and H. Rahnejat. 'Prediction of impulsive vehicle tyre-suspension response to abusive drive-over-kerb manoeuvres'. In: *Proceedings of the Institution of Mechanical Engineers, Part K: Journal of Multi-body Dynamics* 227 (2013), pp. 133–149.

[23] P. W. A. Zegelaar. 'The dynamic response of tyres to brake torque variations and road unevennesses'. PhD thesis. Delft University of Technology, 1998.

[24] D. Adamski. *Simulation in der Fahrwerktechnik*. Wiesbaden: Springer Fachmedien Wiesbaden, 2014.

[25] M. Gipser. 'FTire–the tire simulation model for all applications related to vehicle dynamics'. In: *Vehicle System Dynamics* 45 (2007), pp. 139–151.

[26] C. Oertel. *RMOD-K Formula Documentation*. URL: https://www.rmod-k.com/images/stories/media/downloads/Formula/formula.pdf.

[27] A. Gallrein and M. Bäcker. 'CDTire: a tire model for comfort and durability applications'. In: *Vehicle System Dynamics* 45 (2007), pp. 69–77.

[28] A. Lepold and T. Kroschwald. 'Rechnerische Abschätzung des Lastniveaus bei Sondereregnissen'. In: *Materials Testing* 50 (2008), pp. 671–679.

[29] A. Riepl, W. Reinalter and M. Schmid. 'Application of the tyre model FTire in the vehicle development process at MAGNA STEYR Fahrzeugtechnik'. In: *Vehicle System Dynamics* 43 (2005), pp. 370–383.

[30] C. Berger, K.-G. Eulitz, P. Heuler, K.-L. Kotte, H. Naundorf, W. Schuetz, C. M. Sonsino, A. Wimmer and H. Zenner. 'Betriebsfestigkeit in Germany—an overview'. In: *International Journal of Fatigue* 24.6 (2002), pp. 603–625.

3 Damage equivalent virtual tracks for motorcycles

Damage equivalent virtual tracks for motorcycles

Aptin Haerian[a], Kemal Öztürk[b], Robert Liebich[a]

[a]*Chair of Engineering Design and Product Reliability, Technische Universität Berlin, Berlin, Germany;*[b]*BMW AG, Munich, Germany*

(This is an Accepted Manuscript of an article in International Journal of Vehicle Design, available online: https://www.inderscience.com/jhome.php?jcode=ijvd.©Inderscience.)

The present work deals with the topic of service loads for motorcycles resulting from road excitation. The aim is to create virtual test tracks that can be used representatively for load assumptions. First, different methods from the field of durability engineering were reviewed that centre around the topic of damage equivalency. The methods were evaluated in terms of applicability for virtual test tracks. With an omission approach, a novel method was found to detect relevant track segments for different use cases. The method was successfully applied to create virtual test tracks based on measurements of real tracks with laser scanners. With the proposed method the length of the test tracks and data amount could be decreased by approximately 70%. The gained perceptions enable a faster definition of design loads while additionally saving costs and reducing the amount of data during the early stages of development.

Keywords: Virtual proving ground, multi-body simulation, motorcycle, durability, damage equivalency, omission

3.1 Introduction

In the vehicle development, it is sought to shorten the product development process and reduce costs while maintaining or even increasing the quality of products. In order to achieve this, computer-aided engineering has become more important throughout the years. Particularly in the early stages of the development process,

virtual models help to understand interdependencies and can support decision making. In the field of durability engineering, virtual models allow the developers to predict loads acting on the vehicle or specific components even before a real prototype is built up and measurements have been carried out. The loads can subsequently be used to design components more precisely and reduce the number of revisions for the load assumptions.

In order to predict the loads occurring during the whole product lifecycle and customer usage with virtual models or simulations, it is important to represent all relevant aspects of the real world also in the virtual world. One possible approach, proposed by Küçükay et al. [1], is the 3D method which splits the influencing factors into driver, driving environs, and driven vehicle. The 3D method allows a representation of customer behaviour, and therefore improves the development process as requirements can be defined more precisely. A similar concept is the virtual measurement campaign by Speckert et al. [2] where the distinction is made between vehicle model, environment model, and usage model.

In the field of durability engineering and motorcycles, this separation is also appropriate. The virtual vehicle model needs to represent the relevant characteristics of the real vehicle for a given analysis. For the generation of load profiles resulting from riding manoeuvres, multi-body simulation (MBS) models are common practice. With these types of models, it is possible to determine wheel loads as well as inner loads. Wheel loads represent the outer loads acting on the complete vehicle while inner loads can be directly used for the analysis of specific components.

The environment also needs to be represented virtually with its relevant properties. For durability engineering, these properties result from the structure of the roads that induce loads. Main properties are, for instance, the roughness, curviness, or slope of the road. Lastly, the individual rider influences the loads occurring during usage. For example, a sporty rider travelling on a road with a certain motorcycle will cause different loads than an average rider with the same vehicle on the same road. Exemplary inputs from the rider are the desired velocity, gear, or steering angle. These inputs can also be represented as data or rather time signals. The influencing factors are illustrated in Figure 3.1.

With virtual models, it is possible to evaluate different concepts for a vehicle faster and with lower costs compared to an evaluation based on measurements. For

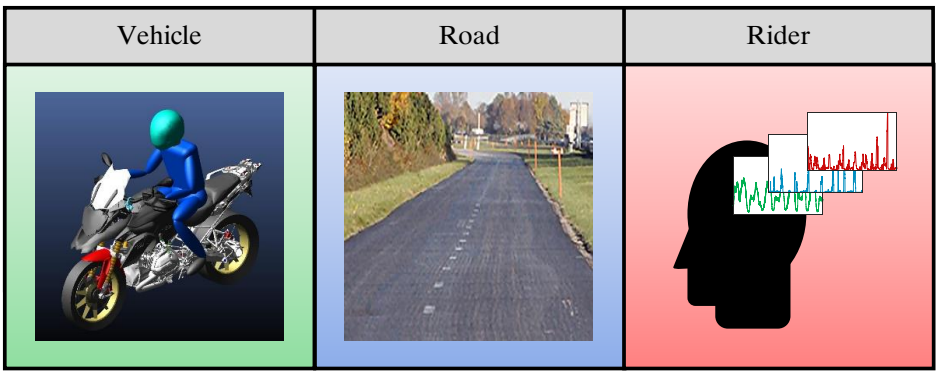

Figure 3.1 – Influences on loads in the virtual world ©BMW AG.

measurements of real vehicles on test tracks, prototypes have to be built including expensive sensors. Additionally, measurement campaigns have a high expenditure of time. Besides economic benefits, using simulations for load analysis has also functional advantages related to durability engineering. First, load assumptions can be made independently of the vehicle. As Mayrböck and Mayr [3] pointed out, load assumptions are generally made based on predecessor models and are, therefore, dependent on the specific vehicle concept. In contrast to that approach, the usage of vehicle independent excitations is expected to deliver better results for the design. This need is met when complete road profiles are used as excitations for full vehicle MBS models. Another advantage of using virtual tracks for load assumptions is the unvarying property of the tracks. On physical test tracks, the conditions depend on the weather, the wear of the track itself, and even vegetation, as mentioned by Warnecke et al. [4]. Thus, virtual test tracks increase reproducibility and enable a more reliable comparison of concepts.

However, considering all different kinds of roads would require a lot of computational time. Also, the amount of stored data would be enormous. Therefore, identifying track segments that are relevant for durability assessment and only simulating those is helpful. The present work aims to present a method by which this can be achieved via simulation. Hence, this research focuses on the second block of Figure 3.1.

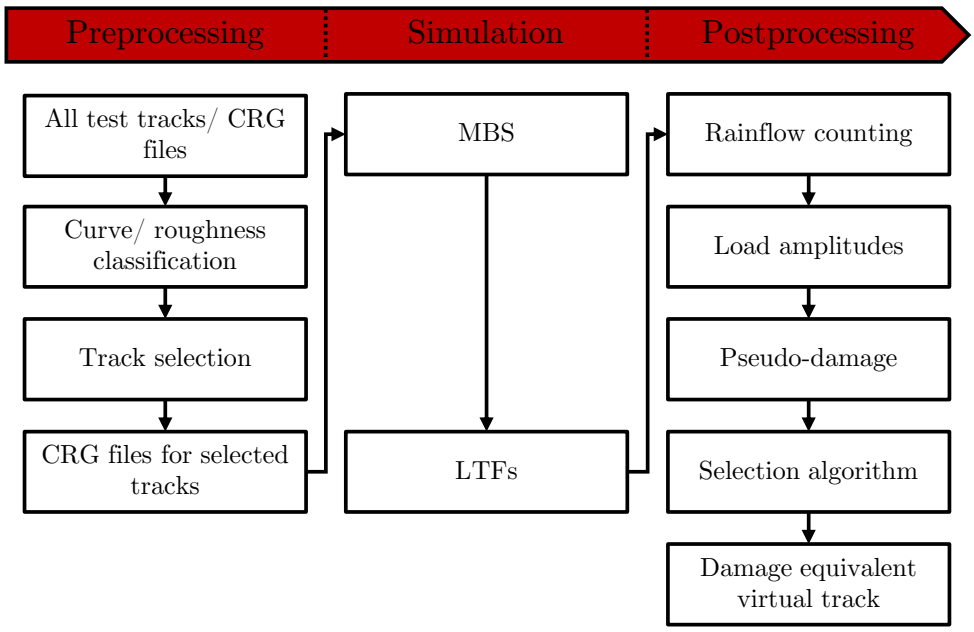

Figure 3.2 – Overall workflow.

The present work is organised as follows. Section 3.2.1 summarises the whole workflow of the analyses in the present work. Section 3.2.2 gives an overview on the state of the art regarding damage equivalency in durability engineering. Section 3.2.3 presents a novel method to identify relevant track segments. Section 3.2.4 highlights how road profiles were measured and classified. Section 3.2.5 shows the MBS model of a motorcycle including the relevant aspects for the simulation of service loads. In Section 3.3.1 the test tracks for the analyses are chosen. Finally, Section 3.3.2 summarises the findings of the analyses. Section 3.4 discusses the findings of the present work and future application.

3.2 Methods

3.2.1 Complete workflow

The overall workflow of the present work can be divided into three parts: preprocessing, simulation, and postprocessing. Figure 3.2 shows the sequence in detail.

First, a dataset of measured test tracks was divided into straight tracks and curved tracks. After that, the test tracks were classified in terms of their roughness class using the vertical profile for each track. Based on these two properties, test tracks were chosen so that a representative database was available for the simulation of various road types. This concluded the preprocessing.

The chosen test tracks were subsequently used as inputs for simulations as CRG files. The input for a single simulation was, therefore, the trajectory as well as the elevation profile of each track. Thus, the vehicle model was excited in the vertical direction by the elevation profile while following the trajectory as the riding path. The outputs of the simulations that were later on analysed in the postprocessing were the loads at decisive spots of the motorcycle.

As a first step during the postprocessing, the load time functions (LTFs) of the mentioned spots were used as inputs for the rainflow counting method in order to obtain load amplitudes. These amplitudes were then used to calculate the pseudo-damage for each spot during one simulation. Finally, the pseudo-damage for each track segment and decisive spot was used as input for the novel selection algorithm as an entry in a three-dimensional damage matrix. The result of the selection algorithm was ultimately the damage equivalent virtual track consisting of the most damaging track segments for one analysis.

3.2.2 Simplification of load time functions

In durability engineering, the damage plays a major role, as this key figure represents the degree of utilization for a component. The damage can be calculated for every component based on a stress time history. Different counting methods lead to a reduced dataset which can subsequently be used for the calculation. In the present work, the rainflow counting method according to Clormann and Seeger [5] was employed. The rainflow method was chosen because it is based on the Masing memory rule, and hence is directly connected to physical properties of the material. Further advantages are the international establishment and the option to transfer the derived results into outcomes of different counting methods [6]. For this work, loads were calculated instead of stresses as the load assumptions should be independent of exact component geometries, and hence effects coming from section modulus or notch factor, for example. Additionally, MBS models are generally used to calculate

loads and compare concepts in the early stages of development where exact geometries might not be modelled yet. Therefore, the pseudo-damage has to be regarded as a qualitative value to evaluate different LTFs and not a quantitative one to calculate fatigue life. In the present work, the rainflow counting method was applied to the LTFs that were obtained through MBS. The resulting load amplitudes L_i were afterwards used to calculate the pseudo-damage d. Additionally, the proportionality constant was neglected to ensure independency of material properties. For the calculation of the pseudo-damage, the Palmgren-Miner rule was used which allows a summation of all considered cycles to one single value. Lastly, the damage exponent was set to $\beta = 5$. According to Johannesson and Speckert [7], this value is typical for automotive components and can be extracted from the S-N curve. The pseudo-damage can then be calculated with Equation 3.1.

$$d = \sum_i L_i^\beta. \tag{3.1}$$

To reduce the necessary time to test and fuse components on test rigs, different principles exist that need to be regarded. One is the damage equivalency and the other one is the shortening and reconstruction of test signals.

The idea behind damage equivalency is to find a different LTF that leads to the same pseudo-damage d as the original LTF. The simplest way is to use an LTF with a constant amplitude. According to Haibach [6], two applications are possible. The first one is to define a specific load amplitude L_a and determine the number of load alternations N_a, according to Equation 3.2.

$$N_a = \frac{d}{L_a^\beta}. \tag{3.2}$$

The second one is to define a specific number of load alternations and determine the necessary load amplitude to obtain the same damage as for the original LTF, according to Equation 3.3.

$$L_a = \left(\frac{d}{N_a}\right)^{\frac{1}{\beta}}. \tag{3.3}$$

Besides the constant amplitude LTF, there are also more complex forms of load collectives that can be utilised to obtain a damage equivalent LTF [8].

As the aim of this paper is to shorten virtual test tracks, it is important to understand how test signals, in general, can be shortened or reconstructed in terms of damage equivalency and whether the methods can be applied to virtual tracks as well. The following six methods were evaluated:

- Increasing the test frequency,
- removing load pauses,
- truncation of peak loads,
- increasing test loads,
- omission of small load cycles,
- reconstruction.

Increasing the frequency of the loads while leaving the amplitudes unchanged that are applied to components is one way to decrease the test duration. This method is useful for test rigs. However, compressing a virtual track so that the amplitudes stay the same while the frequency of the loads increase, is thought to be very difficult.

Removing load pauses is also a possibility to reduce the necessary time for testing on test rigs. Here, time periods where no loads occur are ignored and not applied. This method is also not applicable for virtual tracks, as the vehicle is running constantly on the virtual track, and hence load cycles are generated continuously that need to be accounted for.

The truncation of peak loads also leads to a shorter LTF as peak loads are neglected. According to Vajen [9], this method is suitable when the peak loads are part of special events that occur seldomly. The truncation was also not employed in the present work as the virtual tracks are solely used for simulations of service loads. Special events are fused separately, and hence all the peak loads that occur during the simulation on the virtual test track need to be considered.

The method of increasing test loads can easily be understood with the simplest case of a constant amplitude LTF and Equation 3.2. L_a needs to be set high enough so that the test duration decreases. However, the amplitude cannot be raised arbitrarily as the damage mechanism can change [10]. For virtual tracks, this method is not

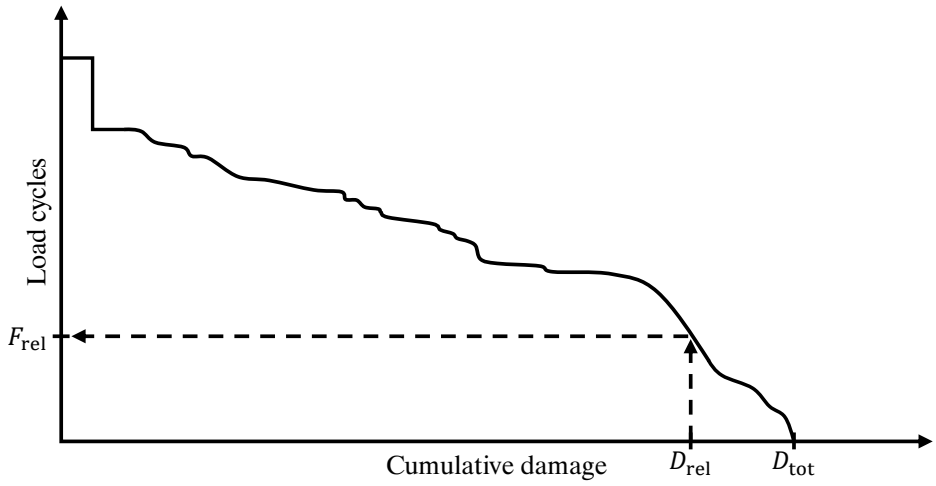

Figure 3.3 – Identifying negligible load cycles.

practicable as the road profile would have to be manipulated in a way that all loads increase with a constant factor.

Another option to reduce the length of an LTF is to use the omission method. In an LTF many load cycles are relatively small compared to the bigger ones and cause negligible damage. Therefore, cutting off those load cycles can reduce the testing time while maintaining the relevant cycles to test the components. Figure 3.3 highlights how the negligible load cycles from an LTF can be identified when the accumulated damage is plotted for the amplitude of the load cycles. In order to obtain the negligible load cycles, the desired damage D_{rel} needs to be defined which can be, for example, 90% of the total damage D_{tot}. Subsequently, the load cycles with amplitudes lower than F_{rel} can be extracted.

This approach was also utilised by Bergold et al. [11]. In their publication, the authors identified track sections from measurements where all the amplitudes of the load cycles were under a threshold and neglected them for the simulations. The simulations were performed with an MBS model of a passenger car driving over a road obtained from GPS data but without vertical excitation from the road or roughness.

The last type of methods are reconstruction methods. These type of approaches make it possible to recreate the input of a system based on measurements from an

output. One method is the spectral reconstruction, mentioned by Johannesson and Speckert [7]. With the power spectral density (PSD) of a load signal it is possible to reconstruct the signal in the time domain. A method to reconstruct road excitations from output signals was used by Bäcker et al. [12] and also Kang et al. [13, 14]. In their publications, random road profiles were generated with either white or pink noise to excite MBS models of four-wheeled vehicles and calculate transfer functions for measured outputs. After that, the outputs were compared in the time domain and an error was calculated. This error was subsequently used for an iteration process to modify the input of the system. The iteration was stopped after the desired outputs reached a defined threshold. The result of the procedure was a virtual road profile that could be used for a simulation with an MBS model to recreate measured signals. These methods are useful when the road profile is unknown or when the used tyre model is not sufficient for durability analysis. In these cases, a fictional road has to be designed in order to recreate signals. The mentioned methods of reconstruction were not employed in the present work as measured data for real test tracks was available as well as a reliable tyre model. Also, the present research aims to reduce the LTF and not to replicate it.

The methods in the literature were mainly applied for four-wheeled vehicles. However, they appear to be vehicle independent, and hence can also be used for motorcycles if the use case is similar.

3.2.3 Selection of representative track segments

The presented method in this section is related to the omission approach. However, the load cycles are not examined separately but rather the damage occurring during a single track segment. The main idea is to separate the segments from the track that result in a negligible amount of damage and only keep the relevant track segments. As a result, the necessary track length would decrease as well as simulation duration and amount of data.

In order to obtain a shortened virtual test track for durability assessments, three indices were defined. The first one is the considered track l out of L total tracks. Different tracks have different properties that influence the loads. Therefore, it can be important to evaluate different tracks separately. The next information is the chosen length of track segments that are considered independently. The chosen length results

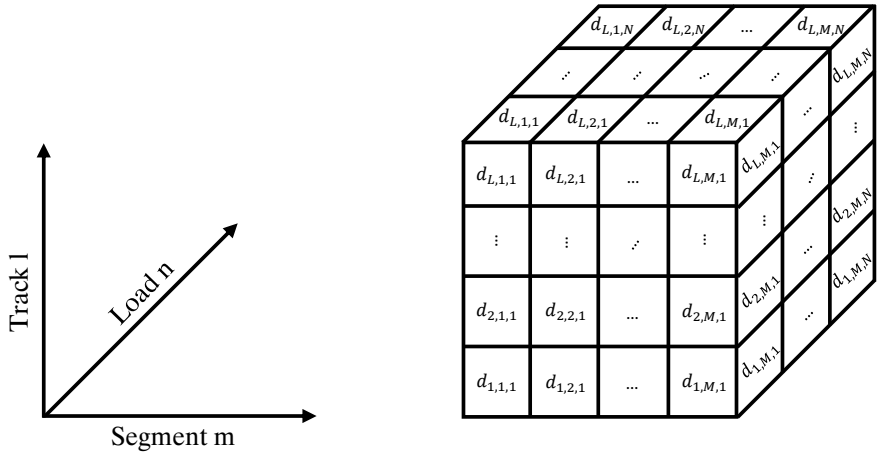

Figure 3.4 – Three-dimensional damage matrix.

in each track being partitioned into M segments and m being the second index. In order to shorten the complete virtual test track, segments with a low amount of damage are neglected. The shorter the chosen segments are the more segments can be found to be neglected. From a durability engineering standpoint, loads are the most important outputs of simulations. Thus, it is important to find a virtual test track that covers the signals necessary for the design of all important components. Therefore, the third index n is the considered signal or in this case component load from N total loads. With the mentioned indices a three-dimensional matrix was designed. The entries of the matrix equal the pseudo-damage occurring for one load on one track segment of one specific track. Figure 3.4 shows how the matrix is structured for tracks having the same length and number of track segments.

Using this matrix, negligible track segments can be identified for different use cases. The simplest use case is depicted in Figure 3.5. If there is only one load that is of interest and only one track is used for testing, the necessary damage entries are reduced to a vector. The sum of the vector equals the total damage d_{tot}. Now a reasonable threshold can be chosen for the desired damage, for instance, 90%, 95%, or 99% of the total damage. Subsequently, track segments can be chosen based on their share of the total damage. Taking this approach a step further, it is possible to pick track segments for one component and multiple tracks including their segments.

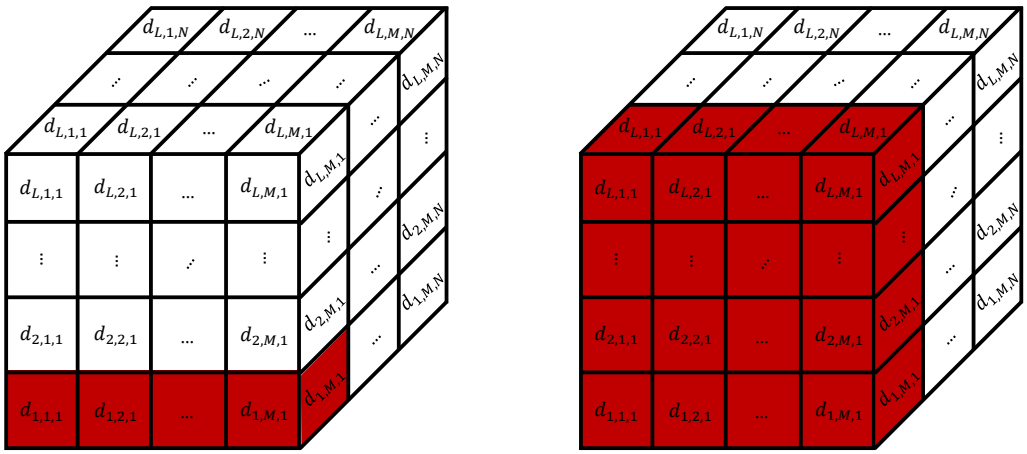

(a) One load and one track

(b) One load and multiple tracks

Figure 3.5 – Single load use cases.

The total damage that has to be related to is now the sum of a two-dimensional matrix when the number of track segments is equal for every track. This use case is also depicted in Figure 3.5.

However, it is also possible to use the presented method for tracks where the number of segments is different for certain tracks. For example, two tracks can have different lengths while the length of the track segments considered for the matrix is the same. Another example is two tracks having the same length but one track having longer track segments as part of the damage matrix. In both cases, this leads to the number of track segments M depending on the track l and possibly being different for each track. This leads to the formulation of Equation 3.4.

$$M \rightarrow M(l). \tag{3.4}$$

Figure 3.6 highlights how the different number of track segments for different tracks affects the damage matrix and how the damage entries need to be transformed.

As shown in the figure, the two-dimensional matrix needs to be transformed into a vector. For this, a substitute index h was used. The composition of the index can be described with Equation 3.5 and leads to the damage vector $\mathbf{d}$, see Equation 3.6.

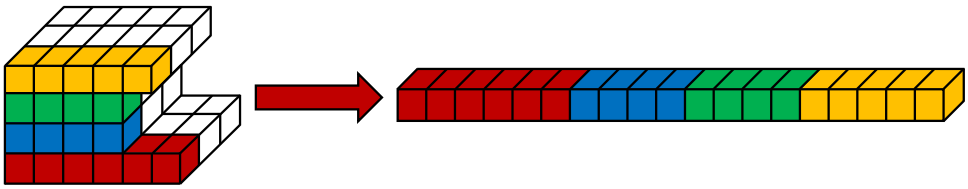

Figure 3.6 – Transformation of deformed damage matrix for single load use case.

$$\mathbf{h} = \{\underbrace{1, 2, ..., M(1)}_{\text{track 1}}, \underbrace{M(1)+1, M(1)+2, ...M(1)+M(2)}_{\text{track 2}}, ..., H\} \quad \text{with} \tag{3.5}$$

$$H = \sum_{l=1}^{L} M(l),$$

$$\mathbf{d} = \begin{Bmatrix} d_1 \\ d_2 \\ \vdots \\ d_H \end{Bmatrix}. \tag{3.6}$$

The first use case is also included when L equals 1. In general, the total damage d_{tot} can be calculated for one chosen load, according to Equation 3.7.

$$d_{\text{tot}} = \sum_{h=1}^{H} d_h. \tag{3.7}$$

Finally, a selection algorithm can pick the entries that accumulate to the threshold while leading to the shortest total track, as depicted in Figure 3.7.

p is the percentage of the total damage that is desired which leads to the relative damage d_{rel}, as shown in Equation 3.8.

$$d_{\text{rel}} = p\, d_{\text{tot}}. \tag{3.8}$$

d_{res} is the sum of the damage for one combination of chosen track segments out of H total segments. This value is compared to d_{rel}. From all combinations where d_{res} exceeds d_{rel} the one that meets the following conditions in order of priority is

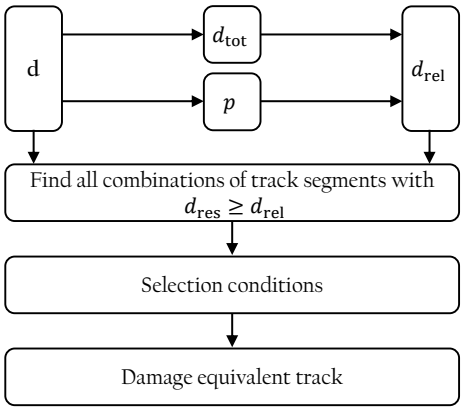

Figure 3.7 – Selection algorithm for single load.

the output of the algorithm:

1. Fewest number of track segments,

2. highest d_{res}.

The first condition is the main focus of the present research as this condition leads to the shortest track. However, multiple solutions may exist with the same amount of track segments. Therefore, the second condition leads to the solution with the highest damage while also having a minimal number of track segments.

As multi-body simulations are used to generate load data for the full vehicle, it is also feasible to further extend this approach to analyse multiple loads. Therefore, the third use case is the treatment of one track but multiple loads. The fourth use case is the treatment of multiple loads and multiple tracks. These two use cases are depicted in Figure 3.8.

For these use cases, the number of track segments can also vary from one track to another. As a result, the substitute index h was also employed which leads to the damage matrix D, see Equation 3.9. Each column of the matrix belongs to one load.

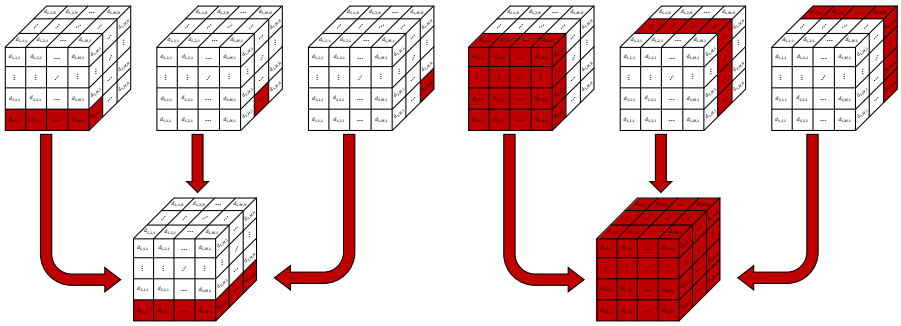

(a) Multiple loads and one track (b) Multiple loads and multiple tracks

Figure 3.8 – Multiple load use cases.

$$\mathbf{D} = \begin{bmatrix} d_{1,1} & d_{1,2} & \dots & d_{1,N} \\ d_{2,1} & d_{2,2} & \dots & d_{2,N} \\ \vdots & \vdots & \ddots & \vdots \\ d_{H,1} & d_{H,2} & \dots & d_{H,N} \end{bmatrix}. \tag{3.9}$$

As the loads have to be handled separately, the selection algorithm also needs to be tuned. Hence, the approach for one load needs to be repeated for every other load as well. For these use cases, the total damage d_{tot} and the value p can be a function of the load n which leads to the relative damage d_{rel} also being dependent on the considered load. This leads to the formulations of the Equations 3.10–3.12.

$$d_{\text{tot}}(n) = \sum_{h=1}^{H} d_{h,n}, \tag{3.10}$$

$$p \to p(n), \tag{3.11}$$

$$d_{\text{rel}}(n) = p(n)\, d_{\text{tot}}(n). \tag{3.12}$$

Additionally, for each load, all sets of possible track segment combinations exceeding the given threshold need to be determined and compared with the combinations resulting from other loads. After this, the track segment combinations that occur in the solution sets of every load are used for a final comparison. Among these fi-

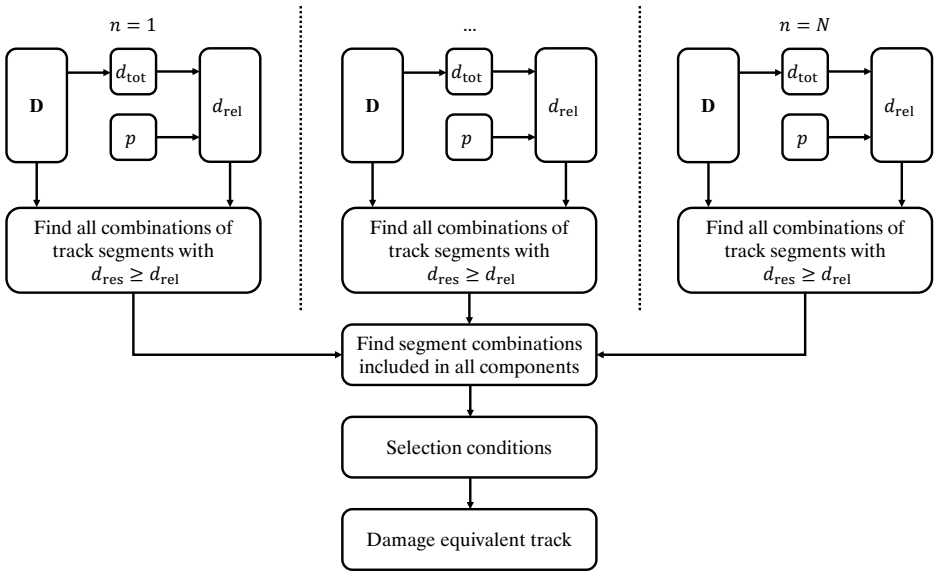

Figure 3.9 – Selection algorithm for multiple loads.

nal combinations, the one fulfilling the earlier mentioned conditions is chosen. The second condition, therefore, also needs to be adjusted as now N different d_{res} exist for each solution. Hence, the second condition for multiple loads is that the sum d_{comp} of all d_{res} should be maximised. d_{comp} can be calculated, according to Equation 3.13.

$$d_{\text{comp}} = \sum_{n=1}^{N} d_{\text{res}}(n). \tag{3.13}$$

Thus, the new selection conditions are:

1. Fewest number of track segments,

2. highest d_{comp}.

Figure 3.9 shows the structure of the algorithm that leads to a track which can be used for the simulation of the full vehicle with the damages of all loads exceeding the given threshold.

For $L = 1$, use case four turns into use case three. For $N = 1$, the use cases three and four turn into the earlier mentioned single load use cases one and two. Overall,

the fourth use case includes the other three use cases as special cases. The use case can be identified as follows:

- Use case 1: $L = 1, N = 1$,
- use case 2: $L \neq 1, N = 1$,
- use case 3: $L = 1, N \neq 1$,
- use case 4: $L \neq 1, N \neq 1$.

3.2.4 Virtual road profiles

The virtual tracks for the present work were created based on measurements of real test tracks and the OpenCRG®-format. The data format CRG is an open standard file format and is used for the evaluation of high-precision microscopic road surface data, the analysis of handling, riding comfort, and more importantly durability. Therefore, this data format was suited for the studies in the present work.

The measurements were performed with a mobile, multi-sensor, measuring system from 3D Mapping Solutions GmbH in a previous measurement campaign. With high-performance laser scanners the road surfaces can be measured three-dimensionally. As a result, all relevant features of the track can be captured in terms of durability analysis. The scanned test tracks were subsequently available as CRG files and could be used as virtual tracks in the ADAMS®environment. For more information on the file format, the reader is referred to [15, 16]. The damage equivalent test tracks were assembled from the track segments that resulted from the selection algorithm by cutting the segments out of the data and simulating them separately.

The tracks for the studies were chosen based on two properties. The first one was the distinction between test tracks that include cornering manoeuvres and ones that only include straight-line manoeuvres. This distinction is important as lateral forces are mainly induced during cornering. The second property was the road roughness since the roughness has an immense influence on the vertical excitation, and thus also the induced loads.

With the *International Roughness Index* (IRI) it is possible to evaluate the roughness of a road with one parameter, see [17]. The IRI can be calculated with a quarter car model which is excited by the road while travelling with $v = 22.22\,\mathrm{m\,s^{-1}}$.

With the model, the suspension motion can be calculated as the difference between sprung mass displacement and unsprung mass displacement. The parameters for the quarter car model are called *The Golden Car*. The accumulated suspension motion is then divided by the length of the road to obtain the IRI. According to Andrén [18], the IRI is related to comfort experience but insufficient for the mathematical description of roads. The author also claims that for vehicle dynamic simulations the distribution of frequencies and amplitudes needs to be considered. This requires a more detailed description of the road. Therefore, a different method was used to evaluate the roughness of the test tracks in the present work. The employed method is described by the *International Organization for Standardization* (ISO) in the ISO 8608 [19] and utilises the power spectral density (PSD) of the road profile. The ISO states that the roughness can be classified into eight classes (A-H) with A being a very smooth road which means that the roughness is relatively low and H being a very poor road with high roughness. With the proposed straight-line fit of the ISO, the roughness coefficient $G_\mathrm{d}(f)$ can be calculated according to Equation 3.14 with $G_\mathrm{d}(f_0)$ being the PSD at the reference spatial frequency f_0.

$$G_\mathrm{d}(f) = G_\mathrm{d}(f_0)\left(\frac{f}{f_0}\right)^{-w} \quad \text{with} \quad f_0 = 0.1\,\mathrm{cycles/m} \quad \text{and} \quad w = 2, \tag{3.14}$$
$$\text{for} \quad 0.011\,\mathrm{cycles/m} < f < 2.83\,\mathrm{cycles/m}.$$

In order to find tracks that cover the whole spectrum of roughness, the test tracks had to be evaluated in terms of their roughness class. Therefore, a classification algorithm was employed that has been presented by Gorges et al. [20] and will shortly be summarised. The method has various advantages. First, it evaluates the roughness class over a frequency range instead of only a reference spatial frequency. Secondly, it summarises the results in multiple octave bands to exactly one road class for the considered track segment. The input of the classification algorithm for the present work was the elevation profile extracted from the CRG file in the centre of the track. First, the PSD of the road profile was smoothed in 10 octave bands which are proposed by the ISO and listed in Table 3.1.

The smoothing algorithm includes the weighted average values of the PSD in the respective octave band. The weighted average is calculated with a normalised

Table 3.1 – Centre frequencies and geometric mean values of octave bands for classification [20].

b	f_c (cycles/m)	Geometric mean values for road classes $G_d(f_c)(10^{-6}\,m^3)$ A	B	C	D	E	F	G	H
1	0.00786	2621	10486	41943	167772	671089	2684354	10737417	42949668
2	0.0156	655	2621	10486	41943	167772	671089	2684354	10737417
3	0.0313	164	655	2621	10486	41943	167772	671089	2684354
4	0.0625	41	164	655	2621	10486	41943	167772	671089
5	0.125	10	41	164	655	2621	10486	41943	167772
6	0.25	2.56	10	41	164	655	2621	10486	41943
7	0.5	0.64	2.56	10	41	164	655	2621	10486
8	1	0.16	0.64	2.56	10	41	164	655	2621
9	2	0.04	0.16	0.64	2.56	10	41	164	655
10	4	0.01	0.04	0.16	0.64	2.56	10	41	164

Gaussian window function. Furthermore, a minimum distance classifier was used to receive one roughness class, according to Equation 3.15. $\mathrm{PSD}_{\mathrm{Smoothed}}(b)$ is the output of the smoothing algorithm for one octave band b and $\mathbf{M}(b, \mathrm{class})$ is the matrix of geometric mean values, see Table 3.1.

$$\text{Road class} = \min\left\{\sum_{b=1}^{10} |\log_{10}[\mathrm{PSD}_{\mathrm{Smoothed}}(b)] - \log_{10}[\mathbf{M}(b, \mathrm{class})]|\right\}. \tag{3.15}$$

Figure 3.10 shows the PSD and smoothed PSD for the complete test track that was used for the simulation of the roughness class C and straight-line manoeuvres.

3.2.5 MBS model

A widely used method to obtain loads for durability assessments virtually is the MBS. For road induced loads, it is important to represent the complete vehicle. Different applications for full vehicle models of passenger cars driving on virtual tracks have been published by other authors. Bäcker et al. [12], as well as Kang et al.[13, 14], created vertical excitations profiles with white and pink noise to recreate LTFs. In [21, 22] tyre models for simulations of trucks on rough roads were evaluated. Kollmer et al. [23] analysed the influence of unevenness and waviness on the loads in order to portray customer usage. The virtual tracks were created with white noise and form

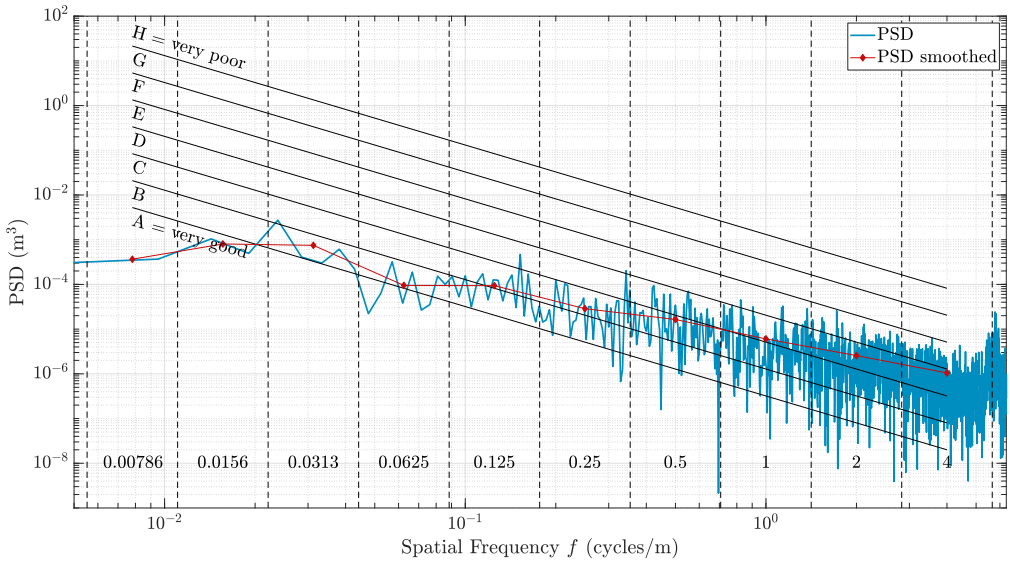

Figure 3.10 – PSD and smoothed PSD for a CRG road profile.

filters. Londhe and Kangde [24] and Roy and Villaire [25] simulated passenger cars riding over virtual roads. Weber [26] analysed the loads and the driving line on a handling circuit which was measured and digitalised. Morr et al. [27] also simulated full vehicle models on digitalised tracks to create excitations for test rig simulations. Rönicke et al. [28] showed how the design of test tracks for bad road surfaces can be improved with results from simulations on digitalised tracks.

The MBS model in the present work also comprised a full vehicle model, but for a motorcycle. The model was assembled with subsystems consisting of mechanical components in ADAMS®, control systems, and a tyre model. Figure 3.11 shows the structure of the co-simulation.

The mechanical components were modelled as flexible bodies based on FE models. Both the control systems and the tyre model ran in a co-simulation. The control systems included were the anti-lock braking system (ABS), the wheelie control, and the semi-active suspension (SAS). Using an appropriate tyre model for simulations is important as the excitations from the road are transmitted via the model into the structure of the full vehicle. As mentioned by Adamski [29], the tyre model has to scan three-dimensional road profiles and transfer the resulting loads and vibrations. Furthermore, the contact patch needs to be discretised so that the model can

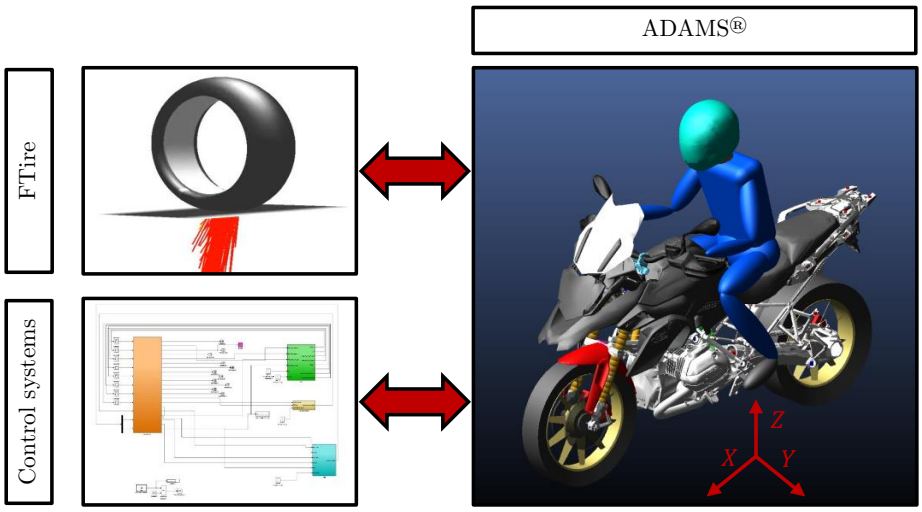

Figure 3.11 – Co-simulation structure.

correctly display the interaction due to deflection of the tyre and the short-wave excitation. The three tyre models suitable for these type of simulations are the FTire by Gipser [30], the RMOD-K by Oertel [31], and the CDTire by Gallrein and Bäcker [32]. The FTire model has been used in different publications in combination with full vehicle models of four-wheeled vehicles and rough roads [21–23, 25, 26, 28]. The results were sufficient, and therefore the FTire model was used for the present work as well.

As stated in Section 3.2.4, the roughness of the measured test tracks was determined for the centre of the tracks. Therefore, also the riding path for the MBS was chosen in the centre of the tracks as well. Additionally, the velocity of the model was set to $15\,\mathrm{m\,s^{-1}}$ for the simulations which is the average velocity that can be observed during customer usage.

For the simulations, the track segments with their associated data were cut out of the original measurement data, as previously mentioned. Afterwards, each segment was used for simulation. To stabilise oscillations that occur during every start of a multi-body simulation before the motorcycle rides on the rough track and interacts with it, a flat surface was attached before and after each track segment. This part of the simulation was later on truncated for the calculation of the pseudo-damage. Figure 3.12 shows the vertical road profile of a track segment with the attached flat

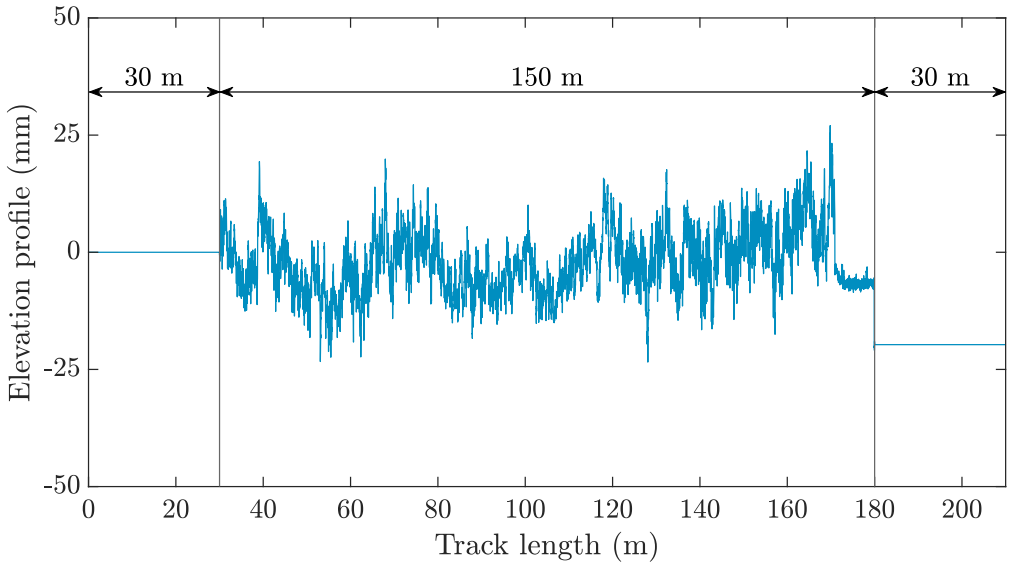

Figure 3.12 – Attached road profiles.

surfaces.

In order to find a representative damage equivalent virtual test track for the full vehicle, decisive spots and loads were chosen from different parts of the motorcycle. These loads are, hence, the N loads of the damage matrix presented in Section 3.2.3. The selection was based on experience from predecessor models and other motorcycles where the chosen loads caused high stresses for components or even cases of damage. The decisive spots and loads are listed in Table 3.2 and depicted in Figure 3.13. F_T is the resulting force of longitudinal and vertical force, see Equation 3.16, and was used for the evaluation of the bolt joints which are designed against transverse shear.

$$F_T = \sqrt{F_X^2 + F_Z^2}. \tag{3.16}$$

3.3 Results

3.3.1 Track selection

For the selection and creation of virtual track profiles, the measured profiles of more than 50 tracks were separated into tracks with and without cornering, as mentioned

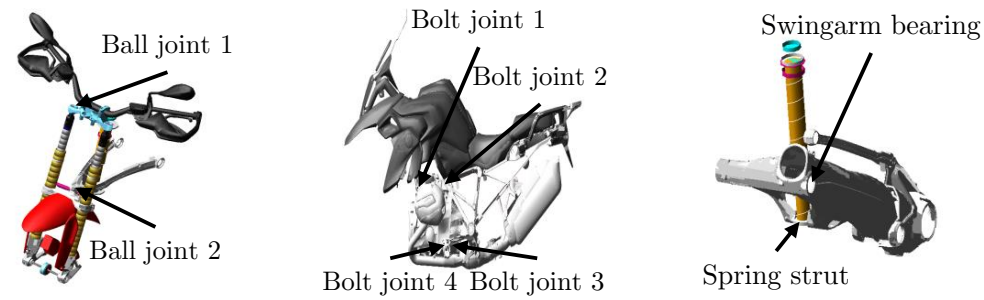

(a) Front suspension (b) Frame (c) Rear suspension

Figure 3.13 – Decisive spots.

Table 3.2 – Decisive spots and respective loads.

Motorcycle part	Spot	Loads
Front wheel	Wheel hub	F_X, F_Y, F_Z, M_Y
Front suspension	Ball joints	F_X, F_Z
Frame	Bolt joints	F_T
Rear suspension	Swingarm bearing, Spring strut	F_X, F_Z
Rear wheel	Wheel hub	F_X, F_Y, F_Z, M_Y

(a) Smooth country road (b) Comfort track

(c) Fine cobblestone (d) Coarse cobblestone

Figure 3.14 – Straight tracks ©BMW AG.

in Section 3.2.1. Additionally, the road roughness classification was used to determine the roughness class of the test tracks according to the ISO. The classification was performed for track segments with a length of 15 metres because the velocity for the MBS model was also set to 15 metres per second. Hence, the classification algorithm identified a roughness class every second. As a result, the share of each roughness class could be determined for every single test track.

Hereafter, each track was assigned to the roughness class that had the major share for the respective track. Finally, the two tracks with the most share of one roughness class were selected and assigned to the roughness class as representative tracks, one being a straight and one a curved track. The length of the virtual tracks was set to 150 metres to ensure uniformity when comparing the resulting damage for different roughness classes. In total, eight tracks were selected, four straight and four curved roads.

Figure 3.14 and 3.15 show pictures of the selected tracks.

Track No. 1 is a smooth country road in the Munich countryside. The low roughness of the road allows riding with higher velocities without high excitation. Track

(a) Highway (b) Poorly maintained country road

(c) Damaged country road (d) Coarse cobblestone

Figure 3.15 – Curved tracks ©BMW AG.

No. 2 is a test track at BMW's test and performance centre and is often used to evaluate the comfort experience that results from long-wave excitations. Test track No. 3 consists of fine cobblestones. This kind of road surface is very common in historical city centres of European cities or also for property gateways with lowered kerbs. Test track No. 4 consists of coarse cobblestones. These kinds of cobblestones can often be found in urban areas and cause short-wave excitation which often forces riders to reduce their speed. The reduced speed, however, increases safety for all road users. Exemplary locations are traffic-calmed sectors like schools or tourist attractions where pedestrians are more likely to be distracted or unfamiliar with the traffic situation. Test track No. 5 is a highway in the surrounding area of Munich. Highways often have a very smooth surface as they are designed to allow road users to travel at a high speed and cover large distances in a short time. This particular highway does not have speed limits for the most part, and hence it is important to ensure a smooth road surface to prevent hazard. Test track No. 6 is a country road in Bavaria and is poorly maintained. Test track No. 7 is also a country road in Bavaria but has worse road conditions and includes damaged road segments. Lastly,

Table 3.3 – ISO class shares - straight tracks.

		ISO class (%)							
Track No.	Description	A	B	C	D	E	F	G	H
1	Smooth country road	100	0	0	0	0	0	0	0
2	Comfort track	0	100	0	0	0	0	0	0
3	Fine cobblestone	0	0	100	0	0	0	0	0
4	Coarse cobblestone	0	0	0	100	0	0	0	0

Table 3.4 – ISO class shares - curved tracks.

		ISO class (%)							
Track No.	Description	A	B	C	D	E	F	G	H
5	Highway	100	0	0	0	0	0	0	0
6	Poorly maintained country road	10	90	0	0	0	0	0	0
7	Damaged country road	0	20	80	0	0	0	0	0
8	Coarse cobblestone	0	0	10	90	0	0	0	0

test track No. 8 is, like track No. 4, composed of coarse cobblestones. It is part of the castle square at the Nymphenburg Palace in Munich which is a tourist attraction. The results of the roughness classification for the chosen test tracks are depicted in Table 3.3 and 3.4.

The distributions clearly show that no measurements were available for tracks with roughness classes higher than D. Roughness classes of C and D already comprise rough and unpaved roads. Roughness classes E and higher are enduro or off-road tracks that cannot be measured reproducibly. That is due to the topology of the road. When the road is not paved or even off-road, the weather, vegetation, and wear of the track itself play a major role as they influence the road profile. Also, when the track consists of loose underground the vehicle itself displaces the underground. These factors would lead to great differences between measurements on two different dates, for example. To sum up, for roughness classes ranging from A to D one straight and one curved test track was chosen based on the share of each class. Table 3.3 and Table 3.4 also highlight that the chosen tracks represent the roughness classes accurately as most tracks only consist of one roughness class. The minimum amount of one roughness class could be observed for the curved track of ISO class C. But

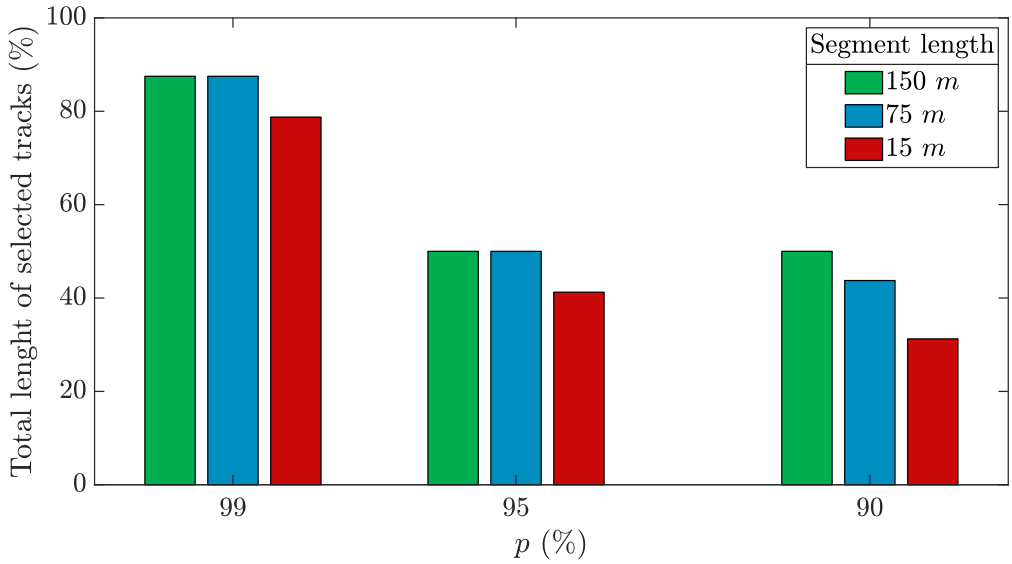

Figure 3.16 – Total length of damage equivalent tracks.

even for that track, 80% consist of one roughness class which is the major share.

3.3.2 Damage equivalent track

The value p for the threshold of the desired damage can be chosen differently for each load. However, for the present work, the value was chosen as a constant value for every load during one analysis. In order to obtain appropriate tracks that represent the major damaging aspects, values of 90%, 95%, and 99% were tested. Additionally, different lengths of track segments were examined. The length of the track segments for the analyses with the damage matrix was set to 15, 75 and 150 metres. With the velocity of the motorcycle being 15 metres per second, this resulted in an analysis of track segments on a one, five and 10 second basis. In the present work, the use case four of Section 3.2.3 was employed because it is the most complex one and also comprises the other three use cases. As the present work aims to present a method for the full vehicle, it is also necessary to consider multiple loads instead of only one load for a specific component. Overall, nine analyses were conducted. For each of the three different track segment lengths and threshold values p, a damage equivalent track was created from the eight selected test tracks. Figure 3.16 shows the total length of the damage equivalent tracks for the nine different analyses.

Table 3.5 – ISO class shares - damage equivalent tracks.

Analysis No.	Segment length (m)	p (%)	ISO class (%) A	B	C	D	E	F	G	H
1	150	99	15.71	30	27.14	27.14	0	0	0	0
2	150	95	0	5	47.5	47.5	0	0	0	0
3	150	90	0	5	47.5	47.5	0	0	0	0
4	75	99	15.71	30	27.14	27.14	0	0	0	0
5	75	95	0	17.5	35	47.5	0	0	0	0
6	75	90	0	5.71	40	54.29	0	0	0	0
7	15	99	23.81	22.22	23.81	30.16	0	0	0	0
8	15	95	0	12.12	30.30	57.58	0	0	0	0
9	15	90	0	8	20	72	0	0	0	0

The figure demonstrates that the total length of simulated tracks decreases with lower values of p which is expected because less damage is sought, and hence fewer track segments have to be considered. Additionally, the total length decreases with lower values of the segment length because the total damage is cut more frequently which allows a more detailed localisation of damaging track segments. For the values 99% and 95% of p, the total length was equal for segment lengths of 150 and 75 metres. The more detailed analyses with segment lengths of 15 metres led to more savings regarding the total length of selected tracks, computational time, and data amount. For segment lengths of 150 metres, the total length of selected tracks was equal for the p-values of 95% and 90% which means that the damage equivalent track for 90% also covers 95% of the damage for each load. Overall, most savings could be achieved with segment lengths of 15 metres and a p-value of 90%. This analysis led to a damage equivalent track that had a length of 31.25% compared to the total length of all tracks.

The resulting damage equivalent tracks and the associated track segments were further examined with regard to the roughness class. For each of the nine analyses, the share of each roughness class was determined. The findings are listed in Table 3.5.

The table highlights that the higher roughness classes account for the major share of the damage equivalent tracks. This means that track segments with higher road roughness also lead to more damage and are more relevant for durability assessments

which was also expected. The share of higher roughness classes also increases with lower values of p. This observation also highlights that the lower roughness classes lead to less damage, but still have to be considered when aiming to cover even more damage.

3.4 Discussion

The present work showed how relevant track segments can be identified in terms of durability engineering and how they can be used for simulations to generate loads that cover the major part of the damage.

First, a novel approach was presented to evaluate the damaging properties of track segments by creating a damage matrix that distinguishes between different tracks, segments, and loads. With a selection algorithm, negligible segments can be identified and dismissed so that computational time decreases as well as the amount of data.

For the validation of the method, test tracks were measured and classified based on two properties. As a first step, the tracks were divided into straight ones and those that include curves. Hereafter, the test tracks were assigned to a roughness class of the ISO 8608 by means of a classification algorithm. As the real customer also rides on roads with different roughness classes it was reasonable to include a variety of tracks to make sure customer usage can also be covered with such an approach. Finally, eight test tracks were used for the validation with four being straight tracks and four having curves. The roughness classes ranged from A to D.

A flexible MBS model of a full motorcycle including the rider was created and used for simulations of the measured test tracks and damage equivalent tracks. The model also included control systems and a tyre model that ran in a co-simulation. However, the findings of the present work can also be transferred to simpler vehicle models.

With the novel method, nine different analyses were conducted. Three different track segment lengths were chosen and three different thresholds. The segment lengths were 15, 75, and 150 metres. The thresholds depict the amount of total damage from the simulations of the complete tracks that is sought. For every segment length, 90%, 95%, and 99% were examined as thresholds. The shorter the segments are chosen for the analysis the shorter the final damage equivalent track becomes because the total damage is partitioned into smaller parts, and hence more negligible

segments can be found. Using smaller thresholds also decreases the size of the final track as less damage is accepted. For the analyses in the present work, savings of up to 70% were possible. As the simulations for the track segments were run sequentially, the savings are equal for total track length, computational time and data amount. To save even more computational time, it is suggested to run the simulations in parallel.

Another advantage of the presented method that identifies representative track segments is the independency of the type of signal used. In the present work, only loads were considered in order to find track segments as this research focuses on durability engineering. However, it is also possible to evaluate other signals, for example, accelerations or displacements. With the method, it is then possible to create equivalent tracks in other fields, like acoustics or comfort assessments.

Future research could take other vehicle concepts into account and compare the results. Furthermore, the implementation of usage models should be investigated as each customer rides the motorcycle differently which leads to different loads. One example is the varying velocity that can be analysed. Furthermore, only the roughness was analysed in detail in regards to the resulting damage. The influence of other road properties was not examined and should be part of upcoming studies. The test tracks used in the present work were chosen solely based on their road properties, and hence only depict a synthetic customer usage profile. For instance, all roughness classes ranging from A to D were represented evenly as each roughness class accounted for 23.75% or 26.25% of the total simulated track length which is a very small gap. This means that for this synthetic usage profile the real customer would have to ride as much on very rough roads as he does on smooth roads. In reality, some of the customers will ride predominantly on smooth roads which means that in the present work the number of rough roads was considered disproportionately. Additionally, some customers will also ride on roads with roughness classes of E and higher. These road segments are even more damaging than the roughness classes examined in the present work. As a result, utilising the presented methods for a real customer usage profile would save even more costs, time, and data amount because more segments with lower roughness and damage contributions can be neglected.

References

[1] F. Küçükay, T. Kassel, M. Eghtessad and H. Kollmer. 'Requirement Engineering using the 3D method'. In: *SAE Technical Paper* No. 2011-26-0012 (2011).

[2] M. Speckert, K. Dreßler, N. Ruf, T. Halfmann and S. Polanski. 'The Virtual Measurement Campaign VMC concept-a methodology for georeferenced description and evaluation of environmental conditions for vehicle loads and energy efficiency'. In: *Proceedings of the 3rd Commercial Vehicle Technology Symposium; 2014 Mar 11-13; Kaiserslautern.* Aachen: Shaker, 2014, pp. 88–98.

[3] R. Mayrböck and A. Mayr. 'Numerische und experimentelle Methoden zur Lastdatenermittlung an Teilmodellen eines Motorrades'. In: *DVM Bericht 143; 2016 Oct 12-13; Steyr.* Berlin: DVM, 2016, pp. 93–106.

[4] U. Warnecke, K. Osterhage and W. Lieven. 'Optimierte Betriebsfestigkeitsauslegung durch Verwendung virtuell ermittelter Betriebslasten für Prüfstandsversuche'. In: *Materials Testing* 51.7-8 (2009), pp. 493–497.

[5] U. H. Clormann and T. Seeger. 'Rainflow-HCM. Ein Zählverfahren für Betriebsfestigkeitsnachweise auf werkstoffmechanischer Grundlage'. In: *Stahlbau* 55.3 (1986), pp. 65–71.

[6] E. Haibach. *Betriebsfestigkeit.* Berlin, Heidelberg: Springer Berlin Heidelberg, 2006.

[7] P. Johannesson and M. Speckert. *Guide to load analysis for durability in vehicle engineering.* Chichester: Wiley, 2014.

[8] G. Genet. 'A statistical approach to multi-input equivalent fatigue loads for the durability of automotive structures'. PhD thesis. Chalmers University of Technology, 2006.

[9] H. Vajen. 'Untersuchung des Einflusses praxisnaher Erprobungsbedingungen auf die Schwingfestigkeit von Bauteilen des Common-Rail-Dieseleinspritzsystems'. PhD thesis. Universität Stuttgart, 2014.

[10] A. Halfpenny. 'Methods for accelerating dynamic durability tests'. In: *Proceedings of the 9th International Conference on Recent Advances in Structural Dynamics; Southampton.* 2006.

[11] M. Bergold, S. Brandes, B. Seufert and D. Bestle. 'Simulation von Kundenmanövern zur Ermittlung repräsentativer Fahrwerksbelastungen'. In: *DVM Bericht 146; 2019 Oct 9-10; Wolfsburg.* Berlin: DVM, 2019, pp. 99–114.

[12] M. Bäcker, T. Langthaler, M. Olbrich and H. Oppermann. 'The hybrid road approach fro durability loads prediction'. In: *SAE Technical Paper* 2005-01-0628 (2005).

[13] D. O. Kang, H. Seungjin and K. Hoiyoung. 'Virtual road profile modeling using equivalent damage method for VPG simulation'. In: *SAE Technical Paper* 2009-01-0814 (2009).

[14] D. O. Kang, K. Park, S.-J. Heo, Y.-I. Ryu and J. I. Jeong. 'Development and application of VPG simulation technique based on equivalent virtual road profile'. In: *International Journal of Precision Engineering and Manufacturing* 11.2 (2010), pp. 265–272.

[15] H. Gimmler, D. Ammon and J. Rauh. 'Road profiles: Mobile measurement, data processing for efficient simulation and assessment of road properties'. In: *VDI Berichte* 1912 (2005), pp. 335–352.

[16] J. Rauh and M. Mössner-Beigel. 'Tyre simulation challenges'. In: *Vehicle System Dynamics* 46.S1 (2008), pp. 49–62.

[17] M. W. Sayers, T. D. Gillespie and A. V. Queiroz. *The international road roughness experiment: establishing correlation and a calibration standard for measurements*. Washington: The World Bank, 1986.

[18] P. Andrén. 'Power spectral density approximations of longitudinal road profiles'. In: *International Journal of Vehicle Design* 40.1-3 (2006), pp. 2–14.

[19] ISO. *Mechanical vibration - Road surface profiles - Reporting of measured data*. Standard No. 8608:2016. Geneva, Switzerland: ISO, 2016.

[20] C. Gorges, K. Öztürk and R. Liebich. 'Road classification for two-wheeled vehicles'. In: *Vehicle System Dynamics* 56.8 (2018), pp. 1289–1314.

[21] S. R. Waser, W. Hirschberg, T. Ille and V. Mladek. 'Evaluierung von Reifen- und Fahrbahnmodellen für die Simulation festigkeitsrelevanter Beanspruchungen von Nutzfahrzeugen'. In: *VDI Berichte, Reifen-Fahrwerk-Fahrbahn*. Düsseldorf: Springer-VDI-Verlag GmbH & Co. KG, 2007, pp. 153–165.

[22] S. R. Waser. 'Generierung der beanspruchungsrelevanten Belastungen von Nutzfahrzeugen mittels Reifen-, Fahrbahn-und Fahrzeugmodellen'. PhD thesis. TU Graz, 2009.

[23] H. Kollmer, F. Küçükay and K. Pötter. 'Measurement and fatigue damage evaluation of road profiles in customer operation'. In: *International Journal of Vehicle Design* 56 (2011), pp. 106–124.

[24] A. Londhe and S. Kangde. 'Virtual Road Approach for Vehicle Durability Simulations'. In: *SAE International Journal of Passenger Cars-Mechanical Systems* 6 (2013), pp. 876–881.

[25] N. Roy and M. Villaire. 'Virtual road load data acquisition using full vehicle simulations'. In: *SAE Technical Paper* 2013-01-1189 (2013).

[26] T. Weber. 'Betriebslasten in der Fahrzeugentwicklung - Simulation Gesamtfahrzeug'. In: *DVM Bericht 141; 2014 Oct 8-9; Ingolstadt*. Berlin: DVM, 2014, pp. 115–128.

[27] M. Morr, T. Minor and T. Maulick. 'Messdatenbasierte virtuelle Lastdatenermittlung für Fahrwerksbauteile und Karosserie'. In: *DVM Bericht 143; 2016 Oct 12-13; Steyr*. Berlin: DVM, 2016, pp. 107–120.

[28] N. Rönicke, A. Ams, S. Brandes and B. Seufert. 'Simulationsgestütztes Design einer Schlechtwegoberfläche für ein neues Automobil-Prüfgelände'. In: *DVM Bericht 143; 2016 Oct 12-13; Steyr*. Berlin: DVM, 2016, pp. 151–164.

[29] D. Adamski. *Simulation in der Fahrwerktechnik*. Wiesbaden: Springer Fachmedien Wiesbaden, 2014.

[30] M. Gipser. 'FTire–the tire simulation model for all applications related to vehicle dynamics'. In: *Vehicle System Dynamics* 45 (2007), pp. 139–151.

[31] C. Oertel. *RMOD-K Formula Documentation*. URL: https://www.rmod-k.com/images/stories/media/downloads/Formula/formula.pdf.

[32] A. Gallrein and M. Bäcker. 'CDTire: a tire model for comfort and durability applications'. In: *Vehicle System Dynamics* 45 (2007), pp. 69–77.

4 Influence of road and rider characteristics on durability of motorcycles

Influence of road and rider characteristics on durability of motorcycles

Aptin Haerian[a], Kemal Öztürk[b], Robert Liebich[a]

[a]*Chair of Engineering Design and Product Reliability, Technische Universität Berlin, Berlin, Germany;*[b]*BMW AG, Munich, Germany*

(This is an Accepted Manuscript of an article in International Journal of Vehicle Systems Modelling and Testing, available online: https://www.inderscience.com/jhome.php?jcode=ijvsmt .©Inderscience.)

The present work deals with the virtualisation of motorcycle customer behaviour. First, a method was found to identify design-relevant customers based on data from classification algorithms involving the vehicle dynamics and onboard signals. For vertical excitations, the roughness of the road and ridden velocities were examined with multi-body-simulations (MBS). A measurement of a real motorcycle equipped with wheel load transducers and data-logging devices on a test track was used for validation. It was shown that especially vertical loads can be estimated via synthetic straight-line simulations. Furthermore, an approach is presented with which virtual tracks are created based on the same dataset and by including data for curvature. A measured speed profile and scatter for the vertical excitation were considered to obtain precise loads via MBS. Besides the virtualisation of the road, a novel algorithm was developed to generate a speed profile based on rider characteristics. The implemented characteristics comprised the bearable accelerations in lateral and longitudinal direction as well as the bearable velocities for different roughness classes. Different synthetic rider types from beginner to expert were defined and compared. The developed methods enable the identification of design-relevant customers and the simulation of load profiles based on real customer behaviour.

Keywords: Virtual environment, motorcycle, driver behaviour, durability, multi-body systems, driver-vehicle systems

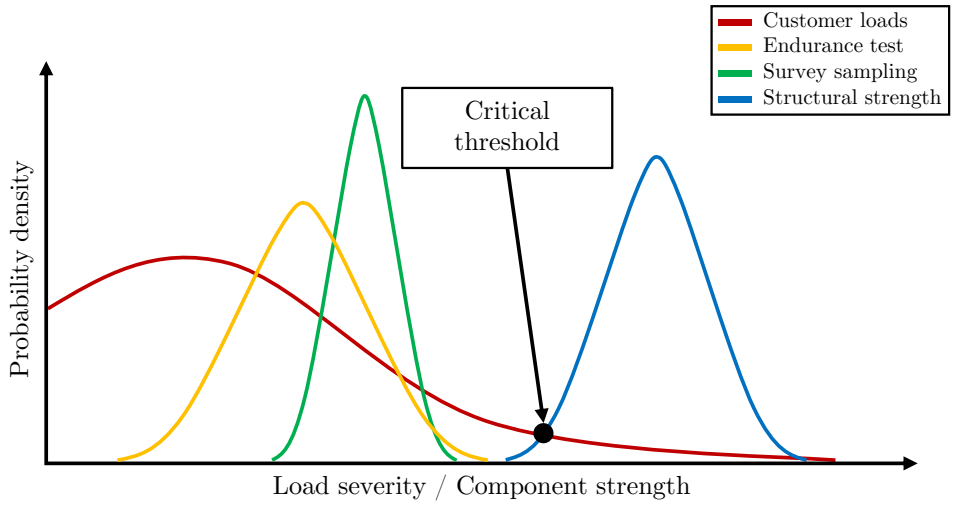

Figure 4.1 – Load distributions.

4.1 Introduction

Throughout the years, digitalisation has become a major part of vehicle development. Especially with increasing computer performance, data availability and transfer rates, the field has shifted more and more towards the implementation of customer usage profiles and simulation. Knowing real customer behaviour has advantages for companies and customers. In an ideal world, the engineer would have all occurring loads during usage. The products could be designed in a way that they would withstand all loads, and hence ensuring safety for customers and preventing recall actions. Additionally, weight and material costs could be reduced, saving money and enabling lightweight construction. In reality, the engineer only has information on predecessor models at best in the early stages of development [1]. In the motorcycle industry, the data is either extracted from survey samplings of predefined customers or endurance tests where measurements are performed on test tracks. These datasets, however, do not cover the whole customer usage as shown in Figure 4.1 and mentioned in [2]. Thus, customer-related data is either not available at all or in an insufficient form, the reason being that memory of devices inside vehicles like motorcycles or passenger cars is still limited. Hence, the recording of signals with high sampling rates is expensive and often not feasible.

That is why a classification of customer usage data is aspired where data amount is reduced while still delivering valuable information. Nowadays, it is possible to collect data from customers in order to classify them for specific use cases. To ensure data security, the data is collected anonymously. The classifications are often results of model-based approaches where different sensor signals are used to calculate a certain quantity. Gorges et al. [2] classified the hilliness, roughness, and curviness of roads with onboard signals of motorcycles. These classifications enable a customer characterisation based on road properties. It is also possible to calculate loads with model-based approaches as in [3–6]. However, they require in-depth knowledge of the cause-effect relationships which results in high complexity. Furthermore, the resulting loads are generally stored in rainflow matrices due to memory limitations and are not available as a load time function (LTF). In addition, the models are limited to specific loads.

Virtual models, on the other hand, can output as many signals as desired. Data amount is less of an issue with simulations. However, it is also not feasible to run simulations for all customers. Some motorcycles are purchased and ridden by thousands of customers worldwide. Simulating all of the customers would lead to immense simulation duration. Therefore, it is important to identify the design-relevant customer whose riding behaviour is more damaging than a certain percentile of the total customer field. In this context, it is also useful to incorporate classified customer usage data by virtualising ridden tracks or different rider behaviours. In doing so, more reliable assumptions can be made. Using simulations to make load assumptions has many advantages. First of all, they can be conducted in the early development stages where real prototypes do not exist yet. In particular, this makes a comparison of different design concepts possible without building up multiple prototypes. Furthermore, the engineer will have no real customer data in the early development stages as the motorcycle is not on the market and in customer hands yet. If vehicle-independent data is, therefore, used in combination with virtual models, it is possible to determine loads more precisely. Such vehicle-independent data are, for example, the road and rider characteristics. Moreover, scatter can easily be created with simulations by the above-mentioned characteristics. Testing a variety of riding styles, for example, is not feasible in a real measurement campaign due to time and cost limiting factors.

The present work is organised as follows. Section 4.2.1 gives an overview of the overall methodology from the data source to the final result including the simulations. Section 4.2.2 presents the method with which design-relevant customers can be identified based on their characteristic behaviour via a combination of classified data and simulations. Section 4.2.3 shows how road characteristics obtained from on-board classifications can be used to recreate virtual road profiles. A novel algorithm to create a speedprofile for a given virtual track and rider characteristics is presented in Section 4.2.4. In Section 4.3.1 the maximum loads for a span of roughness classes and velocities are analysed and classified. Additionally, damages from synthetic simulations are calculated and compared with the measurement of a real motorcycle ridden on a test track. Section 4.3.2 contains the comparison between precise and classified data for curve characteristics. Furthermore, loads and damages resulting from simulations on the recreated virtual track with a specified speed profile are assessed in order to check whether accuracy for load assumptions can be enhanced. Scatter resulting from the random process of the road profile is considered. Section 4.3.3 highlights how additional scatter can be generated with different rider characteristics. Three synthetic rider types are analysed in regards to their speed profiles and resulting damages for the same test track. Finally, the results of the present work are discussed in Section 4.4.

4.2 Methods

4.2.1 Complete workflow

Figure 4.2, depicts the complete workflow for the methods developed in the present work from the real rides to the final load assumptions.

The first part contains the data acquisition process. Customer-related data is collected by classifying the necessary characteristics. This is achieved by utilising the classification algorithms developed in [2] where roughness, curve characteristics, and velocity can be tracked and stored. For the curve characteristics, the banking angle and the vehicle's velocity were measured. The roughness classification requires the front and rear suspension displacements along with the velocity. As these algorithms are not implemented for motorcycles owned by customers currently, a measurement vehicle had to be used for the present work. Data-logging devices were mounted

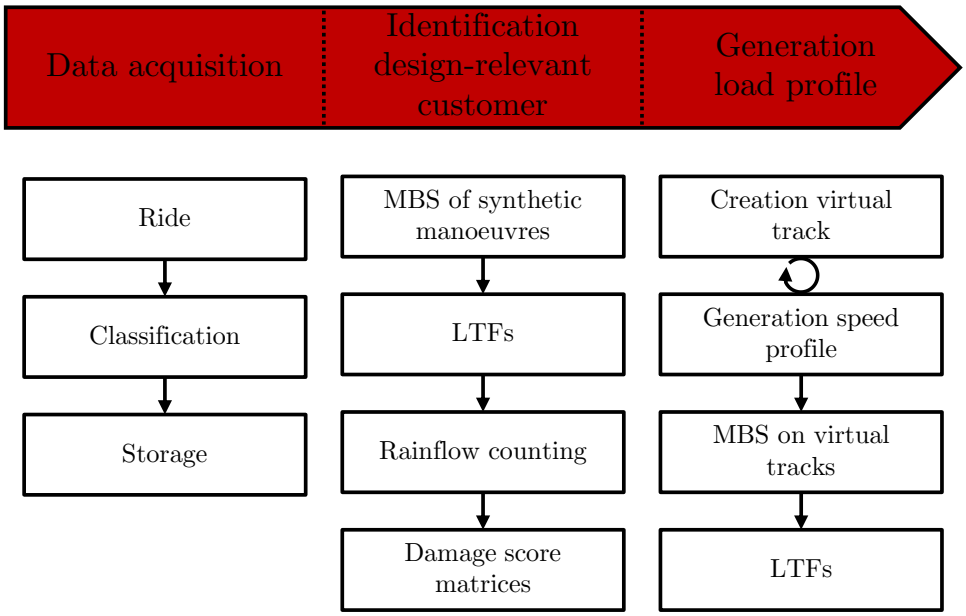

Figure 4.2 – Complete workflow.

to collect onboard signals for a subsequent offline classification. The motorcycle was also equipped with wheel load transducers to measure the loads at the wheel hubs which was necessary for validating the simulations but is not necessary for virtualising customer behaviour in general. The motorcycle was of the type BMW R1200GS. The logged signals are listed in Table 4.1.

The second part deals with the identification of the design-relevant customer. The classified data is used to identify design-relevant customers for vertical excitations with damage scores calculated by means of matrices. For the generation of these damage score matrices, synthetic virtual tracks and manoeuvres have to be created and used in combination with a virtual vehicle model to produce LTFs for a subsequent rainflow counting.

In the present work, multi-body simulations (MBS) were carried out. A full vehicle model of the real motorcycle was used in ADAMS®. Using MBS models to generate load data is common practice and has been part of other publications and ground vehicles like passenger cars or trucks [7–18]. Additionally, relevant control systems and the FTire model by Gipser [19] ran in a co-simulation. The tyre model is able to

Table 4.1 – Logged signals for model and method validation.

Component	Measurand
Vehicle	Velocity GPS longitudinal GPS lateral Banking angle
Front suspension	Displacement
Rear suspension	Displacement
Front wheel hub	X force ($F_{X,\mathrm{ft}}$) Z force ($F_{Z,\mathrm{ft}}$)
Rear wheel hub	X force ($F_{X,\mathrm{rr}}$) Z force ($F_{Z,\mathrm{rr}}$)

scan three-dimensional road profiles and transfer the resulting loads and vibrations. Waser et al. [16] elaborated why the FTire is the most suited model for similar use cases. The FTire model has also been used by other authors to simulate full vehicle MBS models driving over rough roads or obstacles [11, 14, 15, 18, 20]. Using virtual tracks as inputs for the MBS in ADAMS®, the vehicle is excited by the vertical profile and also by following the trajectory when performing cornering manoeuvres.

After the design-relevant customer has been identified, realistic load profiles are generated. The complete virtual track is created based on the classified data. The procedure of creating a virtual road can be repeated so that the scatter resulting from the random process of the vertical profile generation is included. Finally, the speed profile is assigned. Here, it is also possible to generate multiple profiles in order to account for varying riding styles. Again, MBS are run to create LTFs which are the final output and can be used for further investigations during the vehicle development.

4.2.2 Identification of design-relevant customers

The presented approach takes classified data into account and determines which customer causes the highest damage. In doing so, the classified quantities are used to create synthetic simulations and calculate a pseudo-damage for each segment of

the roads that were ridden by the customers. The pseudo-damages of all segments are then added up to a total pseudo-damage for each customer and each analysed load. This final characteristic value makes a comparison of different customers with only a scalar value possible. An LTF is used as input for the rainflow-counting method which is an established method to retrieve load amplitudes [21]. These load amplitudes L_i are subsequently used to calculate the pseudo-damage d with Equation 4.1 where β equals 5 according to Johannesson and Speckert [22].

$$d = \sum_i L_i^\beta. \tag{4.1}$$

For the present work, the parameters influencing vertical loads at the wheel hubs were examined. Loads at the wheel are of great importance as they indicate which loads are transmitted to the full vehicle by the road. Longitudinal loads were considered secondary at this point, as they are examined in more detail in Section 4.2.4 where acceleration and deceleration are included. It is also common practice to analyse different directions in space individually [23].

Vertical loads are mainly induced by the vertical profile of the road. Therefore, the customer dictates the damage based on the roads that are ridden. However, the rider also influences the loads by choosing the vehicle's velocity. These two factors span a two-dimensional matrix. In the present work, velocities were simulated from $5\,\mathrm{m\,s^{-1}}$ to $60\,\mathrm{m\,s^{-1}}$ to cover the entire possible customer spectrum. The roughness classes from the ISO 8608 [24] classify the vertical profile of a road segment and range from A-H. A is a very smooth road, while H is a very rough road. The modelling of virtual roads with different roughness classes is explained in Section 4.2.3.

For each combination of roughness class and vehicle speed, a straight-line simulation of 200 metres was run to calculate forces with the simulation model as road segments up to this length can be regarded with a constant variance regarding the vertical profile according to Johannesson and Rychlik [25]. The forces were then used to determine the pseudo-damage for equal time windows of one second. The resulting matrix $\mathbf{D}$, see Table 4.2, contains all combinations of road types and velocities as well as an associated value for the pseudo-damage which will henceforth be called damage score.

Now, for each customer k, the collected data of roughness class and vehicle velocity that occurred at the same time can be extracted and used to find the respective value

Table 4.2 – Damage matrix **D** for vertical excitation.

	Velocity ($\mathrm{m\,s^{-1}}$)											
ISO Class	5	10	15	20	25	30	35	40	45	50	55	60
H	$d_{8,1}$	$d_{8,2}$	$d_{8,3}$	$d_{8,4}$	$d_{8,5}$	$d_{8,6}$	$d_{8,7}$	$d_{8,8}$	$d_{8,9}$	$d_{8,10}$	$d_{8,11}$	$d_{8,12}$
G	$d_{7,1}$	$d_{7,2}$	$d_{7,3}$	$d_{7,4}$	$d_{7,5}$	$d_{7,6}$	$d_{7,7}$	$d_{7,8}$	$d_{7,9}$	$d_{7,10}$	$d_{7,11}$	$d_{7,12}$
F	$d_{6,1}$	$d_{6,2}$	$d_{6,3}$	$d_{6,4}$	$d_{6,5}$	$d_{6,6}$	$d_{6,7}$	$d_{6,8}$	$d_{6,9}$	$d_{6,10}$	$d_{6,11}$	$d_{6,12}$
E	$d_{5,1}$	$d_{5,2}$	$d_{5,3}$	$d_{5,4}$	$d_{5,5}$	$d_{5,6}$	$d_{5,7}$	$d_{5,8}$	$d_{5,9}$	$d_{5,10}$	$d_{5,11}$	$d_{5,12}$
D	$d_{4,1}$	$d_{4,2}$	$d_{4,3}$	$d_{4,4}$	$d_{4,5}$	$d_{4,6}$	$d_{4,7}$	$d_{4,8}$	$d_{4,9}$	$d_{4,10}$	$d_{4,11}$	$d_{4,12}$
C	$d_{3,1}$	$d_{3,2}$	$d_{3,3}$	$d_{3,4}$	$d_{3,5}$	$d_{3,6}$	$d_{3,7}$	$d_{3,8}$	$d_{3,9}$	$d_{3,10}$	$d_{3,11}$	$d_{3,12}$
B	$d_{2,1}$	$d_{2,2}$	$d_{2,3}$	$d_{2,4}$	$d_{2,5}$	$d_{2,6}$	$d_{2,7}$	$d_{2,8}$	$d_{2,9}$	$d_{2,10}$	$d_{2,11}$	$d_{2,12}$
A	$d_{1,1}$	$d_{1,2}$	$d_{1,3}$	$d_{1,4}$	$d_{1,5}$	$d_{1,6}$	$d_{1,7}$	$d_{1,8}$	$d_{1,9}$	$d_{1,10}$	$d_{1,11}$	$d_{1,12}$

from the matrix and add all values up in order to obtain the total damage score. Equation 4.2 shows how the total damage score d_{tot} is calculated with the number of occurrences $n_{i,j}(k)$ for each entry and the respective damage score $d_{i,j}$ from the matrix. The total damage score can finally be compared for all customers and the design-relevant customer can be chosen for in-depth analysis based on the chosen percentile. The upper limit for the variable i is the number of roughness classes which is constantly 8 and the upper limit for the variable j is the number of simulated velocities J. The value of J influences simulation duration but also accuracy. If more velocities are simulated, the classified data from the customer can be assigned to a bin that is closer to the real velocity. However, increasing the resolution too much will lead to more simulation duration. Therefore, a compromise between the two has to be made. In the present work, the step size was set to $5\,\mathrm{m\,s^{-1}}$, resulting in $J = 12$.

$$d_{\mathrm{tot}}(k) = \sum_{i=1}^{8} \sum_{j=1}^{J} n_{i,j}(k) d_{i,j}. \tag{4.2}$$

The damage scores enable a qualitative evaluation in terms of durability. However, they cannot exactly represent LTFs as each segment is examined separately. This issue will be handled in the upcoming sections.

4.2.3 Recreation of virtual roads

After identifying the design-relevant customer based on general parameters, a virtual track for the simulation of realistic LTFs can be created. Using the approaches from [2], it is possible to classify roughness classes of roads and detect curves. The roughness classification utilises the signals for the front and rear suspension displacements along with the vehicle's velocity. The output is the roughness class according to the ISO 8608 each second and the respective travelled distance. The curve classification also utilises the vehicle's velocity and the banking angle. A curve is detected when a certain threshold of the banking angle is exceeded to prevent the detection of parking and overtaking manoeuvres. For each curve, the length, mean curvature, and maximum curvature are stored.

The vertical profiles of the virtual roads can be modelled each second based on the power spectral density (PSD) of the roughness class according to the ISO 8608. With the proposed straight-line fit and fixed slope w from the ISO , the roughness coefficient $G_\mathrm{d}(f)$ can be calculated according to Equation 4.3, with $G_\mathrm{d}(f_0)$ being the PSD at the defined reference spatial frequency f_0.

$$G_\mathrm{d}(f) = G_\mathrm{d}(f_0)\left(\frac{f}{f_0}\right)^{-w} \quad \text{with} \quad f_0 = 0.1\,\text{cycles/m} \quad \text{and} \quad w = 2, \tag{4.3}$$
$$\text{for} \quad 0.011\,\text{cycles/m} < f < 2.83\,\text{cycles/m}.$$

Different methods to create a synthetic road profile based on the roughness class exist. The method employed in the present work is the superpositioning of sine curves. It has been applied and reviewed in other publications [2, 26–34]. The elevation of the road profile z_R can be determined with Equations 4.4–4.8. The I sine curves have different amplitudes A_i for the spatial frequencies f_i and phase angles Φ_i. The amplitudes can be obtained with $G_\mathrm{d}(f_i)$ from Equation 4.3. The PSD $G_\mathrm{d}(f_0)$ at the reference spatial frequency f_0 can be extracted from Table 4.3. Δf is the increment of the spatial frequency. The minimum and maximum values for the spatial frequencies are the same as in Equation 4.3. The number of superposed sine curves should be high enough and was set to 1000 to ensure an adequate resolution. The phase angles are taken from the uniform distribution $\mathcal{U}$. As the vertical profile is generated through a random process, scatter can be considered when generating

Table 4.3 – Reference values and descriptions according to [2].

ISO Class	$G_\mathrm{d}(f_0)$ $(10^{-6}\,\mathrm{m}^3)$	Description
A	16	Airport runways and superhighways
B	64	Normal pavements
C	256	Unpaved roads and damaged pavements
D	1024	Rough unpaved roads
E	4096	Enduro tracks
F	16384	Off-road tracks
G	65536	Rough off-road tracks
H	262144	Simulation purpose only

a vertical profile for the whole track multiple times which is part of later sections.

$$z_\mathrm{R}(x) = \sum_{i=1}^{I} A_i \sin\left(2\pi f_i x + \Phi_i\right), \tag{4.4}$$

$$A_i = \sqrt{G_\mathrm{d}(f_i)\Delta f}, \tag{4.5}$$

$$f_i = f_1 + (i-1)\Delta f, \tag{4.6}$$

$$\Delta f = \frac{f_I - f_1}{I-1} \quad \text{with} \tag{4.7}$$

$$f_1 = 0.011\,\mathrm{cycles/m},\, f_I = 2.83\,\mathrm{cycles/m} \quad \text{and} \quad I = 1000,$$

$$\Phi_i = \mathcal{U}[0, 2\pi). \tag{4.8}$$

Figure 4.3 shows the PSD of a synthetic vertical profile for the roughness class C. The PSD in the Figure was smoothed according to the algorithm presented in [2] in order to highlight that the PSD can be assigned to one specific roughness class.

The sine curve approach was used in addition to the one-line fit of the PSDs because the classification that served as a database also utilises this assumption. Other methods to create synthetic road profiles based on a target spectrum are reviewed in [31]. More complex models that require additional parameters or measurements from real roads can be found in [25, 35–37]. The more complex models include two- and three-line fits for the PSD or statistical models where the non-stationary and non-homogenous behaviour of real roads is considered. However, it is generally accepted with the current state of the art that by using synthetic road profiles LTFs

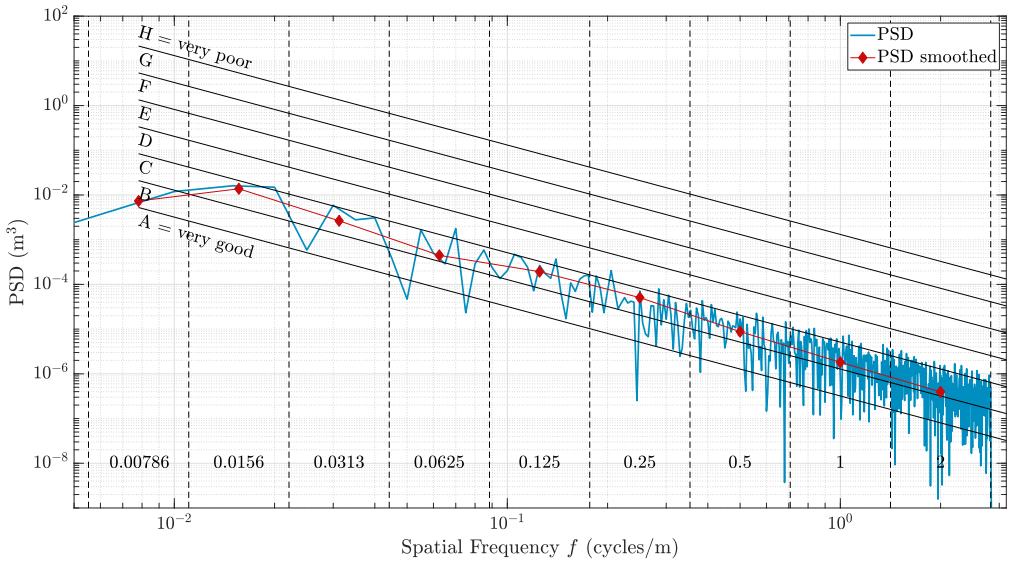

Figure 4.3 – PSD of synthetic road with roughness class C.

cannot be recreated exactly. They rather enable a qualitative evaluation of target quantities related to the interaction of vehicle and road [32, 38].

After creating the vertical profile, the trajectory can be virtualised by recreating curves and straights. A straight segment connects two consecutive curves and the modelling is trivial. The curve modelling is of importance here. As mentioned by Karlsson [23], curves can be described by a trapezoid approximation that displays the change in curvature. The curvature starts at 0 which equals a straight path and rises linearly until the maximum curvature is reached. The curvature stays at the maximum and decreases linearly afterwards until the end of the curve where a straight segment starts again. The linear change in curvature is also known as clothoid. In the present work, another assumption had to be made in order to recreate curves. It was specified that a curve is symmetrical which means that the clothoids at the start and the end of the curve have an equal length. With the total length of the curve s_{tot}, the maximum curvature c_{max}, and the mean curvature $\tilde{c}$, each curve can be characterised. As mentioned in [39], the maximum curvature is expected to have the biggest influence on the loads. Figure 4.4 depicts the trapezoidal shape of the curvature. The length of the clothoids s_1 and s_3 as well as the length of the maximum curvature segment s_2 can be calculated with Equations 4.9–4.11.

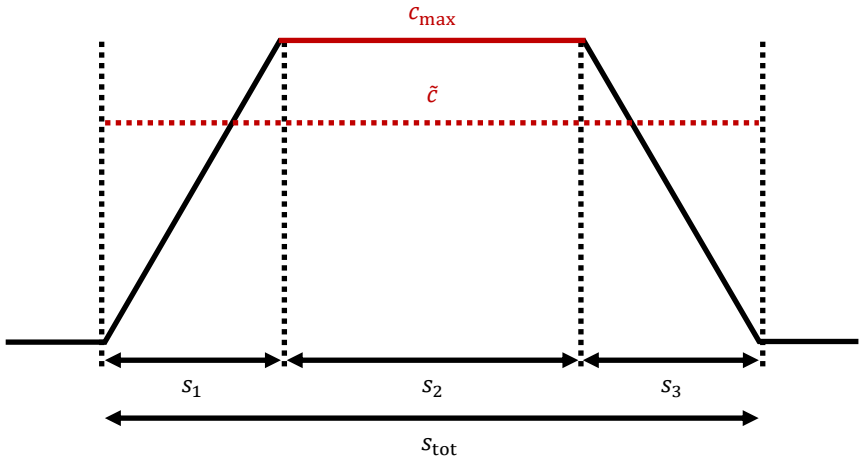

Figure 4.4 – Symmetric trapezoid approach.

$$s_1 = s_{\text{tot}} \left(1 - \frac{\tilde{c}}{c_{\max}}\right), \tag{4.9}$$

$$s_2 = s_{\text{tot}} - 2s_1, \tag{4.10}$$

$$s_3 = s_1. \tag{4.11}$$

The final obtained track contains relevant road characteristics that induce loads and influence the riding style combined with the rider's skills.

4.2.4 Generation of speed profiles

The simplest way to assign a speed profile is to take the measured average velocities for each time window. However, scatter in the riding style has to be considered by running simulations for different riders. Not always does a higher velocity lead to higher loads which will be highlighted in Section 4.3.1.

Generating speed profiles has been the subject of other publications. Karlsson [23] modelled the speed in curves for trucks through a regression where the logarithm of

curvature and speed have a linear relation. The author states that for wider curves other aspects like traffic density or speed limits are the restricting factors. Slimi et al. [40] created a maximum speed profile in curves for motorcycles, including vehicle dynamics, friction, and road geometry. Cossalter et al. [41] showed how an optimal riding manoeuvre can be determined leading to the minimum time for the respective manoeuvre. Speckert et al. [39] modelled the speed profile of four-wheeled vehicles based on traffic density models. Additionally, the driver in their model tries to drive as fast as possible within certain limits of longitudinal and lateral accelerations. This model was utilised in [42] where a tolerance factor was used in order to take into account that customers might not follow the legal speed limit. Biedinger [43] also used the model for her analyses. A comparison of an aggressive and a careful driver for a passenger car showed that the riding style has a relevant influence on loads. Pettersson et al. [44] used a lateral acceleration threshold $a_{\mathrm{lat,th}}$ to define the maximum curve speed v_{max} for four-wheeled vehicles according to Equation 4.12.

$$v_{\mathrm{max}} = \sqrt{\frac{a_{\mathrm{lat,th}}}{c}}. \tag{4.12}$$

The approach in the present work aims to virtualise the customer behaviour of motorcyclists with classified data. It is not required to optimise manoeuvres, control systems, or lap times on race tracks. Instead, road and rider characteristics are taken into account in order to create representative speed profiles. As Will et al. [45] demonstrated, motorcyclists have different riding patterns. These riding patterns can be detected with gg-diagrams where the longitudinal and lateral accelerations are plotted. These diagrams indicate which maximum accelerations are dared as well as a combination of both directions. The distribution of the occurring accelerations looks different for beginners than for experts which was also described by Spiegel [46]. While beginners have lower maximum accelerations and rarely combine both directions in space, experts nearly exploit the whole available acceleration. Shinagawa et al. [47] stated that the longitudinal and lateral accelerations a_{lon} and a_{lat} can be described by a circle that indicates which combination of longitudinal and lateral acceleration is possible, see Equation 4.13. This assumption is based on the more known circle of friction.

$$\sqrt{a_{\mathrm{lon}}^2 + a_{\mathrm{lat}}^2} \leq \mu\, \mathrm{g} \quad \text{with} \quad \mu = 1. \tag{4.13}$$

Table 4.4 – Maximum simulated or proposed velocities in the literature.

Reference	Maximum velocity for road class ($\mathrm{m\,s^{-1}}$) A	B	C	D	E
Jaksic et al. [51]	41.67	41.67	41.67	41.67	41.67
Reza-Kashyzadeh et al. [52]	19.44	19.44	19.44	19.44	19.44
Zhang et al. [53]	33.33	33.33	33.33	33.33	33.33
Huang et al. [54]	33.33	25.00	13.89	8.33	–
Xiao and Zhu [55]	–	–	13.89	1.94	–
Múčka [38]	27.78	27.78	8.61	2.22	0.83
Gorges et al. [2]	60.00	50.00	30.00	20.00	10.00
Vasquez [34]	–	10.00	–	40.00	–

Equations 4.12 and 4.13 were also employed in the present work. Traffic density and speed limits were not considered as motorcyclists tend to behave differently in these situations. Often, they are not constrained by traffic jams because they pass standing vehicles either between or outside of the traffic lanes. This is a very dangerous behaviour and often illegal, but very common. Additionally, motorcyclists are more likely to exceed legal speed limits as mentioned in [48–50].

With the methods presented so far, the generation of speed profiles is possible during curves. For straight segments, an additional criterion has to be defined. This criterion is based on the idea that with higher roughness classes the velocity has to be reduced in order to maintain ride comfort and safety which was also explored by Múčka [38] for a simple quarter-car model. Waser [17] also states that the road roughness limits travelling speed in a natural way. Table 4.4 shows simulated or proposed velocities in other publications.

Most publications defined almost arbitrary velocities to make qualitative comparisons for their respective research question. However, the table shows that some authors already considered that with higher roughness classes the velocity has to decrease. In the present publication, this idea was implemented as each roughness class r was assigned a maximum velocity $v(r)$. Together with the acceleration thresholds g_{th}, three different synthetic riders were defined. Synthetic riders had to be used as no real customer data is available currently. The *beginner* is a motorcycle rider that has little to no experience and will, therefore, ride with velocities lower or equal to the speed limit. The rider will also not perform high acceleration manoeuvres.

Table 4.5 – Thresholds synthetic riders.

		$v(r)$ $(\mathrm{m\,s^{-1}})$				
Rider type	g_{th} (g)	A	B	C	D	E
Beginner	0.36	36	28	17	8	5
Advanced	0.68	48	39	23	14	8
Expert	1.00	60	50	30	20	10

Spiegel [46] states, that there is a natural banking angle of 20 degrees that a beginner will not exceed. This equals a lateral acceleration of 0.36 g. The maximum velocities were chosen based on speed limits of roads that are representative of the roughness classes in Germany. The *advanced* rider was given thresholds in the middle of the two other riders. Lastly, the *expert* rider was given the full acceleration threshold of 1 g. The maximum velocities were defined based on Table 4.3 and the velocities listed in [2]. These velocities are perceived as realistic velocities for real motorcycle customer usage and were also derived from [56]. The three synthetic rider types are listed in Table 4.5.

After all thresholds have been defined, the algorithm to create a speed profile for a given virtual track can be employed. The algorithm predicts the velocity for each upcoming time step based on the circumstances. Road and rider characteristics are included by considering the roughness class, the curvature, and the thresholds of the rider from Table 4.5. The initial speed is solely defined based on the roughness and curvature as no previous time step exists where accelerations need to be considered.

The first step of the algorithm is to determine how much longitudinal acceleration is possible. Figure 4.5a shows the workflow of this step. First, the current curvature $c(i)$ is determined based on the position on the trajectory. This curvature is then used to calculate the current lateral acceleration $a_{\mathrm{lat,curr}}$. Based on the gg-diagram the maximum possible longitudinal acceleration a_{gg} is calculated. As the gg-diagram is symmetrical, the maximum possible deceleration has the same absolute value but a negative sign, see Figure 4.5b.

With a_{gg}, the maximum and minimum possible velocities $v_{\mathrm{max,ap}}$ and $v_{\mathrm{max,an}}$ at the next time step can be calculated and, additionally, the interval where the vehicle will be located at the next time step. That interval is the current position plus the interval of $x_{\mathrm{pos,min}}$ and $x_{\mathrm{pos,max}}$. Now the roughness classes and curvatures can be

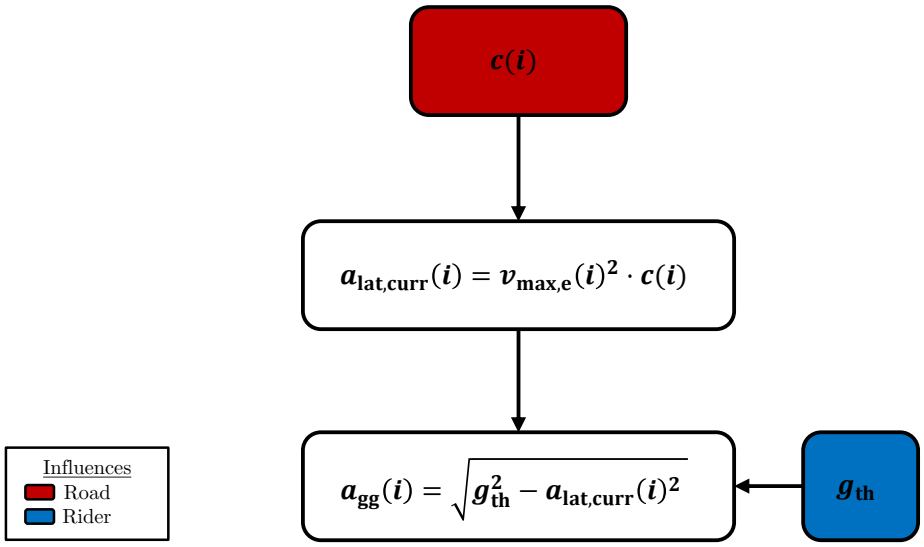

(a) Workflow a_{gg}

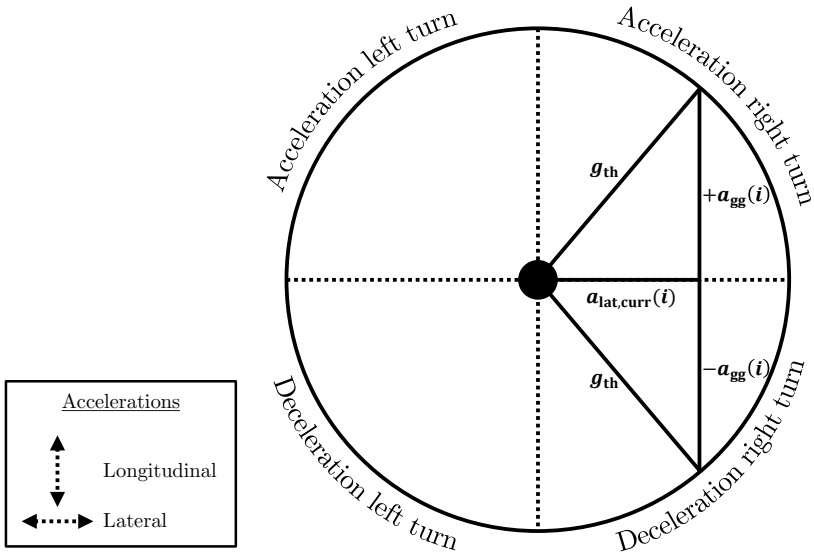

(b) gg-diagram - circle approach

Figure 4.5 – Determination of maximum possible longitudinal acceleration.

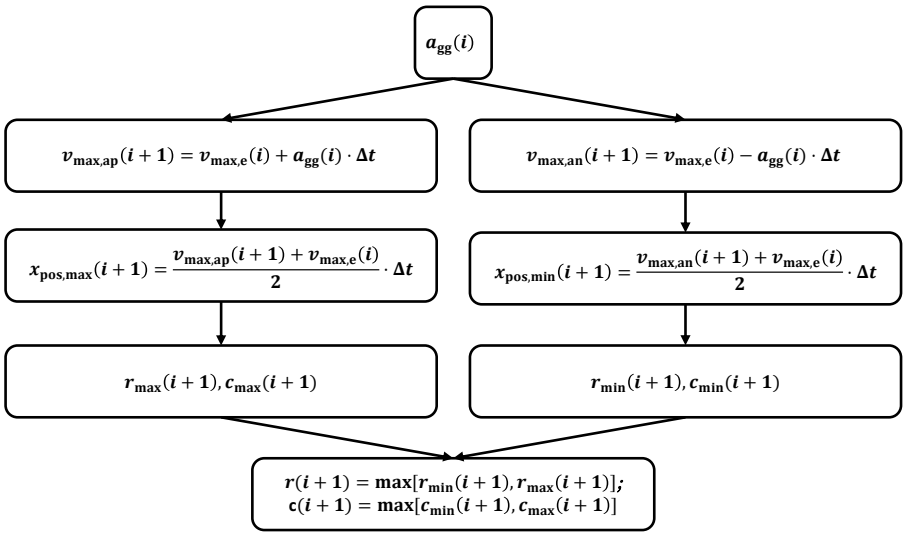

Figure 4.6 – Estimation of roughness and curviness for upcoming time step.

determined for the two boundaries of the interval (r_{min}, r_{max}, c_{min}, c_{max}). These values are then compared and the greater ones are taken in order to obtain the final values r and c respectively for the next time step, see Figure 4.6. This ensures that the worst-case is considered. The assumption is made that there is no worse road condition between the two boundaries. This is a valid assumption when the sampling rate is not too low. In the present work, the speed profile was calculated with a frequency of 10 Hz. With a maximum acceleration of 1 g, this leads to a maximum difference between $x_{\text{pos,min}}$ and $x_{\text{pos,max}}$ of less than 0.1 metre which is negligible.

After the roughness class and curvature are determined, a maximum velocity can be defined according to the workflow in Figure 4.7. g_{th} is taken from Table 4.5 to calculate the maximum velocity $v_{\text{max,c}}$ based on the curvature. $v(r)$ is also taken from Table 4.5 to calculate the maximum velocity $v_{\text{max,r}}$ based on the roughness class. The minimum of both velocities is the threshold defining the maximum velocity $v_{\text{max,s}}$ based on both road characteristics for the next time step.

Hereafter, it has to be checked whether $v_{\text{max,s}}$ lies between the boundaries of $v_{\text{max,ap}}$ and $v_{\text{max,an}}$. If the value is inside the boundaries, it is chosen as the next velocity $v_{\text{max,e}}$, see Figure 4.8a and 4.8c. If $v_{\text{max,ap}}$ is lower than the value, $v_{\text{max,ap}}$ is the next

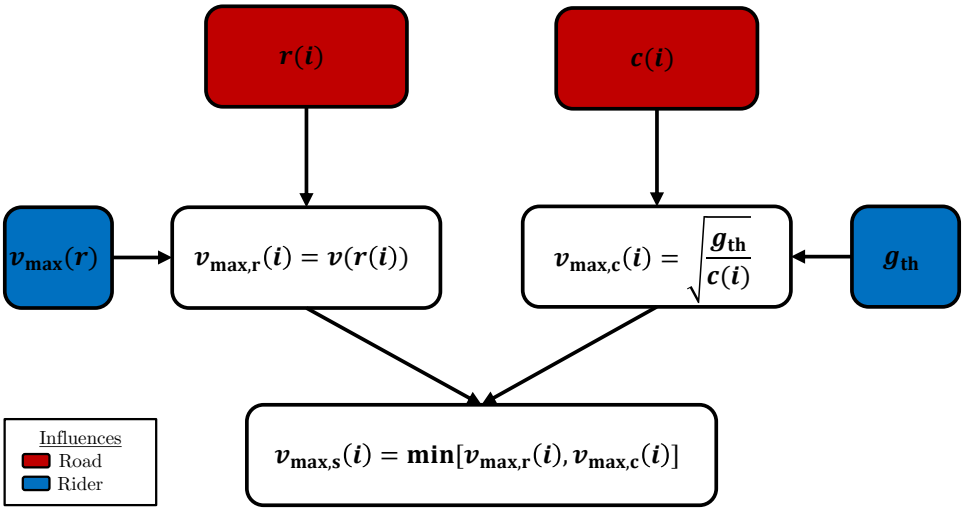

Figure 4.7 – Determination of maximum velocity based on road characteristics.

velocity for the speed profile because the rider cannot accelerate enough to reach $v_{\mathrm{max,s}}$, see Figure 4.8b. The same strategy cannot be applied for the fourth case, see Figure 4.8d. Here $v_{\mathrm{max,s}}$ is lower than $v_{\mathrm{max,an}}$. The rider can only decelerate until $v_{\mathrm{max,an}}$ but should not be allowed to ride with a velocity higher than $v_{\mathrm{max,s}}$. Hence, the velocity has to be adjusted in the current time step by Δv. Additionally, it has to be checked if the new velocity $v_{\mathrm{max,e,n}}$ is inside the acceleration and deceleration boundaries at the current time step. If that is the case, the algorithm can move on without any changes except for the one at the current time step, see Figure 4.9a. If the calculated $v_{\mathrm{max,e,n}}$ is outside the boundaries, the algorithm needs to go back another time step and adjust the maximum velocity there as well, see Figure 4.9b. This procedure is repeated as many steps as necessary.

4.3 Results

4.3.1 Damage scores

First, the maximum vertical loads at the front wheel hub were analysed for the vertical excitation simulations. The reason was that Gorges et al. [57] postulate that with rising velocity and roughness class the loads shift from service to special event

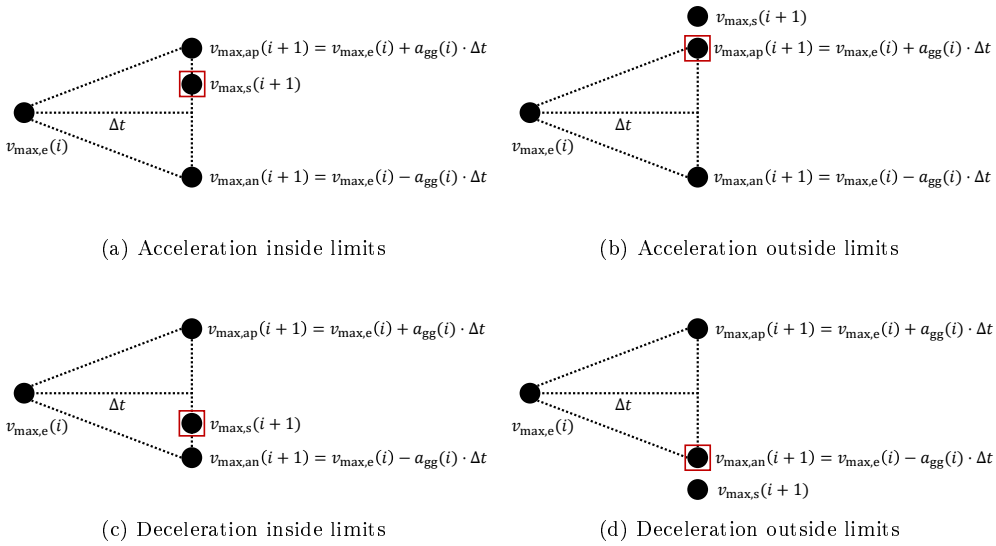

(a) Acceleration inside limits

(b) Acceleration outside limits

(c) Deceleration inside limits

(d) Deceleration outside limits

Figure 4.8 – Checking of longitudinal acceleration thresholds.

and finally to misuse event loads. It is important to specify load categories as misuse events are not part of the intended purpose and can lead to plastic deformations. Special events also have to be fused separately from service loads as these loads are often related to impact situations that occur infrequently but have a big influence on the damage. The hypothesis was, however, not verified in their publication. With virtual models and synthetic roads, it is possible to analyse the influences objectively. The maximum load was extracted for each simulation and entered in the matrix. The hypothesis and the validation are shown in Figure 4.10. The upper limit for service loads which equals the lower limit for special event loads was set to the highest measured value during the measurement campaign of service loads for the real motorcycle. The same procedure was applied for the special event loads where the upper limit equals the lower limit of misuse event loads. The values are presented normalised to the upper limit of service loads.

The Figure demonstrates that the hypothesis is valid, as the shapes of the load categories are similar. Roughness classes from A to C are classified as service loads as well as higher roughness classes with lower velocities except roughness class H. However, as listed in Table 4.3, this roughness class is only used for simulations and is not a realistic road. Special event loads are mainly part of roughness classes D, E,

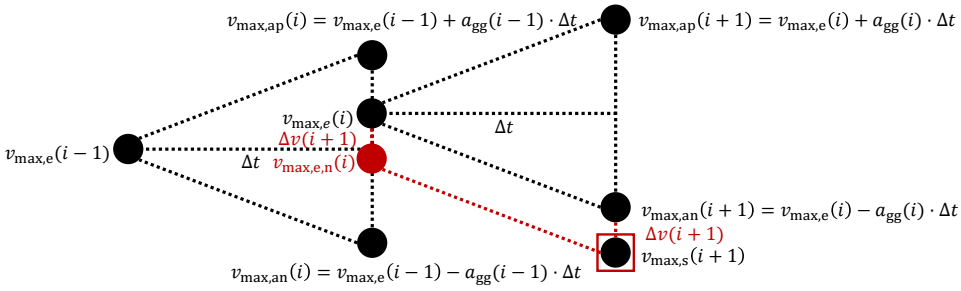

(a) One time step

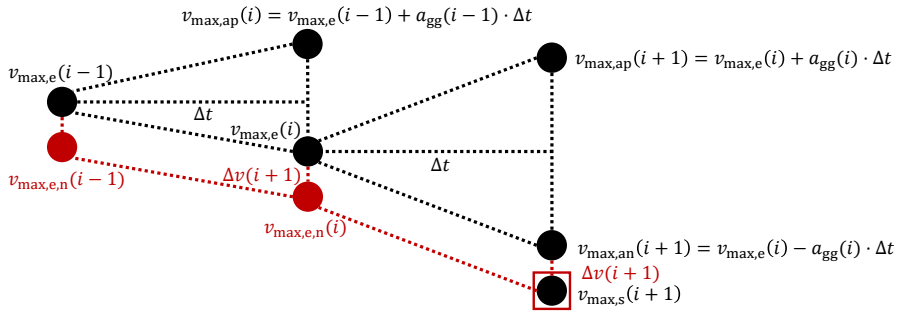

(b) Multiple time steps

Figure 4.9 – Recursive adjustment.

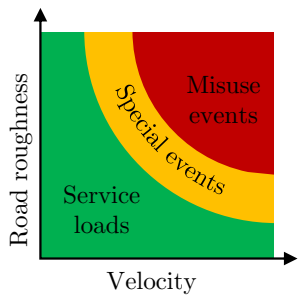

(a) Literature hypothesis [57]

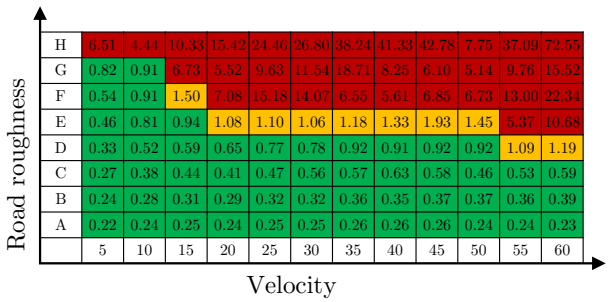

H	6.51	4.44	10.33	15.42	24.46	26.80	38.24	41.33	42.78	7.75	37.09	72.55
G	0.82	0.91	6.73	5.52	9.63	11.54	18.71	8.25	6.10	5.14	9.76	15.52
F	0.54	0.91	1.50	7.08	15.18	14.07	6.55	5.61	6.85	6.73	13.00	22.34
E	0.46	0.81	0.94	1.08	1.10	1.06	1.18	1.33	1.93	1.45	5.37	10.68
D	0.33	0.52	0.59	0.65	0.77	0.78	0.92	0.91	0.92	0.92	1.09	1.19
C	0.27	0.38	0.44	0.41	0.47	0.56	0.57	0.63	0.58	0.46	0.53	0.59
B	0.24	0.28	0.31	0.29	0.32	0.32	0.36	0.35	0.37	0.37	0.36	0.39
A	0.22	0.24	0.25	0.24	0.25	0.25	0.26	0.26	0.26	0.24	0.24	0.23
	5	10	15	20	25	30	35	40	45	50	55	60

(b) Simulation results

Figure 4.10 – Load categories - vertical excitation.

Table 4.6 – Simulation results damage matrix **D** for $F_{Z,\mathrm{ft}}$.

	Velocity ($\mathrm{m\,s^{-1}}$)											
ISO Class	5	10	15	20	25	30	35	40	45	50	55	60
H	–	–	–	–	–	–	–	–	–	–	–	–
G	12292	14415	–	–	–	–	–	–	–	–	–	–
F	833	10981	–	–	–	–	–	–	–	–	–	–
E	268	4367	10840	–	–	–	–	–	–	–	–	–
D	6.63	598	2096	2407	4056	4271	4509	7289	7649	7563	–	–
C	0.38	35	151	210	422	628	896	914	1146	709	1358	1234
B	0.02	1.00	6.84	6.82	13	38	71	99	114	157	302	175
A	0.00	0.04	0.23	0.25	0.33	0.96	1.18	2.44	3.35	3.96	10	10

and F with medium to high velocities.

Hereafter, the damage score matrices were created for the wheel loads. Table 4.6 shows the matrix for the vertical force at the front wheel. The damage score was calculated each second as the onboard roughness classification also delivers results for each second. Afterwards, the median value was extracted and entered into the matrix. The values were normalised with regard to the damage score for $10\,\mathrm{m\,s^{-1}}$ and the roughness class B which portrays travelling on normal pavement with moderate speed.

The tables display that loads and damages do not necessarily rise with higher velocities. If this were so, the values would have to rise row- and column-wise which is not the case. Hence, the vehicle dynamics play a major role as the interaction with the road excitations affects the loads. This can also be observed in the real world where certain roads cause fewer vibrations if ridden faster. Apart from that, the values generally rise column-wise which indicates that higher roughness classes induce higher loads. The empty fields in the matrix represent simulations where special and misuse event loads occurred according to Figure 4.10. These loads are not part of the scope for the present work. Furthermore, loads of this magnitude lead to simulation instabilities as the virtual rider cannot control the vehicle anymore which can also be the case for real riders.

The fact that riding manoeuvres on the same roughness class with the same velocity can lead to different loads is depicted in Table 4.7 where the damage scores for the simulation with $10\,\mathrm{m\,s^{-1}}$ and the roughness class A to E are sorted from minimum to maximum damage during each time window for $F_{Z,\mathrm{ft}}$. Each column

Table 4.7 – Pseudo-damages for $F_{Z,\mathrm{ft}}$ - roughness classes A-E and $10\,\mathrm{m\,s^{-1}}$.

Time-window	Pseudo-damage / roughness class A	B	C	D	E
1	0.17	0.30	0.06	0.52	0.51
2	0.29	0.35	0.42	0.60	0.52
3	0.58	0.36	0.44	0.61	0.53
4	0.59	0.37	0.45	0.65	0.56
5	0.60	0.65	0.58	0.67	0.57
6	0.67	0.67	0.66	0.75	0.69
7	0.80	0.69	0.67	0.76	0.75
8	0.81	0.72	0.86	0.86	0.81
9	0.93	0.88	0.95	0.87	0.88
10	0.97	0.92	0.99	0.90	0.94
Median	1.00	1.00	1.00	1.00	1.00
11	1.03	1.08	1.01	1.10	1.06
12	1.11	1.11	1.30	1.16	1.10
13	1.20	1.12	1.35	1.25	1.19
14	1.31	1.25	1.46	1.53	1.37
15	1.67	1.32	1.51	1.57	1.41
16	1.86	1.50	1.54	1.58	1.45
17	2.20	1.95	1.82	1.63	1.51
18	2.31	2.07	2.05	1.74	1.74
19	2.59	2.45	2.19	1.94	1.78
20	3.59	2.74	2.39	2.12	2.36

was normalised separately in relation to the median value. The deviation between the different entries allows the consideration of scatter by using the damage score matrices and highlights the importance of doing so.

In order to evaluate whether the matrices allow a rough estimation of the occurring damage, the data from the measurement was used to calculate the damage score for the longitudinal and vertical forces at both wheels. The distribution of $n_{i,j}(k)$ resulting from the classification algorithms is presented in Table 4.8.

The table shows that the majority of the track is ridden with higher velocities on roughness classes A and B. Also, all occurring entries are part of service loads. Hereafter, the damage scores were calculated and compared to the total damages

Table 4.8 – $n_{i,j}(k)$ from measurement.

	Velocity ($\mathrm{m\,s^{-1}}$)											
ISO Class	5	10	15	20	25	30	35	40	45	50	55	60
H	0	0	0	0	0	0	0	0	0	0	0	0
G	0	0	0	0	0	0	0	0	0	0	0	0
F	0	0	0	0	0	0	0	0	0	0	0	0
E	0	0	0	0	0	0	0	0	0	0	0	0
D	0	0	0	0	2	0	0	0	0	0	0	0
C	0	0	0	4	18	8	9	2	0	0	0	0
B	0	0	5	17	31	34	27	2	0	0	0	0
A	1	4	14	10	25	22	19	1	0	0	0	0

Table 4.9 – Quotient damage score matrices and measurement.

Load	Minimum	Median	Maximum
$F_{X,\mathrm{ft}}$	0.04	0.10	0.37
$F_{X,\mathrm{rr}}$	0.01	0.03	0.23
$F_{Z,\mathrm{ft}}$	0.87	1.86	4.90
$F_{Z,\mathrm{rr}}$	1.24	2.70	7.52

that were calculated with the rainflow counting for the measured wheel loads. Table 4.9 shows the quotient between the calculated damages from the matrices and the measurement. The target value is one and would mean that the approximation exactly matches the measurement. Values above one represent an overestimation of the damage from the simulations. Values below one represent an underestimation. The quotient was calculated for the median values that were entered in the matrices and also for the minimum and maximum values that were determined for each matrix entry as in Table 4.7.

The results show that the damages for the longitudinal forces are too low in the simulations. This is, however, expected as only constant velocities were simulated for the damage score matrices. Hence, loads resulting from acceleration and braking are not considered. The damages for the vertical forces, on the other hand, can be better estimated. Especially, the results at the front wheel are more accurate as the target value lies within the calculated interval.

4.3.2 Comparison of virtual tracks

In order to increase accuracy and reduce scatter, simulations can be run on a recreated virtual track with a continuous speed profile.

As the MBS model could only be used for straight-line simulations, the developed method to recreate a virtual track could only be validated without cornering manoeuvres. In order to still evaluate the presented symmetric trapezoid approach, the GPS signal from the measurement was compared with the calculated trajectory based on the classified data.

The differences between the resulting trajectories are shown in Figure 4.11a. They result from the symmetric trapezoid approach and segments with small banking angles being classified as straights, see Figure 4.11b. Also, the banking angle and GPS data that are collected onboard have an imprecision. The figures illustrate the idea behind the entire approach. The goal is not to recreate a road identically in the virtual world but to rather build a similar road with a minimum dataset.

In the present work, the virtual track that was used for MBS was created nine times based on the classified data for the roughness classes and the velocity. Figure 4.12 illustrates the measured and simulated loads for one simulation normalised with respect to the particular measurement signal.

The figures demonstrate that the course of the signals can be matched. However, some outliers occur and the amplitudes for the longitudinal forces are smaller in the simulations. The vertical forces show sufficient agreement. The deviation for the front wheel vertical force between 170 and 180 seconds results from a cornering manoeuvre during the measurement where high lateral loads occurred which could not be considered due to the straight-line simulation. Table 4.10 lists the quotient between the recreated simulation and the measurement. Again, minimum, median, and maximum values were determined from all nine simulations for each load separately.

Figure 4.13 shows boxplots for the analysed loads in comparison with the results from the damage score matrices. The damages for the more precise simulations and the damage score matrices are marked with (S) and (D) respectively.

The figure shows that the scatter for the damages was reduced immensely by recreating a continuous virtual track and speed profile. Only the scatter at the front wheel in the longitudinal direction increases slightly. Nevertheless, the target value

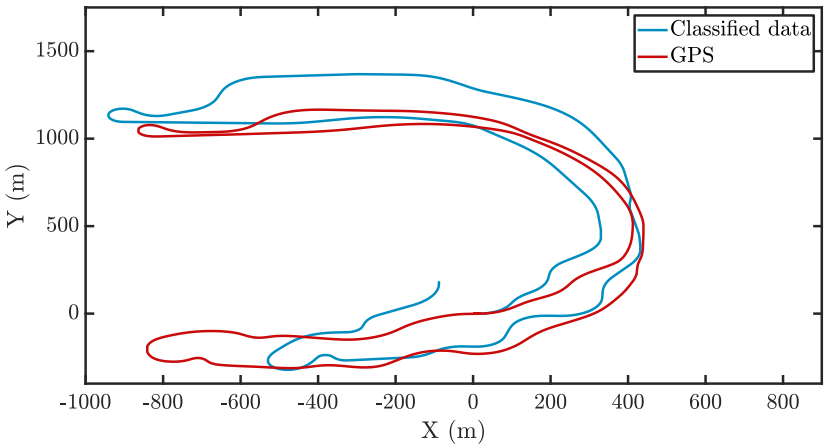

(a) Trajectory

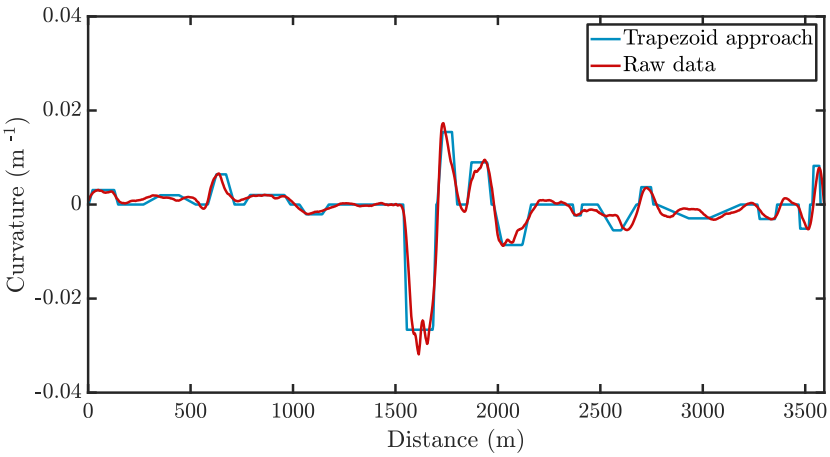

(b) Curvature

Figure 4.11 – Comparison for classified data.

Table 4.10 – Quotient recreated simulations and measurement.

Load	Minimum	Median	Maximum
$F_{X,\mathrm{ft}}$	0.34	0.72	1.59
$F_{X,\mathrm{rr}}$	0.12	0.14	0.18
$F_{Z,\mathrm{ft}}$	1.67	1.87	2.15
$F_{Z,\mathrm{rr}}$	1.55	1.70	2.35

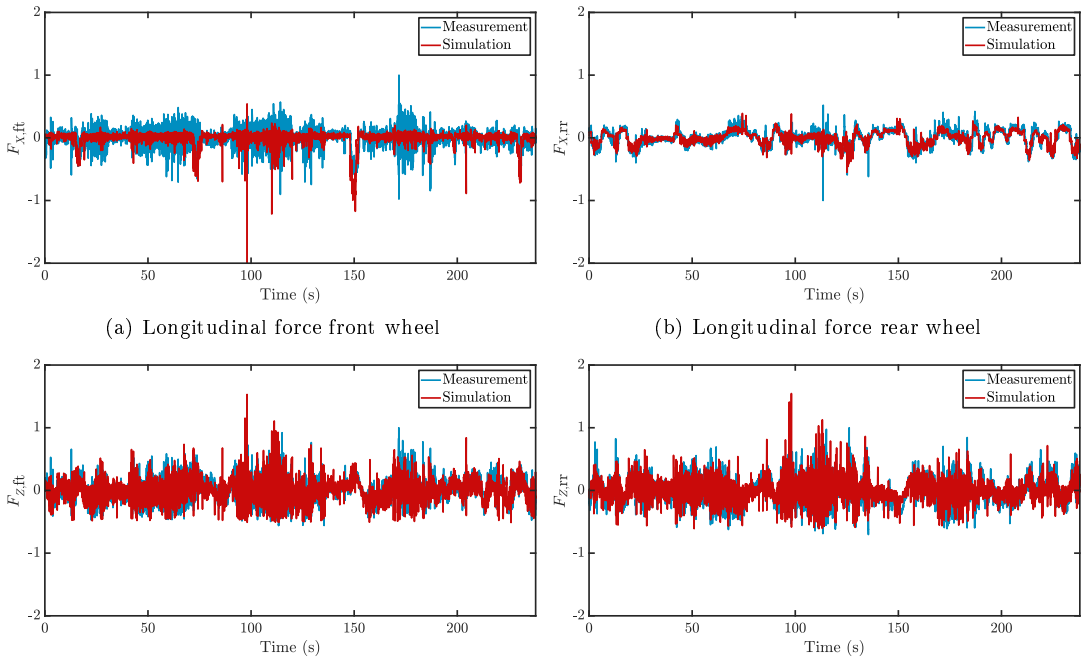

(a) Longitudinal force front wheel

(b) Longitudinal force rear wheel

(c) Vertical force front wheel

(d) Vertical force rear wheel

Figure 4.12 – Load comparison simulation and measurement.

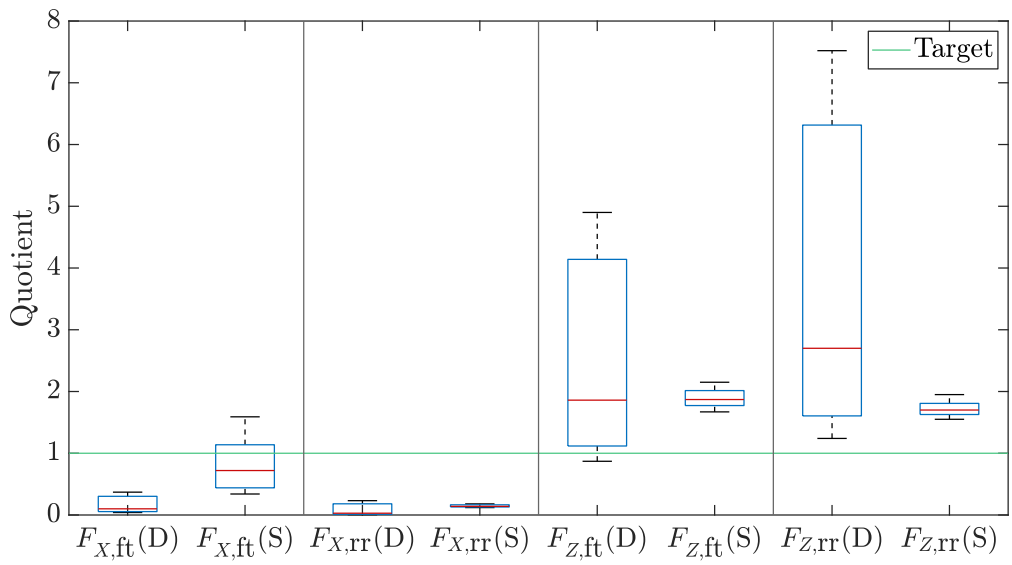

Figure 4.13 – Comparison damage score matrices and recreated simulations.

Table 4.11 – Results synthetic riders and roads.

Analysis No.	Rider type	Round	Duration (s)	Pseudo-damages $F_{X,\mathrm{ft}}$	$F_{X,\mathrm{rr}}$	$F_{Z,\mathrm{ft}}$	$F_{Z,\mathrm{rr}}$
1	Beginner	1	352	0.15	0.20	0.55	0.29
2	Beginner	2	352	0.06	0.30	0.48	0.40
3	Beginner	3	352	0.16	0.21	0.45	0.33
4	Advanced	1	255	1.35	1.03	1.07	0.87
5	Advanced	2	255	1.00	1.00	1.00	1.00
6	Advanced	3	255	0.50	1.26	0.80	1.08
7	Expert	1	204	4.40	0.88	1.70	1.57
8	Expert	2	204	4.64	1.04	1.57	1.38
9	Expert	3	204	3.66	1.29	1.30	1.34

moves inside the boundaries of the box and is closer to the median. For the other loads, an improvement for the median value towards the target value could also be achieved.

4.3.3 Rider influence

In order to create further scatter, the test track was simulated three times for each of the three riders from Table 4.5 which resulted in a total of nine simulations. The generated speed profiles for the riders are highlighted in Figure 4.14a. Figures 4.14b and 4.14c show exemplary segments of the speed profile for the *expert*. Figure 4.14b highlights that the defined speed profile $v_{\mathrm{max,e}}$ is between the acceleration and deceleration limits of $v_{\mathrm{max,ap}}$ and $v_{\mathrm{max,an}}$. Figure 4.14c demonstrates that the maximum velocity $v_{\mathrm{max,s}}$ is correctly chosen from the maximum velocity based on roughness $v_{\mathrm{max,r}}$ and curvature $v_{\mathrm{max,c}}$. Furthermore, the final defined speed profile $v_{\mathrm{max,e}}$ is oriented towards $v_{\mathrm{max,s}}$ but is not equal when the needed deceleration would lead to leaving the boundaries of the gg-diagram. Here, the speed is adapted in the previous time steps, for example, up to the 2250 m mark.

The different durations for the same virtual track as well as the different pseudo-damages for the nine conducted analyses are listed in Table 4.11 and visualised in Figure 4.15. The pseudo-damage was set in relation to the median value from the analyses which was the second simulation of the advanced rider for every load.

The difference in time is enormous compared to race scenarios where split seconds

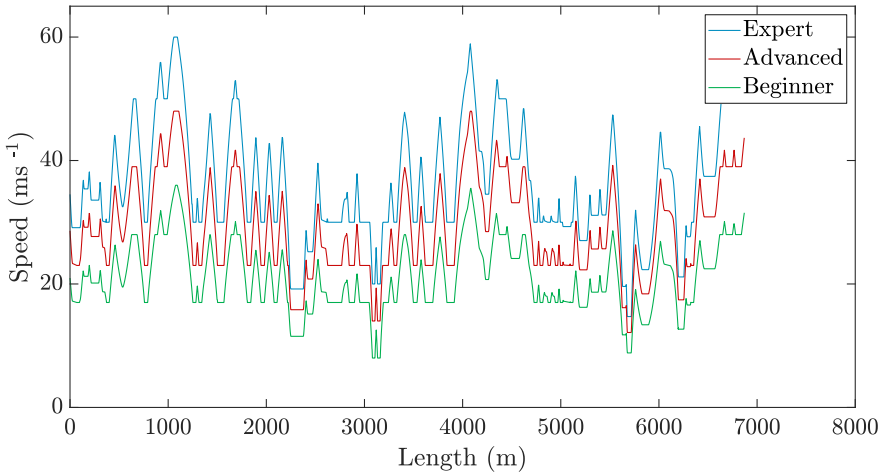

(a) Synthetic speed profiles

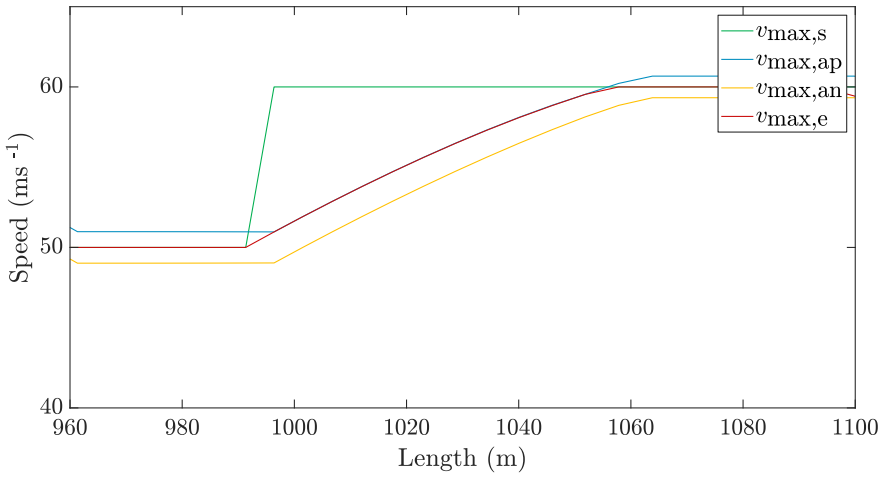

(b) Checking of acceleration thresholds

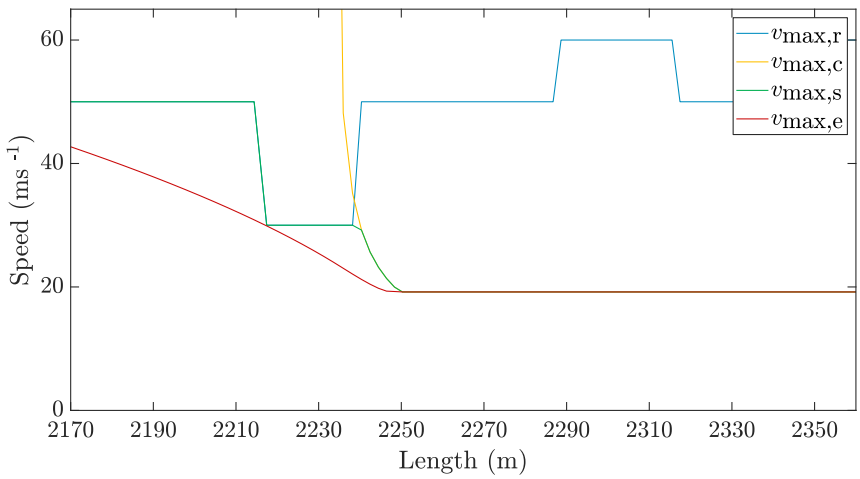

(c) Speed profile adjustment detail

Figure 4.14 – Overview speed profile results.

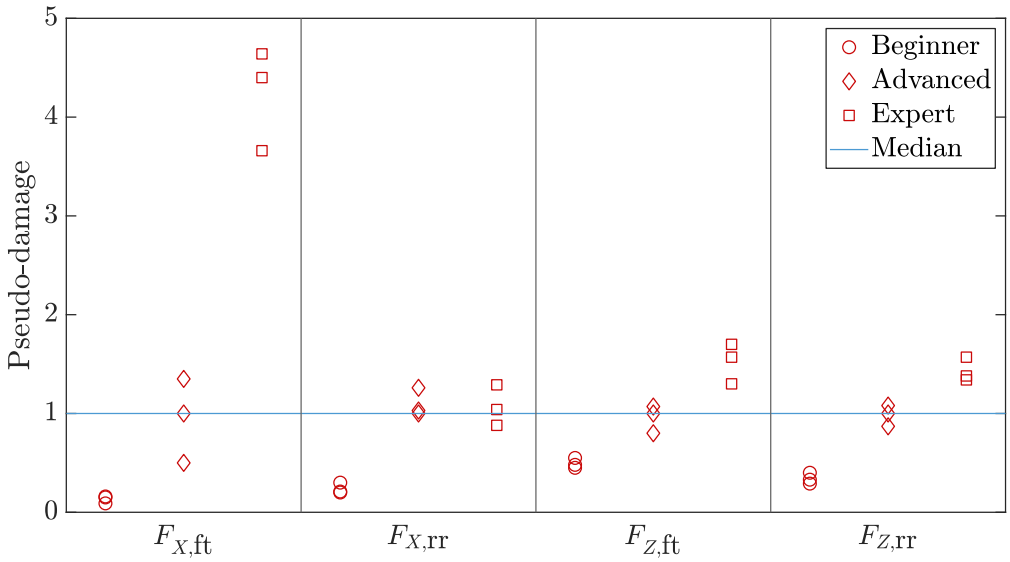

Figure 4.15 – Pseudo-damages for synthetic riders.

decide the winner of a race. The longitudinal force at the front wheel is significantly lower for the beginner compared to the advanced rider and even more so compared to the expert. This is also expected as harsh accelerations and decelerations as well as a higher velocity cause higher loads. Similar observations can be made for the two vertical forces. Here, the effect is not as great, however. This means that the influence of the road itself is greater than the riding style for this direction. Lastly, the longitudinal force at the rear wheel also shows that the beginner causes lower damage. However, there is no significant difference between the advanced and expert rider.

4.4 Discussion

The present work showed how road and rider characteristics can be transferred to the virtual world and used for MBS in order to make load assumptions.

First, a method was presented that enables the identification of design-relevant customers based on damage score matrices. The damage scores can be calculated with MBS models and synthetic virtual roads with less expenditure compared to a simulation of a complete customer usage profile as each possible combination of

roughness and velocity is simulated only once. The roughness classes from the ISO 8608 were utilised to create vertical excitations. It was shown that the matrices deliver first reliable results, especially for vertical loads. The influence of roughness class and velocity on the load category was, further on, examined in order to ensure that only service loads are simulated using the developed methods. The damage scores were assessed for the longitudinal and vertical wheel forces. Inner loads could be analysed in the future. Including inner loads would make it possible to identify design-relevant customers for different components. The assumption that would still have to be satisfied is that the load of interest results predominantly from vertical excitations. It was also shown that the random process used for the generation of vertical road profiles leads to scatter in damage. This scatter should be further investigated and also analysed with measurements of a real motorcycle riding on a variety of roughness classes with a wide range of velocities. This would enable a comparison between the scatter of the approach and real roads. Also, the influence of different loading conditions was not included. The extension of the method to include this aspect is, however, simple as multiple MBS models with pillion or luggage can be modelled and simulated. Lastly, the influencing factors on lateral loads were not examined with the damage score approach. This can be part of upcoming studies. A relevant influence is, for example, the lateral acceleration resulting from velocity and curviness. Additionally, the approach can be extended for longitudinal loads. Different matrices could be created with acceleration and braking manoeuvres of different magnitude.

Furthermore, an approach was described to recreate tracks in the virtual world based on classified data of curves and roughness. For curves, a symmetric trapezoid approach was utilised. For the vertical profile, a common sinusoidal approach was employed. It was demonstrated that the obtained virtual road differs in trajectory, and in the resulting loads when used for simulations. This is, however, expected as the goal of the approach is to recreate virtual roads that include the main characteristics based on a minimum dataset that can be collected onboard. Moreover, the classification algorithms are already subject to inaccuracy. Still, the accuracy could be increased while scatter was decreased in comparison to the damage score approach. An important aspect that should be incorporated in the future is the consideration of curved segments also for the MBS. The model in the present work could only be

used for straight-line simulations. However, a great interdependency exists between the different loads when performing a cornering manoeuvre. Hence, the neglection of these manoeuvres also reduces accuracy for other loads that are analysed. Other aspects leading to deviations due to neglection are the banking of the road and the friction coefficient that can vary due to weather conditions, for example. Nevertheless, these influences have a smaller impact compared to the incorporated aspects. Further on, the approximation of the vertical profile by a superposition of sine curves can also lead to deviations as the real vertical profile might differ. More complex models could be used instead. Another important factor is the rider. Especially for motorcycles, the influence is relevant as the rider moves his or her body and applies loads on the handlebar and footrests. For the model in the present work, the rider was attached rigidly to the frame. Including the mentioned aspects is expected to increase the accuracy when comparing simulations and measurements. The altitude or hilliness was also not modelled in the present work. In order to integrate the hilliness, a trigger would have to be defined which indicates when a hilly segment starts and ends. For the curves, this was possible, as the banking angle indicates whether a cornering manoeuvre is being performed. Furthermore, the influence of hilliness on the rider's behaviour is not clear currently and could, therefore, not be included in the generation of the speed profile. The measurements in the present work did not include hilly tracks which makes the omission of this factor reasonable. Still, the influence of hilliness on loads and especially riding behaviour should be part of future research.

Lastly, a novel method was introduced to generate speed profiles. The method considers customer behaviour in terms of performed accelerations and maximum velocities. The accelerations are used to calculate maximum velocities in curves and also maximum accelerations and decelerations in the longitudinal direction. Additionally, roughness classes are used to define thresholds for the maximum velocity in segments where the curvature plays a minor role. In the present work, only synthetic riders were defined and the acceleration thresholds were set to a constant value, but maximally 1 g. Values higher than this can be implemented easily but require special pairing of tyre and road properties. Furthermore, the motorcycle analysed in the present work is not a sports bike where higher accelerations would be expected. In the future, the method can be applied to real customer data by substituting the

thresholds based on collected data. Furthermore, the thresholds do not have to be static and can be altered throughout the speed profile. This would result in speed profiles where a certain customer does not ride at his capacity limit constantly. One way is to consider real gg-diagrams. In doing so, each lateral acceleration is not assigned one specific value based on an analytical equation. Instead, different longitudinal accelerations are possible each with different probability of occurrence depending on the specific customer. The probabilities could be included by carrying out Monte Carlo simulations. The thresholds for the maximum velocity based on roughness classes should also be examined with real customer data from the field in the future.

References

[1] R. Mayrböck and A. Mayr. 'Numerische und experimentelle Methoden zur Lastdatenermittlung an Teilmodellen eines Motorrades'. In: *DVM Bericht 143; 2016 Oct 12-13; Steyr*. Berlin: DVM, 2016, pp. 93–106.

[2] C. Gorges, K. Öztürk and R. Liebich. 'Road classification for two-wheeled vehicles'. In: *Vehicle System Dynamics* 56.8 (2018), pp. 1289–1314.

[3] C. Matz. 'Online Berechnung von Fahrwerkskräften auf Basis von Onboard-Sensorik'. PhD thesis. Technische Universität Clausthal, 2016.

[4] L. Müller. 'Mehrkörpermodell-basiertes Online Monitoring der Betriebsbeanspruchung am Beispiel eines Nutzfahrzeug-Demonstrators'. PhD thesis. TU Kaiserslautern, 2011.

[5] C. Gorges, K. Öztürk and R. Liebich. 'Customer loads of two-wheeled vehicles'. In: *Vehicle System Dynamics* 55.12 (2017), pp. 1842–1864.

[6] A. Rupp, A. Masieri and T. Dornbusch. 'Durability transfer concept for the monitoring of the load and stress conditions on vehicles'. In: *Innovative Automotive Technology* (2005), pp. 1–8.

[7] M. Bäcker, T. Langthaler, M. Olbrich and H. Oppermann. 'The hybrid road approach fro durability loads prediction'. In: *SAE Technical Paper* 2005-01-0628 (2005).

[8] M. Bergold, S. Brandes, B. Seufert and D. Bestle. 'Simulation von Kundenmanövern zur Ermittlung repräsentativer Fahrwerksbelastungen'. In: *DVM Bericht 146; 2019 Oct 9-10; Wolfsburg*. Berlin: DVM, 2019, pp. 99–114.

[9] D. O. Kang, H. Seungjin and K. Hoiyoung. 'Virtual road profile modeling using equivalent damage method for VPG simulation'. In: *SAE Technical Paper* 2009-01-0814 (2009).

[10] D. O. Kang, K. Park, S.-J. Heo, Y.-I. Ryu and J. I. Jeong. 'Development and application of VPG simulation technique based on equivalent virtual road profile'. In: *International Journal of Precision Engineering and Manufacturing* 11.2 (2010), pp. 265–272.

[11] H. Kollmer, F. Küçükay and K. Pötter. 'Measurement and fatigue damage evaluation of road profiles in customer operation'. In: *International Journal of Vehicle Design* 56 (2011), pp. 106–124.

[12] A. Londhe and S. Kangde. 'Virtual Road Approach for Vehicle Durability Simulations'. In: *SAE International Journal of Passenger Cars-Mechanical Systems* 6 (2013), pp. 876–881.

[13] M. Morr, T. Minor and T. Maulick. 'Messdatenbasierte virtuelle Lastdatenermittlung für Fahrwerksbauteile und Karosserie'. In: *DVM Bericht 143; 2016 Oct 12-13; Steyr.* Berlin: DVM, 2016, pp. 107–120.

[14] N. Rönicke, A. Ams, S. Brandes and B. Seufert. 'Simulationsgestütztes Design einer Schlechtwegoberfläche für ein neues Automobil-Prüfgelände'. In: *DVM Bericht 143; 2016 Oct 12-13; Steyr.* Berlin: DVM, 2016, pp. 151–164.

[15] N. Roy and M. Villaire. 'Virtual road load data acquisition using full vehicle simulations'. In: *SAE Technical Paper* 2013-01-1189 (2013).

[16] S. R. Waser, W. Hirschberg, T. Ille and V. Mladek. 'Evaluierung von Reifen- und Fahrbahnmodellen für die Simulation festigkeitsrelevanter Beanspruchungen von Nutzfahrzeugen'. In: *VDI Berichte, Reifen-Fahrwerk-Fahrbahn.* Düsseldorf: Springer-VDI-Verlag GmbH & Co. KG, 2007, pp. 153–165.

[17] S. R. Waser. 'Generierung der beanspruchungsrelevanten Belastungen von Nutzfahrzeugen mittels Reifen-, Fahrbahn-und Fahrzeugmodellen'. PhD thesis. TU Graz, 2009.

[18] T. Weber. 'Betriebslasten in der Fahrzeugentwicklung - Simulation Gesamtfahrzeug'. In: *DVM Bericht 141; 2014 Oct 8-9; Ingolstadt.* Berlin: DVM, 2014, pp. 115–128.

[19] M. Gipser. 'FTire–the tire simulation model for all applications related to vehicle dynamics'. In: *Vehicle System Dynamics* 45 (2007), pp. 139–151.

[20] S. Engelmann. 'Simulation von fahrwerkdominierten Misuse–Lastfällen zur Unterstützung der virtuellen Crashsensorik'. PhD thesis. Helmut-Schmidt-Universität / Universität der Bundeswehr Hamburg, 2013.

[21] E. Haibach. *Betriebsfestigkeit.* Berlin, Heidelberg: Springer Berlin Heidelberg, 2006.

[22] P. Johannesson and M. Speckert. *Guide to load analysis for durability in vehicle engineering.* Chichester: Wiley, 2014.

[23] M. Karlsson. 'Load modelling for fatigue assessment of vehicles–a statistical approach'. PhD thesis. Göteborg University, 2007.

[24] ISO. *Mechanical vibration - Road surface profiles - Reporting of measured data.* Standard No. 8608:2016. Geneva, Switzerland: ISO, 2016.

[25] P. Johannesson and I. Rychlik. 'Modelling of road profiles using roughness indicators'. In: *International Journal of Vehicle Design* 66.4 (2014), pp. 317–346.

[26] L. Sun. 'Simulation of pavement roughness and IRI based on power spectral density'. In: *Mathematics and computers in simulation* 61.2 (2003), pp. 77–88.

[27] A. González, E. J. O'brien, Y.-Y. Li and K. Cashell. 'The use of vehicle acceleration measurements to estimate road roughness'. In: *Vehicle System Dynamics* 46.6 (2008), pp. 483–499.

[28] F. Tyan, Y.-F. Hong, S.-H. Tu and W. S. Jeng. 'Generation of random road profiles'. In: *Journal of Advanced Engineering* 4.2 (2009), pp. 1373–1378.

[29] H. M. Ngwangwa, P. S. Heyns, F. J. Labuschagne and G. K. Kululanga. 'Reconstruction of road defects and road roughness classification using vehicle responses with artificial neural networks simulation'. In: *Journal of Terramechanics* 47.2 (2010), pp. 97–111.

[30] M. Agostinacchio, D. Ciampa and S. Olita. 'The vibrations induced by surface irregularities in road pavements–a Matlab® approach'. In: *European Transport Research Review* 6.3 (2014), pp. 267–275.

[31] A. Haigermoser, B. Luber, J. Rauh and G. Gräfe. 'Road and track irregularities: measurement, assessment and simulation'. In: *Vehicle System Dynamics* 53.7 (2015), pp. 878–957.

[32] G. Loprencipe and P. Zoccali. 'Use of generated artificial road profiles in road roughness evaluation'. In: *Journal of Modern Transportation* 25.1 (2017), pp. 24–33.

[33] A. Alfadhli, J. Darling and A. J. Hillis. 'The control of an active seat with vehicle suspension preview information'. In: *Journal of Vibration and Control* 24.8 (2018), pp. 1412–1426.

[34] F. Vasquez. 'Optimisation of off-road motorcycle suspensions'. PhD thesis. University of Southampton, 2020.

[35] K. Bogsjö. 'Road profile statistics relevant for vehicle fatigue'. PhD thesis. Lund University, 2007.

[36] K. Bogsjö, K. Podgórski and I. Rychlik. 'Models for road surface roughness'. In: *Vehicle System Dynamics* 50.5 (2012), pp. 725–747.

[37] P. Múčka. 'Longitudinal road profile spectrum approximation by split straight lines'. In: *Journal of transportation engineering* 138.2 (2012), pp. 243–251.

[38] P. Múčka. 'Simulated road profiles according to ISO 8608 in vibration analysis'. In: *Journal of Testing and Evaluation* 46.1 (2017), pp. 405–418.

[39] M. Speckert, K. Dreßler, N. Ruf, T. Halfmann and S. Polanski. 'The Virtual Measurement Campaign VMC concept-a methodology for georeferenced description and evaluation of environmental conditions for vehicle loads and energy efficiency'. In: *Proceedings of the 3rd Commercial Vehicle Technology Symposium; 2014 Mar 11-13; Kaiserslautern.* Aachen: Shaker, 2014, pp. 88–98.

[40] H. Slimi, H. Arioui, L. Nouvelière and S. Mammar. 'Motorcycle speed profile in cornering situation'. In: *Proceedings of the 2010 American Control Conference; 2010 Jun 30- Jul 2; Baltimore.* New York City: IEEE, 2010, pp. 1172–1177.

[41] V. Cossalter, R. Lot and D. Tavernini. 'Optimization of the centre of mass position of a racing motorcycle in dry and wet track by means of the "optimal maneuver method"'. In: *IEEE International Conference on Mechatronics (ICM); 2013 Feb 27- Mar 1; Vicenza.* New York City: IEEE, 2013, pp. 412–417.

[42] M. Speckert, M. Lübke, B. Wagner, T. Anstötz and C. Haupt. 'Representative road selection and route planning for commercial vehicle development'. In: *Proceedings of the 5th Commercial Vehicle Technology Symposium; 2018 Mar 13-15; Kaiserslautern.* Aachen: Shaker, 2018, pp. 117–128.

[43] C. Biedinger. 'Automatic Usage Modeling for Automotive Applications'. PhD thesis. TU Kaiserslautern, 2019.

[44] P. Pettersson, S. Berglund, B. Jacobson, L. Fast, P. Johannesson and F. Santandrea. 'A proposal for an operating cycle description format for road transport missions'. In: *European Transport Research Review* 10.2 (2018), pp. 1–19.

[45] S. Will, B. Metz, T. Hammer, M. Mörbe, M. Henzler, F. Harnischmacher and G. Matschl. 'Methodological considerations regarding motorcycle naturalistic riding investigations based on the use of gg diagrams for rider profile detection'. In: *Safety Science* 129 (2020).

[46] B. Spiegel. *Die obere Hälfte des Motorrads: über die Einheit von Mensch und Maschine.* Stuttgart: Motorbuch, 2009.

[47] A. Shinagawa, H. Nozawa and T. Masuda. 'Data Analysis of Motorcycle in a Motard Race'. In: *Symposium on the Dynamics and Control of Single Track Vehicles; 2019 Sep 9-11; Padova.* 2019, pp. 1–8.

[48] D. Walton and J. Buchanan. 'Motorcycle and scooter speeds approaching urban intersections'. In: *Accident Analysis & Prevention* 48 (2012), pp. 335–340.

[49] S. Buld, S. Will, A. Kaussner and H.-P. Krüger. *Entwicklung eines Verfahrens zur Erfassung der Fahrerbeanspruchung beim Motorradfahren.* Bremen: Fachverlag NW, 2014.

[50] D. Q. Nguyen-Phuoc, C. de Gruyter, H. A. Nguyen, T. Nguyen and D. N. Su. 'Risky behaviours associated with traffic crashes among app-based motorcycle taxi drivers in Vietnam'. In: *Transportation research part F: traffic psychology and behaviour* 70 (2020), pp. 249–259.

[51] V. Jaksic, A. O'Connor and V. Pakrashi. 'Damage detection and calibration from beam–moving oscillator interaction employing surface roughness'. In: *Journal of Sound and Vibration* 333.17 (2014), pp. 3917–3930.

[52] K. Reza-Kashyzadeh, M. J. Ostad-Ahmad-Ghorabi and A. Arghavan. 'Investigating the effect of road roughness on automotive component'. In: *Engineering Failure Analysis* 41 (2014), pp. 96–107.

[53] Y. Zhang, S. C. S. Cai and L. Deng. 'Piezoelectric-based energy harvesting in bridge systems'. In: *Journal of intelligent material systems and structures* 25.12 (2014), pp. 1414–1428.

[54] B. Huang, C.-Y. Hsieh, F. Golnaraghi and M. Moallem. 'Development and optimization of an energy-regenerative suspension system under stochastic road excitation'. In: *Journal of Sound and Vibration* 357 (2015), pp. 16–34.

[55] L. Xiao and Y. Zhu. 'Sliding-mode output feedback control for active suspension with nonlinear actuator dynamics'. In: *Journal of Vibration and Control* 21.14 (2015), pp. 2721–2738.

[56] M. W. Sayers and S. M. Karamihas. *The little book of profiling.* Ann Arbor: University of Michigan, 1998.

[57] C. Gorges, K. Öztürk and R. Liebich. 'Impact detection using a machine learning approach and experimental road roughness classification'. In: *Mechanical Systems and Signal Processing* 117 (2019), pp. 738–756.

5 Discussion

5.1 Summary of the developed methods

This cumulative PhD thesis shows the development and validation of methods for virtually acquiring load data profiles with consideration of real customer behaviour.

The first publication deals with the categorisation of loads. The categories service loads, special events, misuse events, and crashes are described. The first two categories belong to the so-called intended purpose which comprises loads that have to be endured without restricting customer usage, while the latter two are not part of the intended purpose. During misuse events and crashes, plastic deformations can occur, which is why the simulation of such events with standard MBS models is not appropriate. On the other hand, the simulation of loads for the intended purpose was part of the scope of all three publications. In the first publication, special events were simulated. A test motorcycle was ridden over different obstacles on a real test track. The vehicle's dynamic behaviour and the loads at the front and rear wheel hub were validated. Therefore, it was shown that the simulation of such manoeuvres with MBS models delivers accurate results. Furthermore, a novel method to identify representative special events was introduced. With this method, it is possible to choose the most important events either for simulation studies or measurement campaigns if time is limited. For the measurement campaign in the present work, the kerb, sleeper, and bumper event lead to the highest loads. Besides the simulations, novel definitions for special and misuse events are proposed based on signal characteristics. The presented definitions make a product-independent distinction of load categories possible. Both definitions include durability related quantities, like load and damage, and put them in relation to the event character. The event character describes the fact that an event makes up a short track segment compared to the entire product lifecycle of a vehicle. This resulted in a novel key figure called damage ratio. This ratio was calculated for the measured special events and compared

with measurement from service load testing. It was shown that the damage ratio for special events is significantly higher than for service loads.

The second publication focuses on service loads. First, a variety of laser-scanned test tracks in the CRG format were analysed in terms of their roughness and the existence of curves. The roughness was classified according to the ISO 8608. For all relevant roughness classes, one straight and one curved track was used for simulations. By utilising already existing CRG tracks, it was ensured that the created MBS model could be used for the simulation of service loads. However, the main content of the publication was the development of a method for determining damage equivalent virtual tracks. For this purpose, a literature survey was first carried out which presented existing methods in the field of durability engineering related to damage equivalency. Subsequently, it was evaluated which methods are feasible for the simulation of riding manoeuvres. An omission approach was extended with a segmentation and a selection algorithm for different use cases. The developed method makes the creation of damage-equivalent virtual tracks that induce the major share of damage possible. The use cases distinguish between whether one or more tracks serve as input and whether one or multiple loads should be considered as a target quantity. The simulation duration for a synthetic customer usage profile could be decreased immensely.

The third publication deals with the implementation of customer behaviour into the virtual load data acquisition process. As simulating all customers is not feasible due to the high expenditure of time, a method was developed to identify the so-called design-relevant customer. The load profile of said customer is more severe than the loads from a certain percentile of the entire customer population. This percentile can be 50%, 90%, 95%, or 99%, for example. The method utilises classified data and synthetic manoeuvres to create damage score matrices. The classification algorithm from [46] for the roughness classes according to the ISO 8608 [47] is summarised in Appendix B. By simulating different velocities paired with different roughness classes from the ISO 8608, the damage scores can be assigned for vertical excitations. Using the synthetic manoeuvres from the matrix, simulation duration can be reduced as repeating combinations do not have to be simulated multiple times. Instead, the value from the damage score matrices can be summed up to have a scalar value to rank the customers. For example, travelling on a highway for many kilometres with

a narrow speed range can be represented with the simulation of a short segment of up to 200 metres. Comparing the matrices with measurements on a real test track, it was shown that a rough estimation can be achieved. In order to enhance accuracy, complete virtual tracks and measured speed profiles were virtualised afterwards. Based on the same dataset and implementing data for curvature, an approach to recreate virtual tracks was developed. With the superposition of sine curves, the vertical profile of the track was recreated. For the trajectory, a symmetric trapezoid approach was incorporated to model the curvature. The aim was to ascertain if a real track can be recreated based on a minimum dataset in the virtual world and whether the loads are comparable. This approach was proven with minor deviations. Lastly, a novel algorithm is demonstrated that creates a speed profile for a given virtual track and a certain customer behaviour. Again, the roughness and curvature were used as inputs. Based on rider skills, the algorithm calculates an associated profile. The skills include bearable velocities and accelerations. Depending on the roughness class, maximum velocities are defined. In parallel, the algorithm checks the current curvature and evaluates how fast the specified rider can travel without exceeding the bearable lateral acceleration limits. Additionally, it is checked if the longitudinal acceleration limit would be exceeded. If so, the algorithm adjusts the speed recursively. By varying the rider characteristics and thresholds, scatter can be considered. Scatter resulting from the vertical profile of the track can be included by creating multiple virtual tracks with the same roughness dataset as the superpositioning method involves a random process.

In conclusion, the developed methods enable a virtual load data acquisition in two different ways. Firstly, existing measurement campaigns can be transferred into the virtual world immediately by utilising MBS models of motorcycles. The feasibility of simulating special events, laser-scanned test tracks, and synthetically recreated tracks was proven in the publications. The models comprised full vehicle MBS models of motorcycles with the addition of FTire models and relevant control systems through co-simulations. Secondly, derived customer usage profiles can be used as inputs for the simulation of realistic customer load profiles. Using the presented methods, it is possible to recreate riding manoeuvres in the virtual world based on classified data from onboard signals. The implementable characteristics include the ridden roads and the rider's skills.

5.2 Implementation into the vehicle development process

The implementation into the vehicle development process can best be understood with Figure 5.1. The figure shows the well-known v-model with which the process for durability engineering can also be described [48]. The left branch includes the design, while the right branch describes the testing. First, pre-defined load cases are adapted. After first concepts have been developed, virtual models with geometry data are created in computer-aided design (CAD) systems. The following two steps cover the content of the present work. Based on the existing virtual models, MBS models can be built and used initially for the determination of special event loads. Further on, the service loads can be simulated. Both simulation types result in wheel loads and inner loads. These quantities are subsequently available for FE simulations. In these simulations, exact geometries and material properties can be integrated to derive stresses for components and to perform a holistic fatigue life assessment. In the branch of the testing, component test beds are served first of all. For this purpose, the loads that are determined via the MBS can be used as input for the excitation of a component test bed. Depending on the test bed layout, however, the result of an FE calculation can also be used as an input for test bed operation. After components have been tested, the measurements of loads are carried out with the first test drives of a prototype. Here, the assumptions made in the left branch of the v-model are checked. In the further course, system tests are carried out in which entire assemblies are excited on test beds. The last part of the durability engineering timeline is the so-called endurance run. During this run, the motorcycle is ridden many kilometres to ensure that the entire vehicle meets the requirements. Although the process is displayed sequentially, steps can be swapped or repeated. Furthermore, development loops and comparisons between different steps of the process are possible. Thus, the figure should be regarded as a simplified representation.

The above-mentioned procedure describes the general implementation into the development process. Following, the detailed application and connection of the developed methods will be described.

The present work has shown that special event manoeuvres with motorcycles can be reproduced by simulations. Similarly, the determination of resulting maximum loads is possible with sufficient accuracy. Thus, in the future, MBS models can be created in the early phases of development to simulate the maximum loads of relevant

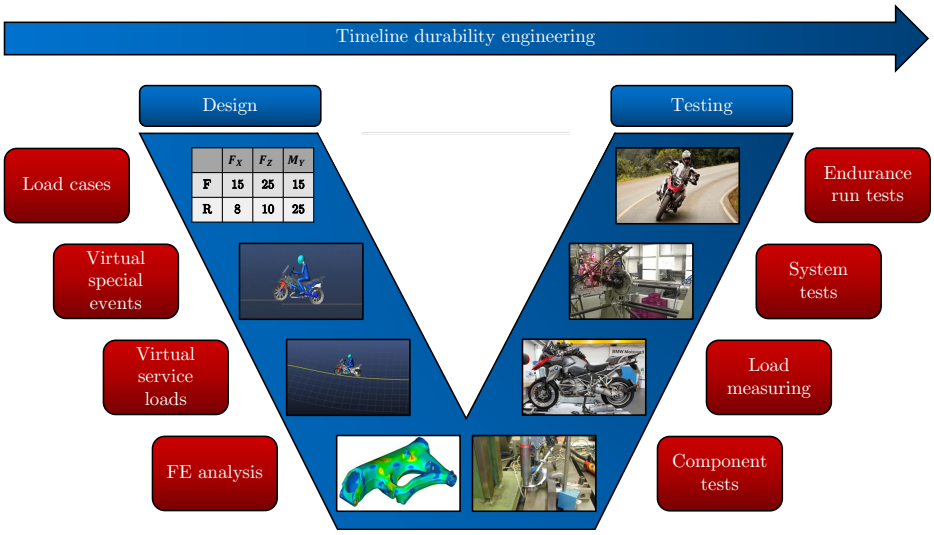

Figure 5.1 – V-model vehicle development.

components and provide further simulations and test beds with inputs as mentioned earlier. The developed method for identifying representative special events can be used to reduce either the simulation duration or measurement campaign duration by neglecting irrelevant special events. The new definition for special and misuse events can be used in the future to enable consistent handling of load categories across industries or departments. The substitution of such manoeuvres in the event of an unintentional occurrence is another use case that can be part of future research.

After special event loads have been derived, the next step is to determine service loads. In order to obtain realistic load profiles, the customer behaviour needs to be studied and integrated in the simulations. First of all, design-relevant customers have to be determined as not all motorcycle customers can be simulated due to the high expenditure of time. Using the damage score matrices, these customers can be identified for vertical excitations. After the design-relevant customers have been identified, virtual test tracks can be designed with a similar dataset. Based on rider characteristics, speed profiles can be assigned for the virtual test tracks with the developed method. With the speed profile and virtual test track, service loads for a realistic customer usage profile can be determined and used for further investigations.

Scattering can be accounted for by varying speed profiles and repeating the creation of the virtual test track multiple times. Apart from that, the developed method to recreate virtual tracks can be used to recreate real test tracks in the virtual world without expensive laser scanner measurements. Existing testing cycles containing a certain riding style and mixture of test tracks could, hence, be transferred directly into the virtual environment.

Finally, the method to create damage equivalent virtual tracks can be employed. There are multiple possibilities to combine this method with the above-mentioned methods. The first option is to identify the most damaging segments from the damage score matrices. The resulting virtual track that is created immediately contains only the relevant segments for a customer. The second option is to create a full virtual track and later on run the algorithm to detect the most damaging segments and shorten the virtual test track. This can be performed for virtual tracks obtained from the customer field or existing test tracks that are transferred into the virtual environment as mentioned above. Either way, the simulation duration can be reduced tremendously.

For all mentioned aspects, however, customer usage profiles have to be derived. Hence, enough data has to be collected and classified first. The data must then be processed in such a way that it can be used for the simulations. Afterwards, information about maximum velocities during special events and normal usage, ridden roughness classes, curves, and accelerations can be used as inputs for a holistic virtual vehicle design process using the presented methods. The end-to-end realisation of collecting customer data and making it available in the vehicle development process is discussed by Grupp et al. [49]. The authors highlight the state of the art regarding onboard classifications and possible data transfer over the air for passenger cars.

5.3 Application to other vehicles or products

The applicability of the developed methods to other vehicles or industries was an important issue for the present work. The definition of special and misuse events can be adopted one to one for every other ground vehicle. For other products, the aspect that the damage or loads occur during a short track segment could be replaced by a short time period and should be investigated in more detail. The possibility to simulate special events with MBS models has been the subject of other

publications for four-wheeled vehicles as well. However, the presented method to identify representative special events has not been applied for other vehicles and should be done in order to objectively decide which special events are of importance.

The algorithm to create damage equivalent virtual tracks can also be used for other vehicles without any limitations. Additionally, the method can be applied for other products. The distinction between different tracks, however, cannot be made and should be replaced with respective testing scenarios or operating states. Instead of track segments, time intervals could be used to partition the LTFs.

The identification of design-relevant customers based on damage score matrices is also suited for other vehicles. Therefore, it has to be assured that a comparable database is available including customer information on the roughness and driving speed. Virtual test tracks can then be created identical to the approach presented in this work. A speed profile can be assigned by defining the same parameters that were specified in the present work, namely the boundaries of the gg-diagram and the maximum velocity based on the driven roughness class. Therefore, realistic assumptions have to be made or customer data needs to be evaluated in order to derive the relevant characteristics. The method to consider scatter by simulating multiple speed profiles and creating vertical profiles via a random process can be transferred as well.

5.4 Additional studies

This section presents further studies that were conducted but not included in the previous sections due to their smaller extent or untraceable inconsistencies in simulation results.

Concept comparison:

In order to ascertain whether the representative special events depend on the vehicle concept, a first simulation study was conducted. A second motorcycle that, for example, differed in the front suspension concept was built up in ADAMS®. The previous motorcycle model will hereinafter be referred to as Model A and the new motorcycle model as Model B. All special events from Table 2.3 were simulated with Model B as well. In order to objectively compare the events, only the loads at the wheel hubs were compared. Table 5.1 lists all representative special events for the

Table 5.1 – Comparison representative special events.

Motorcycle part	Spot	Load	Representative event Model A	Model B
Front wheel	Wheel hub	F_X	Kerb	Kerb
		F_Z	Sleeper	Sleeper
Rear wheel	Wheel hub	F_X	Bumper	Sleeper
		F_Z	Bumper	Sleeper

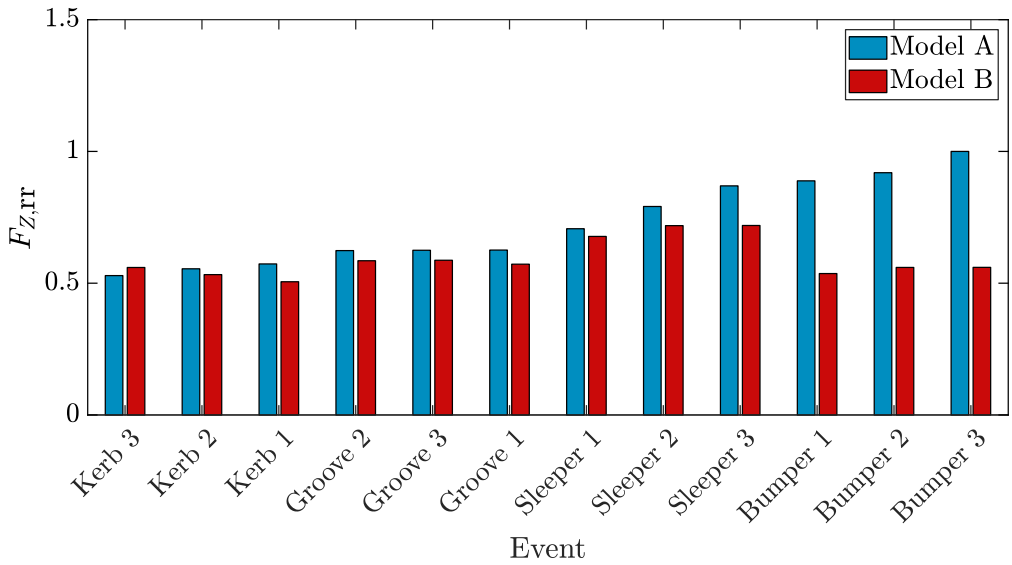

Figure 5.2 – Comparison $F_{Z,\mathrm{rr}}$ for special events.

two models and each wheel load.

The comparison at the front wheel showed that the same special events were the most decisive in terms of maximum loads. For the longitudinal direction, the kerb event was the decisive event while for the vertical direction the sleeper led to the highest loads. Unlike Model A, the highest loads in both directions at the rear wheel also occurred during the sleeper event for Model B which means that the bumper event is negligible for this motorcycle. Figure 5.2 shows the loads at the rear wheel in the vertical direction for the two models and each event.

It becomes apparent that the models differ in terms of the level of the maximum

loads but also the event which induces the maximum loads for the respective model.

Rigid bodies:

In order to decide which components can be modelled as rigid bodies in an early design stage, a study was carried out for the kerb and bumper event and all loads from Table 2.4. The components that were evaluated and modelled as rigid and flexible bodies were the same as in Figure 2.4.

A fractional factorial experimental design was used, according to the design of experiments (DOE) principle. This experimental design makes it possible to examine the effect of several parameters on a defined target quantity. In addition to the main effects, this design also provides the interactions between the parameters. The chosen parameters are the different components and have two states. The components can either be flexible or rigid. Therefore, the factors are categorical and have a nominal scaling. This means that there is no state between the rigid and the flexible modelling, as there is no such thing as a partly flexible and partly rigid body. This leads to a two-stage fractional factorial experimental design. Compared to a full fractional design the number of experiments is significantly decreased. A full factorial experimental plan with 10 factors would lead to 1024 simulations, while a fractional factorial experimental plan leads to 128 necessary simulations. The number of experiments, or in this case simulations n_{sim}, can be determined using Equation 5.1 with f being the number of factors and p being the fraction factor. The fraction factor indicates to what extent the experimental plan is reduced, compared to a full factorial design. In the present work, p was chosen to three, which means that the number of simulations was reduced by a factor of 8, as can be seen in Equation 5.2.

$$n_{\text{sim}} = 2^{f-p}, \tag{5.1}$$

$$\Leftrightarrow n_{\text{sim}} = 2^{f} \cdot \frac{1}{2^{p}}. \tag{5.2}$$

The disadvantage of fractional factorial designs is that effects are being blended. In the case of a fractional factorial design with 10 factors and a fraction factor of three, this leads to the blending of the last three factors with the interaction of four other factors and the blending of two-factor interactions with three-factor interactions.

Assigning the 10 factors letters from A to J, the blending of the last three factors can be described with Equation 5.3.

$$H = ABCG, I = BCDE, J = ACDF. \tag{5.3}$$

However, the blending can be regarded as uncritical with a resolution of V in this case. To sum up, the fractional factorial design reduces computing time significantly while focusing more on main effects and interactions of lower order. For more information on DOE as well as full and fractional factorial designs, the reader is referred to [50].

For each simulation, the maximum value of the loads was extracted. The reply variable for the DOE was defined as the absolute deviation $\Delta_{i,j}$ of the maximum load j between the simulation model consisting of all available flexible bodies $F_{\text{flex,j}}$ and the maximum load for the respective simulation of the model i containing rigid bodies $F_{i,j}$, according to Equation 5.4.

$$\Delta_{i,j} = \frac{F_{i,j} - F_{\text{flex,j}}}{F_{\text{flex,j}}} \tag{5.4}$$

The resulting deviations were afterwards analysed with the statistical softwares Minitab® and Optimus®. Different regression models and machine learning approaches were applied. However, the results were without exception not plausible. Hence, it was not possible to determine which influence the individual rigid bodies had on the accuracy of the simulation. The fact that the analyses did not provide meaningful results was discovered by looking at whether, according to the prognosis models, the model variant which consists fully of flexible bodies had the highest accuracy. This has to be fulfilled in any case since the simulation in which no rigid bodies were used was taken as the reference value $F_{\text{flex,j}}$. Hence, no deviation or only a small one should exist. This was not the case as all models suggested using some rigid bodies to reach the highest accuracy. In conclusion, the question of which bodies of a motorcycle can be modelled as rigid in MBS could not be answered with this approach. The cause are the inaccurate simulation results from ADAMS®, the resulting dataset, and not the statistical evaluation methods. In the future, other simulation models could be built up in order to check whether this specific model caused the issue or the software.

Lateral damage score matrix:

The influence for lateral loads was also examined with the MBS model from the present work. The relation between the lateral acceleration, the vehicle's velocity, and the curvature is described by Equation 5.5.

$$a_{\mathrm{lat}} = v^2 c. \tag{5.5}$$

Analogous to the vertical damage score matrices, a matrix can be created by simulating different curvatures with velocities. Hence, the customer influences the loads by two different decisions. The rider chooses if particularly curvy roads are ridden. This is especially interesting for motorcycles where enthusiasts like to travel extra curvy roads in order to experience high lateral accelerations. In this context, the customer also chooses the respective velocity for each curve based on his or her abilities.

The matrix also contains the velocities from $5\,\mathrm{m\,s^{-1}}$ to $60\,\mathrm{m\,s^{-1}}$. On the vertical axis, curvature serves as the second parameter. The simulated curvatures were calculated based on Equation 5.5 where a_{lat} was set constantly 1g. This resulted in 12 different curvatures that were used for simulation. The matrix (Table 5.2) is only filled diagonally as with rising curvature higher velocities would lead to lateral accelerations exceeding the threshold of 1g. For example, all curvatures can be paired with a velocity of $5\,\mathrm{m\,s^{-1}}$. However, the highest curvature cannot be paired with a velocity of $60\,\mathrm{m\,s^{-1}}$, because the highest curvature is based on a lateral acceleration of 1g with a velocity of $5\,\mathrm{m\,s^{-1}}$.

The design-relevant customer for lateral loads can then be identified through Equation 5.6. In order to have a standardised cornering manoeuvre, all curves and simulations were created in a way that the transition from straight to maximum curvature and vice versa was one second. The section where the maximum curvature is maintained was also set to one second.

$$d_{\mathrm{tot}}(k) = \sum_{i=1}^{I} \sum_{j=1}^{J(i)} n_{i,j}(k) d_{i,j} \quad \text{with} \quad J(i) = I - (i-1) \quad \text{and} \quad I = 12. \tag{5.6}$$

For each simulation, the damage was calculated and entered into the matrix.

Table 5.2 – Damage matrix for lateral excitation.

	Velocity ($\mathrm{m\,s^{-1}}$)											
Curvature ($\mathrm{m^{-1}}$)	5	10	15	20	25	30	35	40	45	50	55	60
0.3924	$d_{12,1}$	–	–	–	–	–	–	–	–	–	–	–
0.0981	$d_{11,1}$	$d_{11,2}$	–	–	–	–	–	–	–	–	–	–
0.0436	$d_{10,1}$	$d_{10,2}$	$d_{10,3}$	–	–	–	–	–	–	–	–	–
0.0245	$d_{9,1}$	$d_{9,2}$	$d_{9,3}$	$d_{9,4}$	–	–	–	–	–	–	–	–
0.0157	$d_{8,1}$	$d_{8,2}$	$d_{8,3}$	$d_{8,4}$	$d_{8,5}$	–	–	–	–	–	–	
0.0109	$d_{7,1}$	$d_{7,2}$	$d_{7,3}$	$d_{7,4}$	$d_{7,5}$	$d_{7,6}$	–	–	–	–	–	–
0.0080	$d_{6,1}$	$d_{6,2}$	$d_{6,3}$	$d_{6,4}$	$d_{6,5}$	$d_{6,6}$	$d_{6,7}$	–	–	–	–	–
0.0061	$d_{5,1}$	$d_{5,2}$	$d_{5,3}$	$d_{5,4}$	$d_{5,5}$	$d_{5,6}$	$d_{5,7}$	$d_{5,8}$	–	–	–	–
0.0048	$d_{4,1}$	$d_{4,2}$	$d_{4,3}$	$d_{4,4}$	$d_{4,5}$	$d_{4,6}$	$d_{4,7}$	$d_{4,8}$	$d_{4,9}$	–	–	–
0.0039	$d_{3,1}$	$d_{3,2}$	$d_{3,3}$	$d_{3,4}$	$d_{3,5}$	$d_{3,6}$	$d_{3,7}$	$d_{3,8}$	$d_{3,9}$	$d_{3,10}$	–	–
0.0032	$d_{2,1}$	$d_{2,2}$	$d_{2,3}$	$d_{2,4}$	$d_{2,5}$	$d_{2,6}$	$d_{2,7}$	$d_{2,8}$	$d_{2,9}$	$d_{2,10}$	$d_{2,11}$	–
0.0027	$d_{1,1}$	$d_{1,2}$	$d_{1,3}$	$d_{1,4}$	$d_{1,5}$	$d_{1,6}$	$d_{1,7}$	$d_{1,8}$	$d_{1,9}$	$d_{1,10}$	$d_{1,11}$	$d_{1,12}$

Table 5.3 – Simulation results lateral damage matrix for lateral force front wheel.

	Velocity ($\mathrm{m\,s^{-1}}$)											
Curvature ($\mathrm{m^{-1}}$)	5	10	15	20	25	30	35	40	45	50	55	60
0.3924	36378146	–	–	–	–	–	–	–	–	–	–	–
0.0981	9767	1298956	–	–	–	–	–	–	–	–	–	–
0.0436	37221	17190	744856	–	–	–	–	–	–	–	–	–
0.0245	23628	1640	85023	8.18	–	–	–	–	–	–	–	–
0.0157	20297	0.48	0.21	0.15	21	–	–	–	–	–	–	
0.0109	24669	52	1640	0.11	0.21	7568001	–	–	–	–	–	–
0.0080	21487	17	537	0.18	194777	1.80	4633390	–	–	–	–	–
0.0061	45736	4.43	128	0.11	52460	0.20	12	550078	–	–	–	–
0.0048	24108	4.52	51	0.08	17194	235228	160092	282138	0.25	–	–	–
0.0039	46579	0.44	17	276	6087	66953	0.16	160095	0.15	30997	–	–
0.0032	47322	1.00	4.10	128	2644	30977	0.16	0.07	0.07	30977	195352	–
0.0027	47322	0.95	4.13	51	969	12449	12449	0.07	0.07	0.05	15027043	2641

The values were normalised with regard to the damage score for $10\,\mathrm{m\,s^{-1}}$ and the curvature of $0.0032\,\mathrm{m^{-1}}$. Table 5.3 shows the results.

The table highlights that the results from the simulation are not plausible. For example, the values do not rise row- and column-wise. Furthermore, the damages on the diagonal vary immensely, although the lateral accelerations are equal. The cause is suspected to be the interaction between the MBS and rider model as the manoeuvres could not be simulated consistently. The rider which is represented by controllers in the simulation environment tries to make the motorcycle travel the given trajectory. For instance, if the current riding line deviates from the desired trajectory, a steering angle is applied. The simulation results revealed that during

some cornering manoeuvres implausible steering angles were applied by the controller. This goes to show that either the controller needs to be adjusted or that the vehicle's response to the inputs of the controller are not as expected. Thus, the interaction between vehicle and rider model should be analysed more detailed in the future.

5.5 Outlook

The present work has shown that MBS models can be used to simulate service and special event loads for motorcycles. Furthermore, methods to include customer behaviour were developed and shown to be promising. In order to include the approaches in the vehicle development, relevant customer data has to be collected or specified first. One possibility is to define so-called personas that represent a certain customer, for example, commuters, racers, or tour riders. The personas might differ in ridden roads, maximum velocities, or the gg-diagram which displays the occurring accelerations in the longitudinal and lateral direction in space. The derived characteristics can further be used to run Monte Carlo simulations, creating a whole customer population. This would account for additional scatter and implement the idea of recent publications where Monte Carlo simulations were employed to randomly mix load profiles and find reference customer load spectrums [39–44]. The method could be applied to measured maximum velocities for different roughness classes or curvatures. Further on, the distribution for the combination of longitudinal and lateral accelerations could be portrayed by taking gg-diagrams and assigning each data point a probability corresponding to the frequency of occurrence, see Figure 5.3. This data could be used to generate multiple speed profiles with the method presented in the present work, for example.

The presented damage score matrices can be used to find patterns with statistical models or machine learning. Some exemplary methods can be found in [49]. The frequency of occurrence for each matrix entry could be analysed for different customers. A typical form of presentation is the colouration for a two-parameter distribution function as depicted in Figure 5.4. The figure highlights that different

[1] Reprinted from Safety Science, 129, S. Will et al., Methodological considerations regarding motorcycle naturalistic riding investigations based on the use of g-g diagrams for rider profile detection, Copyright (2020), with permission from Elsevier.

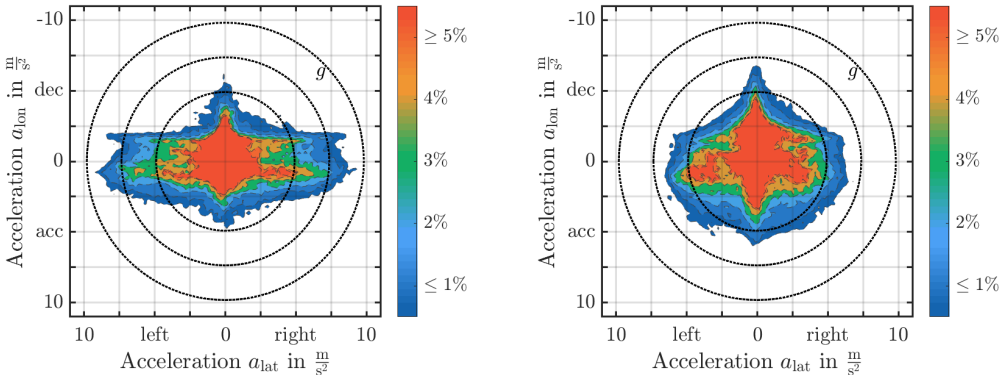

(a) Profile 1 (b) Profile 2

Figure 5.3 – GG-diagrams for different motorcycle riders[1].

areas of the engine map containing engine speed and torque can appear more often depending on riding style and the environment.

Additional damage score matrices could be created for longitudinal and lateral excitations. As a result, design-relevant customers could be identified for these directions as well. For longitudinal loads, acceleration and braking manoeuvres could be analysed. For lateral loads, the acceleration resulting from curvature and ridden velocity could be of relevance. However, the consistent simulation of cornering manoeuvres has to be ensured first. Therefore, it is important to identify suitable rider models for the ADAMS® environment as mentioned in Section 5.4.

The MBS simulations and methods can be further improved by the following investigations and enhancements:

- Retaining rigid bodies,
- determining the necessary number of modes,
- including an accurate structural damping approach,
- including rider movement,
- including differing friction coefficients,
- including road slope,

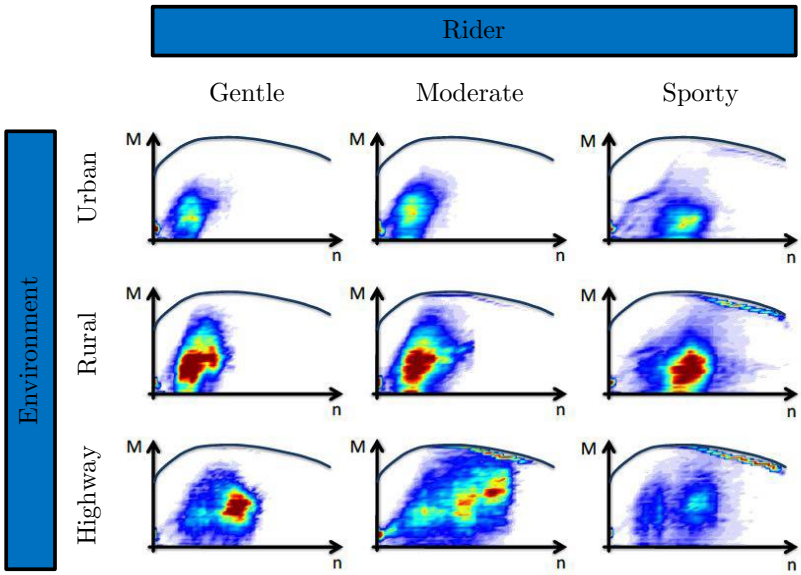

Figure 5.4 – Exemplary customer patterns for engine map.

- including road banking,
- including loading conditions.

As mentioned earlier, the implementation of flexible bodies instead of rigid bodies leads to a higher modelling effort and simulation duration. Thus, identifying components that can be retained as rigid bodies is valuable. The study in Section 5.4 did not provide plausible results. In the future, therefore, different approaches should be tested in order to answer this question methodologically. In general, it is conceivable that the validity of modelling a body rigidly increases with rising stiffness due to diminishing deformations.

A different aspect influencing the dynamic behaviour of the simulation model is the number of modes that are included to represent the flexible characteristics of components. As mentioned earlier, 10 normal modes were considered in order to reduce simulation duration while taking the recommended minimum number of modes into consideration. The accuracy of simulations can further be improved if more modes are taken into account. The decision on the number of modes depends on the aspired accuracy and the acceptable simulation duration. Based on these two

factors, the engineer has to make a practical decision. The exact selection of modes can be achieved through different methods. Three of the most common ones are:

- Total number of modes,
- relevant frequency range,
- ranking of modes.

The first approach is the simplest and enables a standardised procedure that does not require further investigations and adjustments for new components or models. A fixed number of modes that are taken into account is defined. However, the disadvantage can be that relevant frequency ranges are not represented. For this purpose, the second approach is suitable in which the occurring excitation frequencies are looked at first. Afterwards, approximately twice that value is chosen as the highest considered mode [17, 51]. This procedure allows to determine which, and thus also how many modes must be included per component. This can result in a lower total number of modes for some components, while for others it can result in a higher total number. The last method is the approach via ranking modes based on certain criteria. One example is the effective interface mass (EIM). Here, the extent to which an individual mode contributes to the loads at the interfaces of a structural component is quantified. The modes are then sorted so that the most important ones are taken into account. As a result, consecutive modes do not always have to be taken into account. For more information on the EIM method, the reader is referred to [52, 53]. Figure 5.5 shows exemplary diagrams for modes of a component with their associated EIMs. After the EIMs have been calculated, the cumulative EIM can be determined by adding up the values of the sorted modes until a defined threshold is exceeded. The figure highlights that the cumulative EIM of the sorted modes is generally higher compared to the one without sorting. Hence, less modes have to be considered to reach a certain threshold. In [51], a possible standardisation for the integration of flexible structures into MBS models is described. Various selection criteria, as well as previous simulations, serve as inputs for an algorithm that identifies relevant modes. However, the implementation of the method requires more effort and must also be extensively validated with more complex models. Other selection methods and a novel energy-based approach are presented in [54]. The method was

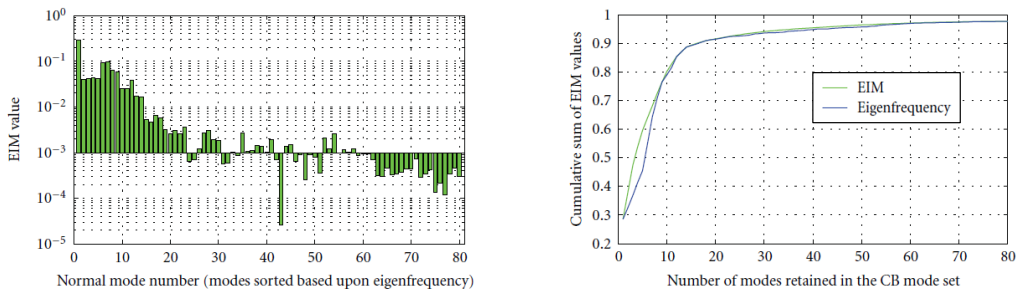

(a) EIM (b) Cumulative EIM

Figure 5.5 – EIM curves[2].

shown to reduce the number of selected modes significantly compared to other reduction methods for harmonic excitations. Even though ranking methods have the potential to reduce simulation duration while including the relevant dynamic characteristics of structural components, the problem of selecting modes shifts towards the decision on the aspired percentage of the target quantity for the respective criterion. The influence of this value on the accuracy of loads, which are the most important outputs for durability related simulations, should be investigated in the future. A combination of the three presented approaches is also conceivable. The implementation through software is carried out by defining the selection method in the FE models when they are transferred to the MBS environment.

Another improvement in accuracy can be achieved by modelling the damping of the structural components in more detail. In the present work, a standard modal damping approach was applied which is common for MBS of longer manoeuvres. In order to identify exact damping parameters, experiments would have to be carried out which is, however, time and cost-intensive, especially for full vehicle models containing numerous components [17]. For instance, complex structures could be enhanced by means of locally damped FE models as in [55].

Further on, the rider in the MBS model was rigidly attached to the frame of the motorcycle and did not perform any movements. However, it is common for motorcyclists to exercise movements on the vehicle. The posture is adjusted, and

[2] 'EIM values of fixed-interface normal modes' and 'Cumulative EIM sum according to the modal ordering schemes based upon EIM value and eigenfrequency, respectively' (https://www.hindawi.com/journals/ijrm/2011/143523/) by Stefano Ricci et al. are licensed under CC BY 3.0. (https://creativecommons.org/licenses/by/3.0/)

thus the COG shifts in relation to the motorcycle. At the same time, low-frequency excitations are induced. Additionally, arms and legs provide vibration isolation. The mentioned aspects, thus, influence the vehicle dynamics. Especially in borderline cases such as special event manoeuvres, a strongly deviating behaviour compared to the rigidly connected rider can be observed. Another example is the cornering with high lateral acceleration in which some riders influence the manoeuvre by again shifting their COG. Several publications elaborated on the subject of rider and rider movement modelling [56–60]. The implementation of these aspects in the ADAMS® environment and the simulation studies presented in this work should be part of upcoming studies and provide further insights.

In the present work, the friction and banking of the road were not modelled. These factors, however, have a smaller influence on the loads compared to the aspects that were considered. The banking of the road is of special interest for motorcycles riding on race tracks where the banking increases towards the outside of curves so that higher speeds can be ridden without skidding or tipping over due to the centrifugal forces. Nevertheless, both factors could be implemented in the presented approaches if a sufficient database exists. The slope of the roads was left out for the creation of synthetic virtual tracks and speed profiles. Reason being that there is currently no method to classify and recreate the slope of a road segmentally. Furthermore, the influence of slope on motorcycle rider behaviour is not explored as of yet. These interactions should, therefore, be examined in upcoming research.

Different loading conditions were not analysed either in the present work. However, the implementation is simple. Pillion riders and luggage can be created in ADAMS® like other components or the already included rider. Afterwards, simulations can be conducted in the same way. The methods to identify design-relevant customers, simulate their associated load profile, and create damage equivalent virtual tracks should be adjusted so that all relevant loading conditions are considered. This would, therefore, result in multiple simulations of virtual tracks with each relevant loading condition. At the same time, this would equal the approach that is currently employed for real measurement campaigns where certain test tracks are additionally ridden with luggage and pillion riders.

As shown in Section 5.4, representative special events might differ for different motorcycles. In future research, more obstacles and special events should be ana-

lysed. First, measurement campaigns should be carried out to validate new simulation models. Further on, representative special events should be identified with a larger database. Therefore, it is also advisable to examine even more vehicles to see whether the representative special events are still vehicle-independent or not.

The definition for special events and the introduced damage ratio factor should be further investigated. Using statistical models or also machine learning algorithms can be employed in order to identify and substitute special events that occur during the testing for service loads. Extracting the special events from service loads prevents incorrect load assumptions.

Another use case for MBS models are digital twins. These models represent a real object in the digital world. Additionally, there is an exchange of information between the real and virtual model. For example, data could be measured during real customer operation and transmitted to the digital twin which uses complex or simplified MBS models to calculate loads that the vehicle is currently experiencing in the hands of the customer. This makes it possible to detect whether a component will wear out or fail in the near future. As a result, the customer could be notified to have the vehicle inspected in a workshop to prevent actual damage or unintended immobilisation time. This approach is also known as predictive maintenance.

Bibliography

[1] A. Haerian, K. Öztürk and R. Liebich. 'Special and misuse events for motorcycles'. In: *International Journal of Vehicle Systems Modelling and Testing* (in press).

[2] A. Haerian, K. Öztürk and R. Liebich. 'Damage equivalent virtual tracks for motorcycles'. In: *International Journal of Vehicle Design* (in press).

[3] A. Haerian, K. Öztürk and R. Liebich. 'Influence of road and rider characteristics on durability of motorcycles'. In: *International Journal of Vehicle Systems Modelling and Testing* (in press).

[4] M. Köhler, S. Jenne, K. Pötter and H. Zenner. *Zählverfahren und Lastannahme in der Betriebsfestigkeit.* Berlin, Heidelberg: Springer Berlin Heidelberg, 2012.

[5] M. Karlsson. 'Load modelling for fatigue assessment of vehicles–a statistical approach'. PhD thesis. Göteborg University, 2007.

[6] C. Gorges. 'Identifying customer usage profiles of two-wheeled vehicles'. PhD thesis. TU Berlin, 2018.

[7] M. Meywerk. *CAE-Methoden in der Fahrzeugtechnik.* Berlin, Heidelberg: Springer Berlin Heidelberg, 2007.

[8] B. Bergman and B. Klefsjö. *Quality from customer needs to customer satisfaction.* Lund: Studentlitteratur AB, 2010.

[9] F. Küçükay, T. Kassel, M. Eghtessad and H. Kollmer. 'Requirement Engineering using the 3D method'. In: *SAE Technical Paper* No. 2011-26-0012 (2011).

[10] M. Speckert, K. Dreßler, N. Ruf, T. Halfmann and S. Polanski. 'The Virtual Measurement Campaign VMC concept-a methodology for georeferenced description and evaluation of environmental conditions for vehicle loads and energy efficiency'. In: *Proceedings of the 3rd Commercial Vehicle Technology Symposium; 2014 Mar 11-13; Kaiserslautern.* Aachen: Shaker, 2014, pp. 88–98.

[11] R. Mayrböck and A. Mayr. 'Numerische und experimentelle Methoden zur Lastdatenermittlung an Teilmodellen eines Motorrades'. In: *DVM Bericht 143; 2016 Oct 12-13; Steyr.* Berlin: DVM, 2016, pp. 93–106.

[12] M. Sautter and G. Greim. 'Betriebsfester Leichtbau von Motorrädern'. In: *Materials Testing* 47 (2005), pp. 396–403.

[13] U. Warnecke, K. Osterhage and W. Lieven. 'Optimierte Betriebsfestigkeitsauslegung durch Verwendung virtuell ermittelter Betriebslasten für Prüfstandsversuche'. In: *Materials Testing* 51.7-8 (2009), pp. 493–497.

[14] M. Kuchler and R. Schrupp. 'Multiaxial motorcycle wheel load transducer'. In: *VDI* 1616 (2001), pp. 249–278.

[15] M. Meywerk. *Vehicle dynamics*. Chichester: Wiley, 2015.

[16] R. Benz. 'Fahrzeugsimulation zur Zuverlässigkeitsabsicherung von karosseriefesten Kfz-Komponenten'. PhD thesis. Universität Karlsruhe, 2008.

[17] P. Johannesson and M. Speckert. *Guide to load analysis for durability in vehicle engineering*. Chichester: Wiley, 2014.

[18] M. Gipser. 'FTire–the tire simulation model for all applications related to vehicle dynamics'. In: *Vehicle System Dynamics* 45 (2007), pp. 139–151.

[19] D. Adamski. *Simulation in der Fahrwerktechnik*. Wiesbaden: Springer Fachmedien Wiesbaden, 2014.

[20] S. Engelmann. 'Simulation von fahrwerkdominierten Misuse–Lastfällen zur Unterstützung der virtuellen Crashsensorik'. PhD thesis. Helmut-Schmidt-Universität / Universität der Bundeswehr Hamburg, 2013.

[21] H. Kollmer, F. Küçükay and K. Pötter. 'Measurement and fatigue damage evaluation of road profiles in customer operation'. In: *International Journal of Vehicle Design* 56 (2011), pp. 106–124.

[22] A. Lepold and T. Kroschwald. 'Rechnerische Abschätzung des Lastniveaus bei Sonderereignissen'. In: *Materials Testing* 50 (2008), pp. 671–679.

[23] A. Riepl, W. Reinalter and M. Schmid. 'Application of the tyre model FTire in the vehicle development process at MAGNA STEYR Fahrzeugtechnik'. In: *Vehicle System Dynamics* 43 (2005), pp. 370–383.

[24] N. Rönicke, A. Ams, S. Brandes and B. Seufert. 'Simulationsgestütztes Design einer Schlechtwegoberfläche für ein neues Automobil-Prüfgelände'. In: *DVM Bericht 143; 2016 Oct 12-13; Steyr*. Berlin: DVM, 2016, pp. 151–164.

[25] N. Roy and M. Villaire. 'Virtual road load data acquisition using full vehicle simulations'. In: *SAE Technical Paper* 2013-01-1189 (2013).

[26] S. R. Waser, W. Hirschberg, T. Ille and V. Mladek. 'Evaluierung von Reifen- und Fahrbahnmodellen für die Simulation festigkeitsrelevanter Beanspruchungen von Nutzfahrzeugen'. In: *VDI Berichte, Reifen-Fahrwerk-Fahrbahn*. Düsseldorf: Springer-VDI-Verlag GmbH & Co. KG, 2007, pp. 153–165.

[27] S. R. Waser. 'Generierung der beanspruchungsrelevanten Belastungen von Nutzfahrzeugen mittels Reifen-, Fahrbahn-und Fahrzeugmodellen'. PhD thesis. TU Graz, 2009.

[28] T. Weber. 'Betriebslasten in der Fahrzeugentwicklung - Simulation Gesamtfahrzeug'. In: *DVM Bericht 141; 2014 Oct 8-9; Ingolstadt.* Berlin: DVM, 2014, pp. 115–128.

[29] H. Gimmler, D. Ammon and J. Rauh. 'Road profiles: Mobile measurement, data processing for efficient simulation and assessment of road properties'. In: *VDI Berichte* 1912 (2005), pp. 335–352.

[30] J. Rauh and M. Mössner-Beigel. 'Tyre simulation challenges'. In: *Vehicle System Dynamics* 46.S1 (2008), pp. 49–62.

[31] G. Rill and T. Schaeffer. *Grundlagen und Methodik der Mehrkörpersimulation.* Wiesbaden: Springer Vieweg, 2014.

[32] M. Bäcker, T. Langthaler, M. Olbrich and H. Oppermann. 'The hybrid road approach fro durability loads prediction'. In: *SAE Technical Paper* 2005-01-0628 (2005).

[33] D. O. Kang, H. Seungjin and K. Hoiyoung. 'Virtual road profile modeling using equivalent damage method for VPG simulation'. In: *SAE Technical Paper* 2009-01-0814 (2009).

[34] D. O. Kang, K. Park, S.-J. Heo, Y.-I. Ryu and J. I. Jeong. 'Development and application of VPG simulation technique based on equivalent virtual road profile'. In: *International Journal of Precision Engineering and Manufacturing* 11.2 (2010), pp. 265–272.

[35] A. Londhe and S. Kangde. 'Virtual Road Approach for Vehicle Durability Simulations'. In: *SAE International Journal of Passenger Cars-Mechanical Systems* 6 (2013), pp. 876–881.

[36] M. Morr, T. Minor and T. Maulick. 'Messdatenbasierte virtuelle Lastdatenermittlung für Fahrwerksbauteile und Karosserie'. In: *DVM Bericht 143; 2016 Oct 12-13; Steyr.* Berlin: DVM, 2016, pp. 107–120.

[37] C. Blanchette, M. Boisvert, N. Joubert, D. Rancourt and A. Desrochers. 'Dynamic input loads evaluation of a recreational vehicle frame using multibody dynamics hybrid modeling validated with experimental and full analytical modeling data'. In: *Advances in Mechanical Engineering* 13.8 (2021).

[38] A. Janßen, H. Kollmer and F. Küçükay. 'Entwicklung von Fahrwerks-und Antriebsstrangbauteilen durch Simulation kundennaher Betriebsbelastungen'. In: *Materials Testing* 49.9 (2007), pp. 468–473.

[39] M. Wagner, A. Opalinski and F. Küçükay. 'Determining Customer-Correlated Loads by Using the Monte Carlo Method'. In: *Proceedings of the 3rd Commercial Vehicle Technology Symposium; 2014 Mar 11-13; Kaiserslautern.* Aachen: Shaker, 2014, pp. 69–77.

[40] K. Dreßler, M. Speckert, R. Müller and C. Weber. 'Customer loads correlation in truck engineering'. In: *Berichte des Fraunhofer ITWM.* Vol. 151. 2009.

[41] A. Streit, K. Dreßler, M. Speckert, J. Lichter, T. Zenner and P. Bach. 'Anwendung statistischer Methoden zur Erstellung von Nutzungsprofilen für die Auslegung von Mobilbaggern'. In: *Berichte des Fraunhofer ITWM.* Vol. 163. 2009.

[42] C. Eckstein, P. Pirro, M. Speckert and A. Streit. 'Determination of test scenarios for durability verification of tractors under consideration of their usage variability'. In: *Proceedings of the 3rd Commercial Vehicle Technology Symposium; 2014 Mar 11-13; Kaiserslautern.* Aachen: Shaker, 2014, pp. 78–87.

[43] C. Eckstein. 'Ermittlung repräsentativer Lastkollektive zur Betriebsfestigkeit von Ackerschleppern'. PhD thesis. TU Kaiserslautern, 2017.

[44] R. Müller, D. Weiberle and R. Lenerz. 'Ableitung von einsatzspezifischen Auslegungslasten der Betriebsfestigkeit'. In: *Proceedings of the 4th Commercial Vehicle Technology Symposium; 2016 Mar 08-10; Kaiserslautern.* Aachen: Shaker, 2016, pp. 491–500.

[45] C. Biedinger. 'Automatic Usage Modeling for Automotive Applications'. PhD thesis. TU Kaiserslautern, 2019.

[46] C. Gorges, K. Öztürk and R. Liebich. 'Road classification for two-wheeled vehicles'. In: *Vehicle System Dynamics* 56.8 (2018), pp. 1289–1314.

[47] ISO. *Mechanical vibration - Road surface profiles - Reporting of measured data.* Standard No. 8608:2016. Geneva, Switzerland: ISO, 2016.

[48] J. Ungermann. 'Zuverlässigkeitsnachweis und Zuverlässigkeitsentwicklung in der Gesamtfahrzeugerprobung'. PhD thesis. ETH Zürich, 2009.

[49] B. Grupp, S. Salber and A. Haug. 'Nutzung von Kundenkollektiven und Data-Analytics-Methoden zur Präzisierung der Betriebsfestigkeitsanforderungen'. In: *DVM Bericht 146; 2019 Oct 9-10; Wolfsburg.* Berlin: DVM, 2019, pp. 59–75.

[50] T. Ryan. *Modern Experimental Design.* Hoboken: John Wiley & Sons, Inc, 2007.

[51] S. Litter. 'Integration von flexiblen Strukturen in Mehrkörpersysteme: Modellerstellung und automatisierte Selektion von Ansatzfunktionen'. PhD thesis. Universität der Bundeswehr München, 2014.

[52] D. C. Kammer and M. J. Triller. 'Selection of component modes for Craig-Bampton substructure representations'. In: *Journal of Vibration and Acoustics* 118.2 (1996), pp. 264–270.

[53] S. Ricci, M. Troncossi and A. Rivola. 'Model reduction of the flexible rotating crankshaft of a motorcycle engine cranktrain'. In: *International Journal of Rotating Machinery* 2011 (2011).

[54] R. Belotti, I. Palomba, D. Richiedei and A. Trevisiani. 'Interior mode selection in the Craig Bampton reduction technique based on an energy approach'. In: *Sixth International Operational Modal Analysis Conference; 2015 May 12-14; Gijón*. New York: Red Hook, 2015.

[55] A. Lion. 'Einsatz flexibler Körper in der numerischen Lebensdauersimulation von Kraftfahrzeugen: Methoden, Beispiele und offene Fragen'. In: *NAFEMS Magazin* 1 (2005), pp. 21–31.

[56] V. Keppler. 'Analysis of the biomechanical interaction between rider and motorcycle by means of an active rider model'. In: *Proceedings, Bicycle and Motorcycle Dynamics; 2010 Oct 20-22; Delft*. Delft: BMD, 2010.

[57] M. Bova, M. Massaro and N. Petrone. 'A Three-Dimensional Parametric Biomechanical Rider Model for Multibody Applications'. In: *Applied Sciences* 10.13 (2020).

[58] G. Sequenzia, S. M. Oliveri, G. Fatuzzo and M. Calì. 'An advanced multibody model for evaluating rider's influence on motorcycle dynamics'. In: *Proceedings of the Institution of Mechanical Engineers, Part K: Journal of Multi-body Dynamics* 229.2 (2015), pp. 193–207.

[59] F. Vasquez. 'Optimisation of off-road motorcycle suspensions'. PhD thesis. University of Southampton, 2020.

[60] S. Zhu, S. Murakami and H. Nishimura. 'Motion analysis of a motorcycle taking into account the rider's effects'. In: *Vehicle System Dynamics* 50.8 (2012), pp. 1225–1245.

[61] R. Gasch, K. Knothe and R. Liebich. *Strukturdynamik: Diskrete Systeme und Kontinua*. Berlin, Heidelberg: Springer-Verlag Berlin Heidelberg, 2012.

[62] R. Craig and M. Bampton. 'Coupling of substructures for dynamic analyses'. In: *AIAA journal* 6 (1968), pp. 1313–1319.

[63] E. Woschke, C. Daniel and J. Strackeljan. 'Reduktion elastischer Strukturen für MKS Anwendungen'. In: *Magdeburger Maschinenbau-Tage* 8 (2007), pp. 187–195.

A Flexible bodies

In order to take flexible properties into account, the components for the MBS can be imported from existing FE models. Therefore, the attachment points in both environments have to be matching, for example, the location and orientation of a bearing. In addition, the constraints have to be the same in both environments. One key assumption is that the infinite number of degrees of freedom (DOF) of a body can be approximated with a number of finite element DOF and the linear combination of mode shapes. As MBS can only operate effectively with significantly less DOF than FE models, a modal reduction needs to be executed to reduce the number of DOF. The main goal of modal reduction methods is to decrease the size of the state vector by means of a transformation matrix. Gasch et al. [61] illustrate how a transformation matrix $\mathbf{\Phi}$ with n rows and m columns can be used to reduce the size of the state vector $\mathbf{u}$ from n rows to a vector $\mathbf{q}$ with m rows, see Equation A.1. This reduction can then be applied to a system of equations of motion, like Equation A.2. $\mathbf{M}$ depicts the mass matrix, $\mathbf{K}$ is defined as the stiffness matrix, and $\mathbf{f}$ generally represents the vector of external loads.

$$\underbrace{\begin{Bmatrix} u_1 \\ u_2 \\ \vdots \\ u_n \end{Bmatrix}}_{\mathbf{u}} = \underbrace{\begin{bmatrix} \Phi_{1,1} & \Phi_{1,2} & \dots & \Phi_{1,m} \\ \Phi_{2,1} & \Phi_{2,2} & \dots & \Phi_{2,m} \\ \vdots & \vdots & \ddots & \vdots \\ \Phi_{n,1} & \Phi_{n,2} & \dots & \Phi_{n,m} \end{bmatrix}}_{\mathbf{\Phi}} \underbrace{\begin{Bmatrix} q_1 \\ q_2 \\ \vdots \\ q_m \end{Bmatrix}}_{\mathbf{q}}, \; m < n, \tag{A.1}$$

$$\mathbf{M}\ddot{\mathbf{u}} + \mathbf{K}\mathbf{u} = \mathbf{f}. \tag{A.2}$$

A widely used method that is also implemented in the ADAMS® environment is the method by Craig and Bampton [62]. First, a distinction between inner and outer nodes is made. The outer nodes or also boundary DOF ($\mathbf{u_B}$) represent the

attachment points to the MBS model. They are assigned a certain mass and also used to induce the outer loads. The inner nodes or also interior DOF ($\mathbf{u_I}$), on the other hand, describe the system behaviour in the FE environment. Utilising this definition leads to Equation A.3. The indices **B** and **I** stand for boundary and interior respectively.

$$\underbrace{\begin{bmatrix} \mathbf{M_{BB}} & \mathbf{M_{BI}} \\ \mathbf{M_{IB}} & \mathbf{M_{II}} \end{bmatrix}}_{\mathbf{M}} \underbrace{\begin{Bmatrix} \ddot{\mathbf{u}}_\mathbf{B} \\ \ddot{\mathbf{u}}_\mathbf{I} \end{Bmatrix}}_{\ddot{\mathbf{u}}} + \underbrace{\begin{bmatrix} \mathbf{K_{BB}} & \mathbf{K_{BI}} \\ \mathbf{K_{IB}} & \mathbf{K_{II}} \end{bmatrix}}_{\mathbf{K}} \underbrace{\begin{Bmatrix} \mathbf{u_B} \\ \mathbf{u_I} \end{Bmatrix}}_{\mathbf{u}} = \underbrace{\begin{Bmatrix} \mathbf{f_B} \\ \mathbf{f_I} \end{Bmatrix}}_{\mathbf{f}}. \tag{A.3}$$

The mode shapes are divided into two categories: the constraint modes and the normal modes. The normal modes represent the modes of the system with fixed outer nodes. Eigensolutions are then computed. The number of normal modes can be defined individually for every component. The constraint modes on the other hand are determined by fixing every outer node except for one. The one node that is not fixed is given a unit displacement. This procedure is carried out subsequently for the remaining outer nodes [19]. The total number of modes ω_{tot} that is used to describe the flexible behaviour of a component is, therefore, the sum of six rigid body modes ω_{R}, the number of constraint modes ω_{C}, and lastly the number of normal modes ω_{N}, see Equations A.4–A.6. The number of constraint modes equals the number of outer nodes n_{B} multiplied by six because of three translational and three rotational unit displacements.

$$\omega_{\mathrm{tot}} = \omega_{\mathrm{R}} + \omega_{\mathrm{C}} + \omega_{\mathrm{N}}, \tag{A.4}$$

$$\omega_{\mathrm{R}} = 6, \tag{A.5}$$

$$\omega_{\mathrm{C}} = n_{\mathrm{B}} \cdot 6. \tag{A.6}$$

The state vector containing the boundary DOF $\mathbf{u_B}$ and the interior DOF $\mathbf{u_I}$ can then be described with the transformation matrix $\mathbf{\Phi}$ and the modal coordinates of the two different mode categories according to Equation A.7. The modal coordinates of the constraint modes are labelled as $\mathbf{q_C}$ and the modal coordinates of the normal modes are labelled as $\mathbf{q_N}$. The transformation matrix contains the identity matrix $\mathbf{I}$, the zero matrix $\mathbf{0}$ and the displacements of the interior DOF in the constraint modes $\mathbf{\Phi_{IC}}$ and normal modes $\mathbf{\Phi_{IN}}$. The indices **C** and **N** stand for constraint and normal

respectively.

$$\underbrace{\begin{Bmatrix} \mathbf{u_B} \\ \mathbf{u_I} \end{Bmatrix}}_{\mathbf{u}} = \underbrace{\begin{bmatrix} \mathbf{I} & \mathbf{0} \\ \mathbf{\Phi_{IC}} & \mathbf{\Phi_{IN}} \end{bmatrix}}_{\mathbf{\Phi}} \underbrace{\begin{Bmatrix} \mathbf{q_C} \\ \mathbf{q_N} \end{Bmatrix}}_{\mathbf{q}}. \tag{A.7}$$

$\mathbf{\Phi_{IC}}$ and $\mathbf{\Phi_{IN}}$ can be derived from Equation A.8 and A.9, where $\boldsymbol{\omega}$ are the eigen-frequencies [63].

$$\mathbf{\Phi_{IC}} = -\mathbf{K_{II}}^{-1}\mathbf{K_{IB}}, \tag{A.8}$$

$$(\mathbf{K_{II}} - \boldsymbol{\omega}^2\mathbf{M_{II}})\mathbf{\Phi_{IN}} = 0. \tag{A.9}$$

The transformation matrix and its transposed $\mathbf{\Phi^T}$ can then be used to determine the generalised mass and stiffness matrices $\mathbf{M^{gen}}$ and $\mathbf{K^{gen}}$ according to Equation A.10 and A.11.

$$\mathbf{M^{gen}} = \mathbf{\Phi^T M \Phi}, \tag{A.10}$$

$$\mathbf{K^{gen}} = \mathbf{\Phi^T K \Phi}. \tag{A.11}$$

These generalised matrices are not diagonal, and hence the Craig-Bampton modes are not a set of orthogonal modes. Besides that, the raw Craig-Bampton method cannot be directly applied for dynamic simulations in the ADAMS® environment because of the following deficiencies:

- The six rigid body DOF are provided by ADAMS®, and therefore need to be eliminated from the constraint modes,
- the constraint modes are obtained through static condensation and hence do not have associated natural frequencies,
- disabling constraint modes has the same effect as applying a constraint to the system.

In order to use the Craig-Bampton method in the ADAMS® environment, a mode shape orthonormalisation has to be conducted. This is achieved by solving the

following eigenvalue problem:

$$\mathbf{K^{gen}q} = \boldsymbol{\lambda}\mathbf{M^{gen}q}. \tag{A.12}$$

The obtained eigenvectors $\boldsymbol{\lambda}$ can then be arranged in a new transformation matrix, named $\mathbf{B}$. This matrix transforms the Craig-Bampton modal basis to an equivalent basis with modal coordinates $\mathbf{q_e}$ that is orthogonal. The relation between the two bases is depicted by Equation A.13.

$$\mathbf{q} = \mathbf{Bq_e}. \tag{A.13}$$

Inserting the previous findings into Equation A.2 results in Equation A.14, which is now modally decoupled and has a reduced number of DOF.

$$\mathbf{B^T M^{gen} B\ddot{q}_e} + \mathbf{B^T K^{gen} Bq_e} = \mathbf{B^T f}. \tag{A.14}$$

As the last step, damping needs to be considered. Therefore, a modal damping matrix $\hat{\mathbf{D}}$ is added after the orthonormalisation. This damping matrix is diagonal and the amount of damping is dependant on the frequency of the modes. Higher frequencies are in general damped with a higher percentage with regard to the critical damping. In the present work, the damping was set to 1% for modes lower than 100 Hz, 10% for modes between 100 Hz and 1000 Hz, and 100% for modes over 1000 Hz based on experience values. Furthermore, the frequency range of interest for durability issues is typically under 100 Hz which justifies the values [17]. Using $\hat{\mathbf{M}}$ and $\hat{\mathbf{K}}$ as abbreviations leads to the final Equation A.15.

$$\hat{\mathbf{M}}\ddot{\mathbf{q}}_\mathbf{e} + \hat{\mathbf{D}}\dot{\mathbf{q}}_\mathbf{e} + \hat{\mathbf{K}}\mathbf{q_e} = \mathbf{B^T f} \tag{A.15}$$
$$\text{with} \quad \hat{\mathbf{M}} = \mathbf{B^T M^{gen} B} \quad \text{and} \quad \hat{\mathbf{K}} = \mathbf{B^T K^{gen} B}.$$

B Roughness classification

For the allocation of a roughness class according to the ISO 8608, the PSD of the road input has to be obtained. As this quantity cannot be measured directly during customer usage, onboard signals are used instead. The algorithm utilises the vehicle's velocity as well as the front and rear suspension displacements.

First, an in-plane full vehicle model is used to describe the system dynamics, as illustrated in Figure B.1.

The model consists of three rigid bodies and has four DOF. The sprung mass m_{s} is lumped in the COG and has the moment of inertia J_{s}. It is connected via dampers and springs (d_{ft}, d_{rr}, k_{ft}, k_{rr}) to the front and rear unsprung masses (m_{ft}, m_{rr}) which in turn are connected via springs and dampers representing the tyres (d_{T}, k_{T}) to the road which excites the system. Hence, the input of the system is the road profile z_{R}. The road stimulates the model both at the front wheel and at the rear wheel with a time delay which can be determined using the wheelbase p. The distance between COG and front as well as rear wheel is titled a and b respectively. The sprung mass comprises the chassis, the engine, the frame, the rider, and parts of the front and rear suspension system. The rear and front unsprung masses comprise the brakes, the wheel, and parts of the suspension systems respectively. The sprung mass can perform vertical and pitch motion (z_{s}, Θ_{s}) whereas the unsprung masses can only perform vertical motion (z_{ft}, z_{rr},). As suspension displacements can be recorded onboard, the transfer behaviour between the input and the spring displacements (s_{ft}, s_{rr}) needs to be determined. For this, the equations of motion have to be considered on the assumption of constant vehicle velocity v, see Equation B.1 to B.5.

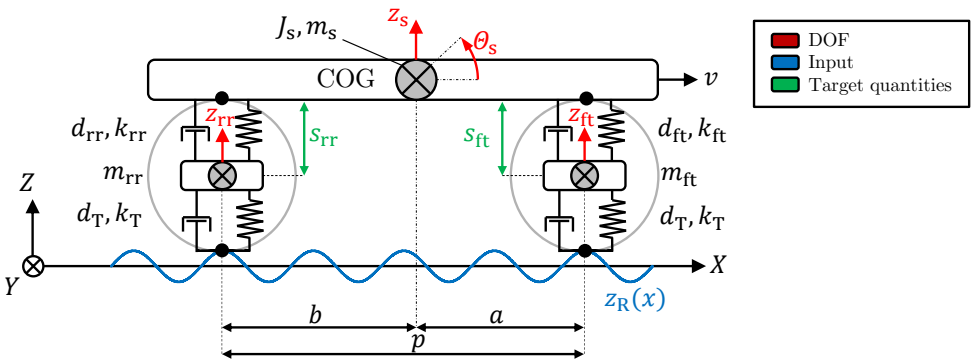

Figure B.1 – Full vehicle model.

$$\mathbf{M}\ddot{\mathbf{x}} + \mathbf{D}\dot{\mathbf{x}} + \mathbf{K}\mathbf{x} = \mathbf{f} \quad \text{with} \tag{B.1}$$

$$\mathbf{x} = \begin{pmatrix} z_s \\ \Theta_s \\ z_{ft} \\ z_{rr} \end{pmatrix}, \quad \mathbf{M} = \begin{bmatrix} m_s & 0 & 0 & 0 \\ 0 & J_s & 0 & 0 \\ 0 & 0 & m_{ft} & 0 \\ 0 & 0 & 0 & m_{rr} \end{bmatrix}, \tag{B.2}$$

$$\mathbf{D} = \begin{bmatrix} d_{ft} + d_{rr} & d_{ft}a - d_{rr}b & -d_{ft} & -d_{rr} \\ d_{ft}a - d_{rr}b & d_{ft}a^2 + d_{rr}b^2 & -d_{ft}a & d_{rr}b \\ -d_{ft} & -d_{ft}a & d_{ft} + d_T & 0 \\ -d_{rr} & d_{rr}b & 0 & d_{rr} + d_T \end{bmatrix}, \tag{B.3}$$

$$\mathbf{K} = \begin{bmatrix} k_{ft} + k_{rr} & k_{ft}a - k_{rr}b & -k_{ft} & -k_{rr} \\ k_{ft}a - k_{rr}b & k_{ft}a^2 + k_{rr}b^2 & -k_{ft}a & k_{rr}b \\ -k_{ft} & -k_{ft}a & k_{ft} + k_T & 0 \\ -k_{rr} & k_{rr}b & 0 & k_{rr} + k_T \end{bmatrix}, \tag{B.4}$$

$$\mathbf{f} = \begin{pmatrix} 0 \\ 0 \\ k_T z_R(t) + d_T \dot{z}_R(t) \\ k_T z_R(t-\tau) + d_T \dot{z}_R(t-\tau) \end{pmatrix} \quad \text{with} \quad \tau = \frac{p}{v}. \tag{B.5}$$

The parameters are described in Table B.1.

Table B.1 – Parameters full vehicle model.

Symbol	Description
Perpendicular distance of COG from front-wheel Z-axis	a
Perpendicular distance of COG from rear-wheel Z-axis	b
Reduced damping coefficient front suspension	d_{ft}
Reduced damping coefficient rear suspension	d_{rr}
Tyre damping coefficient	d_{T}
Pitch sprung mass	Θ_{s}
Rotational inertia sprung mass	J_{s}
Reduced stiffness coefficient front suspension	k_{ft}
Reduced stiffness coefficient rear suspension	k_{rr}
Tyre stiffness coefficient	k_{T}
Front unsprung mass	m_{ft}
Rear unsprung mass	m_{rr}
Sprung mass	m_{s}
Wheelbase	p
Spring displacement front	s_{ft}
Spring displacement rear	s_{rr}
Time delay	τ
Vehicle velocity	v
Displacement unsprung mass front	z_{ft}
Road excitation	z_{R}
Displacement unsprung mass rear	z_{rr}
Displacement sprung mass	z_{s}

The linear time-invariant system can be analysed in the time as well as the frequency domain. In the latter, the relation between input $X(s)$ and target quantity $Y(s)$ can be described with the transfer function $H(s)$, according to Equation B.6.

$$H(s) = \frac{Y(s)}{X(s)}. \tag{B.6}$$

The relation between the spring displacements that are collected onboard and the DOF from the full vehicle model depicted in Figure B.1 is described by Equations B.7 and B.8. Here, the transformation to the frequency domain is also considered.

$$S_{\mathrm{ft}}(s) = Z_{\mathrm{s}}(s) + a\Theta(s) - Z_{\mathrm{ft}}(s), \tag{B.7}$$

$$S_{\mathrm{rr}}(s) = Z_{\mathrm{s}}(s) - b\Theta(s) - Z_{\mathrm{rr}}(s). \tag{B.8}$$

The transfer functions for the spring displacements are presented in Equations B.9 and B.10.

$$H_{\mathrm{ft}}(s, v) = \frac{S_{\mathrm{ft}}(s)}{Z_{\mathrm{R}}(s)}, \tag{B.9}$$

$$H_{\mathrm{rr}}(s, v) = \frac{S_{\mathrm{rr}}(s)}{Z_{\mathrm{R}}(s)}. \tag{B.10}$$

These functions can be derived numerically for defined velocities. For this, the equations of motion are transferred into a state-space model with delayed inputs, see Equations B.11–B.16.

$$\dot{\boldsymbol{x}}(t) = \mathbf{A}\boldsymbol{x}(t) + \mathbf{B}_1\boldsymbol{u}(t) + \mathbf{B}_2\boldsymbol{u}(t-\tau), \tag{B.11}$$

$$\boldsymbol{y}(t) = \mathbf{C}\boldsymbol{x}(t) + \mathbf{D}_1\boldsymbol{u}(t) + \mathbf{D}_2\boldsymbol{u}(t-\tau), \tag{B.12}$$

with

$$\mathbf{A} = \begin{bmatrix} 0 & 0 & 0 & 0 & 1 & 0 & 0 & 0 \\ 0 & 0 & 0 & 0 & 0 & 1 & 0 & 0 \\ 0 & 0 & 0 & 0 & 0 & 0 & 1 & 0 \\ 0 & 0 & 0 & 0 & 0 & 0 & 0 & 1 \\ \frac{-(k_{\mathrm{ft}}+k_{\mathrm{rr}})}{m_{\mathrm{s}}} & \frac{-k_{\mathrm{ft}}a+k_{\mathrm{rr}}b}{m_{\mathrm{s}}} & \frac{k_{\mathrm{ft}}}{m_{\mathrm{s}}} & \frac{k_{\mathrm{rr}}}{m_{\mathrm{s}}} & \frac{-(d_{\mathrm{ft}}+d_{\mathrm{rr}})}{m_{\mathrm{s}}} & \frac{-d_{\mathrm{ft}}a+d_{\mathrm{rr}}b}{m_{\mathrm{s}}} & \frac{d_{\mathrm{ft}}}{m_{\mathrm{s}}} & \frac{d_{\mathrm{rr}}}{m_{\mathrm{s}}} \\ \frac{-k_{\mathrm{ft}}a+k_{\mathrm{rr}}b}{J_{\mathrm{s}}} & \frac{-(k_{\mathrm{ft}}a^2+k_{\mathrm{rr}}b^2)}{J_{\mathrm{s}}} & \frac{k_{\mathrm{ft}}a}{J_{\mathrm{s}}} & \frac{-k_{\mathrm{rr}}b}{J_{\mathrm{s}}} & \frac{-(d_{\mathrm{ft}}a+d_{\mathrm{rr}}b)}{J_{\mathrm{s}}} & \frac{-(d_{\mathrm{ft}}a^2+d_{\mathrm{rr}}b^2)}{J_{\mathrm{s}}} & \frac{d_{\mathrm{ft}}a}{J_{\mathrm{s}}} & \frac{-d_{\mathrm{rr}}b}{J_{\mathrm{s}}} \\ \frac{k_{\mathrm{ft}}}{m_{\mathrm{ft}}} & \frac{k_{\mathrm{ft}}a}{m_{\mathrm{ft}}} & \frac{-(k_{\mathrm{ft}}+k_{\mathrm{T}})}{m_{\mathrm{ft}}} & 0 & \frac{d_{\mathrm{ft}}}{m_{\mathrm{ft}}} & \frac{d_{\mathrm{ft}}a}{m_{\mathrm{ft}}} & \frac{-(d_{\mathrm{ft}}+d_{\mathrm{T}})}{m_{\mathrm{ft}}} & 0 \\ \frac{k_{\mathrm{rr}}}{m_{\mathrm{rr}}} & \frac{-k_{\mathrm{rr}}b}{m_{\mathrm{rr}}} & 0 & \frac{-(k_{\mathrm{rr}}+k_{\mathrm{T}})}{m_{\mathrm{rr}}} & \frac{d_{\mathrm{rr}}}{m_{\mathrm{rr}}} & \frac{-d_{\mathrm{rr}}b}{m_{\mathrm{rr}}} & 0 & \frac{-(d_{\mathrm{rr}}+d_{\mathrm{T}})}{m_{\mathrm{rr}}} \end{bmatrix}, \tag{B.13}$$

$$\boldsymbol{x} = \begin{pmatrix} z_{\mathrm{s}} \\ \Theta \\ z_{\mathrm{ft}} \\ z_{\mathrm{rr}} \\ \ddot{z}_{\mathrm{s}} \\ \ddot{\Theta} \\ s_{\mathrm{ft}} \\ s_{\mathrm{rr}} \end{pmatrix}, \quad \mathbf{B}_1 = \begin{bmatrix} 0 \\ 0 \\ \frac{d_{\mathrm{T}}b}{m_{\mathrm{ft}}} \\ 0 \\ \frac{(d_{\mathrm{ft}}d_{\mathrm{T}})}{(m_{\mathrm{s}}m_{\mathrm{ft}})} \\ \frac{(d_{\mathrm{ft}}d_{\mathrm{T}})a}{(J_{\mathrm{s}}m_{\mathrm{ft}})} \\ \frac{(-d_{\mathrm{ft}}d_{\mathrm{T}}-d_{\mathrm{T}}^2+k_{\mathrm{T}}m_{\mathrm{ft}})}{m_{\mathrm{ft}}^2} \\ 0 \end{bmatrix}, \quad \mathbf{B}_2 = \begin{bmatrix} 0 \\ 0 \\ \frac{d_{\mathrm{T}}b}{m_{\mathrm{rr}}} \\ 0 \\ \frac{(d_{\mathrm{rr}}d_{\mathrm{T}})}{(m_{\mathrm{s}}m_{\mathrm{rr}})} \\ \frac{(d_{\mathrm{rr}}d_{\mathrm{T}})a}{(J_{\mathrm{s}}m_{\mathrm{rr}})} \\ \frac{(-d_{\mathrm{rr}}d_{\mathrm{T}}-d_{\mathrm{T}}^2+k_{\mathrm{T}}m_{\mathrm{rr}})}{m_{\mathrm{rr}}^2} \\ 0 \end{bmatrix}, \tag{B.14}$$

$$\mathbf{C} = \begin{bmatrix} 1 & 0 & 0 & 0 & 0 & 0 & 0 & 0 \\ 0 & 1 & 0 & 0 & 0 & 0 & 0 & 0 \\ 0 & 0 & 1 & 0 & 0 & 0 & 0 & 0 \\ 0 & 0 & 0 & 1 & 0 & 0 & 0 & 0 \\ -(k_{\mathrm{ft}}+k_{\mathrm{rr}}) & k_{\mathrm{rr}}b-k_{\mathrm{ft}}a & k_{\mathrm{ft}} & k_{\mathrm{rr}} & -(d_{\mathrm{ft}}+d_{\mathrm{rr}}) & d_{\mathrm{rr}}b-d_{\mathrm{ft}}a & d_{\mathrm{ft}} & d_{\mathrm{rr}} \\ k_{\mathrm{rr}}b-k_{\mathrm{ft}}a & -(k_{\mathrm{ft}}a^2+k_{\mathrm{rr}}b^2) & k_{\mathrm{ft}}a & -k_{\mathrm{rr}}b & d_{\mathrm{rr}}b-d_{\mathrm{ft}} & -(d_{\mathrm{ft}}a^2+d_{\mathrm{rr}}b^2) & d_{\mathrm{ft}}a & -d_{\mathrm{rr}}b \\ 1 & a & -1 & 0 & 0 & 0 & 0 & 0 \\ 1 & -b & 0 & -1 & 0 & 0 & 0 & 0 \end{bmatrix}, \tag{B.15}$$

$$\mathbf{D}_1 = \begin{bmatrix} 0 \\ 0 \\ 0 \\ 0 \\ \frac{(d_{\mathrm{ft}} d_{\mathrm{T}})}{(m_{\mathrm{s}} m_{\mathrm{ft}})} \\ \frac{(d_{\mathrm{ft}} d_{\mathrm{T}}) a}{(J_{\mathrm{s}} m_{\mathrm{ft}})} \\ 0 \\ 0 \end{bmatrix}, \quad \mathbf{D}_2 = \begin{bmatrix} 0 \\ 0 \\ 0 \\ 0 \\ \frac{(d_{\mathrm{rr}} d_{\mathrm{T}})}{(m_{\mathrm{s}} m_{\mathrm{rr}})} \\ \frac{-(d_{\mathrm{rr}} d_{\mathrm{T}}) b}{(J_{\mathrm{s}} m_{\mathrm{rr}})} \\ 0 \\ 0 \end{bmatrix}, \quad u = z_{\mathrm{R}}. \tag{B.16}$$

In order to calculate the PSD of the road $\mathrm{PSD}_{\mathrm{Road}}(f)$, Equation B.17 has to be used with $\mathrm{PSD}_{\mathrm{Res}}(f)$ being the PSD of the response signal and $H(f)$ the respective transfer function from the numeric computation.

$$|H(f)|^2 = \frac{\mathrm{PSD}_{\mathrm{Res}}(f)}{\mathrm{PSD}_{\mathrm{Road}}(f)} \quad \rightarrow \quad \mathrm{PSD}_{\mathrm{Road}}(f) = \frac{\mathrm{PSD}_{\mathrm{Res}}(f)}{|H(f)|^2}. \tag{B.17}$$

The PSD has to be transformed from the time frequency domain f to the spatial frequency domain n due to consistency with the ISO 8608, see Equation B.18. Implementing the transformation in Equation B.17 leads to the final Equation B.19.

$$n = \frac{f}{v} \quad \rightarrow \quad \mathrm{PSD}_{\mathrm{Road}}(n) = v\,\mathrm{PSD}_{\mathrm{Road}}(f), \tag{B.18}$$

$$\mathrm{PSD}_{\mathrm{Road}}(n) = \frac{v\,\mathrm{PSD}_{\mathrm{Res}}(f)}{|H(f)|^2}. \tag{B.19}$$

Hereafter, the PSD is smoothed in different octave bands. In the present work, the transfer functions for the front and rear spring displacements were used. Hence, both signals and the respective transfer function lead to a separate PSD. In order to obtain only one PSD for the road profile classification, the mean for the two provided PSDs is calculated. Finally, a minimum distance classifier is employed to find the closest roughness class as described in Section 3.2.4. Computing and storing the transfer functions beforehand for a span of velocities enables a continuous online classification when the velocity is averaged during a small time window.